UNIVERSITY OF ALBERTA

Coupling a time-dependent two-cylinder cumulus model with a time-dependent hail growth model to forecast maximum hail size on the ground

By

Fusheng Jia 

A thesis submitted to the Faculty of Graduate Studies and Research
in partial fulfillment of requirements for the degree of Master of Sciences

Department of Earth and Atmospheric Sciences

Edmonton, Alberta

Fall 2007

Your file Votre référence
ISBN: 978-0-494-33268-9
Our file Notre référence
ISBN: 978-0-494-33268-9

DEDICATION

For my wife, my daughter and son who always believed in me.

ABSTRACT

A time-dependent, two-cylinder cumulus model coupled with a time-dependent hail growth model is developed to simulate hail growth and forecast maximum hail size on the ground. Observed upper air soundings were used as input to initialize the coupled cumulus-hail model. Sensitivity experiments were carried out to examine the influence of changes of cloud and hail parameters on the hail growth. The new coupled cumulus-hail model technique was used to simulate hail storms for three summers of 1983 to 1985, using afternoon sounding data sampled over the Alberta Hail Project (AHP) area. For each day, the forecast hail size on the ground was compared with daily observations of maximum hail size collected within the AHP area. The skillfulness of the new model was quantified by calculating various forecasting skill scores.

The time-dependent coupled cumulus-hail model with precipitation effects was skillful in forecasting the occurrence and size of hail. The forecasting of maximum hail size was improved by including the parameterization of precipitation in the cumulus model. Overall, the model improved forecasting of maximum hail size compared against the operationally used method, HAILCAST, which was based on a steady-state cloud model. This improvement was attributed to the employment of the time-dependent cloud model as the evolution of the fields of cloud water, vertical velocity and the in-cloud temperature provided more realistic surrounding conditions for hail growth. Using the time-dependent coupled cumulus-hail model improved the forecasting of hail size compared to a traditional algorithm, NOMOGRAM, which related maximum hail size on the ground to the cloud maximum updraft velocity and the temperature at the altitude of maximum updraft.

ACKNOWLEDGEMENTS

I am greatly indebted to many individuals who provide encouragement and helps to me during this undertaking. In particular I wish to thank Dr. Gerhard Reuter so much, my thesis supervisor. His guidance, comments and suggestions are invaluable and very much appreciated. I also like to thank Dr. Maxwell Dupilka for his generous assistance with computer drafting of Golden Software, as well as his constructive comments and suggestions. Special thanks are given to Mr. Julian Charles Brimelow, profitable discussions with him about the model framework and his suggestions on the model modification and improvements are appreciated.

TABLE OF CONTENTS

LIST OF FIGURES

LIST OF TABLES

Chapter 1 INTRODUCTION

1.1 Forecasting maximum hail size

Hailstones are pieces of ice in the structure of layered or onionskin-like, which typically are transparent or partially opaque. A hailstone size ranges from that of small peas to that of golf balls or larger. Falling hailstones can destroy crops, break windows, dent cars, batter roofs of homes, and sometimes even cause extensive damage to livestock and people. The damage inflicted by a falling hailstone is determined primarily by its kinetic energy (KE). For a spherical hailstone with diameter of D, the KE is proportional to D^4 as the hailstone's mass and terminal velocity are proportional to D^3 and $D^{0.5}$, respectively. Figure 1.1 depicts the increases of a hailstone's kinetic energy and the terminal velocity with the increase of the hailstone's diameter.

In order to prevent or mitigate hail damage it is necessary to determine the potential of hailstone damage. For this purpose, it is very important to forecast expected maximum hail size. One of the primary mandates of the Meteorological Service of Canada (MSC) of Environment Canada is to issue weather watches or weather warnings for violent summer weather. One of the criteria used to issue watches and warnings for hail fall is that the expected maximum hail exceeds 2 cm in diameter. The useful lead time for a severe weather watch or warning is about 12 hours. This means that a severe weather warning for late afternoon thunderstorms should be issued in the morning. Sufficient hours of severe weather warning in advance of upcoming hailstorms would provide enough time to disseminate the news and allow to protect potentially hail-affected properties by implementing precautions with enough lead time.

Weather radar is used to monitor the structure, severity and evolution of severe convective storms. It can also detect and nowcast hail fall. However, the radar-derived hail algorithms reveal some significant caveats in forecasting hailstones. They only indicate hail after it commences or is imminent. Thus, there is little or even no lead time

to disseminate hail warnings. In addition, the radar-derived hail techniques showed limited skills at forecasting the actual hail size on the ground (Edwards and Thompson 1998). A wide variety of operationally used numerical weather prediction (NWP) models provide guidance for the synoptic scale weather patterns several hours in advance, but they do not predict hail size on the ground surface.

In order to forecast maximum hail size, this thesis research plans to investigate the feasibility of using numerical models to simulate the process of hail growth and to forecast maximum hail size on the ground. The scientific motivation is to study how to couple a time-dependent two-cylinder cumulus model with a time-dependent hail growth model to forecast maximum hail size on the ground. Furthermore, this work will examine how the evolution of storm cloud and precipitation in the cumulus model affect hail growth and the final hail size in the coupled model technique. The overall objective is that the coupled cumulus-hail model approach could eventually provide an effective numerical tool to aid weather forecasters in forecasting maximum hail size and issuing hail warnings for operational job.

1.2 Review of hail forecasting techniques using numerical models

Different numerical models have been used in the past to forecast hail size with lead times up to 12 hours. Most of these models are a type of cumulus cloud model initialized with an observed (or NWP-model predicted) thermodynamic sounding. The simplest approach is based on correlating hail size with sounding derived parameters such as convective available potential energy (CAPE) or vertical velocity at specific temperature levels. Renick and Maxwell (1977) developed a NOMOGRAM to provide a simple algorithm to forecast hail size. The NOMOGRAM relates maximum hail size on the ground to the maximum storm updraft velocity and the temperature at the height of maximum updraft. The maximum updraft speed was diagnosed from a stationary cloud model (being essentially a tephigram analysis). The NOMOGRAM technique relies on the concept that higher CAPE is capable of producing severe convective storms with stronger updraft velocity to support larger hailstones. However, it is not always the case

that higher CAPE leads to larger hailstones. The NOMOGRAM sometimes failed to discriminate between large and small hail size (Doswell et al 1982) because of the oversimplification of the cloud conditions and the neglect of microphysical processes such as melting and water shedding.

Moor and Pino (1990) used a steady-state, one-dimensional cloud model of Athens (1977) to calculate the profile of vertical velocity of storm cloud, and then, hail diameters were related to the vertical velocity at the level of temperature as –10°C. Skill of the method proved far superior to those based only on the maximum updraft velocity derived from CAPE for severe hail events over the southern plains of the United States. However, the technique has yet to be evaluated for no-hail and non-severe hail days.

Brimelow et al (2002a) developed a numerical model, HAILCAST, to predict maximum hail size on the ground. HAILCAST was a model technique that coupled a steady-state one-dimensional cloud model with a time-dependent hail growth model. The cloud model was similar to that of Anthes (1977), Moore and Pino (1990), and the hail growth model was adopted from that of Dennis and Musil (1973), Rasmussen and Heymsfield (1987a, b). The steady-state, one-dimensional cloud model is initialized using observed balloon sounding data. Alternatively, prognostic soundings derived from NWP models can be used to provide the cloud model's initial conditions. The steady-state cloud model predicts updraft velocity, in-cloud temperature and liquid water content (LWC) within the main storm updraft column. These vertical profiles of updraft, temperature and LWC are used as input for the hail growth model. Based on water budget and heat budget for hail stones, the hail model computes the evolution of the size, temperature, and trajectory of the hailstone. The hail growth microphysics includes dry growth, wet growth, melting and shedding of excess liquid water within surrounding conditions provided by the cloud model output. Combining the steady-state one-dimensional cloud model with the time-dependent hail growth model allows a modeling tool for predicting maximum hail size based on atmospheric soundings.

HAILCAST was verified based on the Alberta Hail Project (AHP) data for three summers of 1983 to 1985. Afternoon balloon soundings released from Penhold every day were used to initialize model runs. Model forecast maximum hail size on the ground was compared with hailstone observations within the AHP area. It was found that HAILCAST was more accurate and robust than the traditionally used NOMOGRAM technique in forecasting maximum hail size based on the same AHP data. HAILCAST was used operationally in the Prairie and Arctic Storm Prediction Center (PASPC) during summers of 2002 through 2005 to assist in issuing storm warnings (Brimelow, 2005). It was also used in Argentina (Brimelow, 2002b), South Africa and the USA.

In recent years NWP models have improved such that the model predicted soundings frequently resemble observed profiles of temperature and humidity. This makes it possible to utilize model-predicted soundings as input for HAILCAST, rather than relying on the observed sounding data, which are available only twice daily at any upper air sounding station. Moreover, the upper air stations are distributed on highly sparse networks. For example, there is only one upper air sounding station, Stony Plain, in operation for Alberta. And the distance between Stony Plain and a nearest sounding station, The Pas in Saskatchewan, is about 1000 km. Brimelow et al (2005) alternatively used prognostic GEM model soundings for the summer of 2000. For each summer day contour maps of forecast maximum hail size were obtained by running HAILCAST on grid points of more than 1500 GEM prognostic soundings. The forecast hail size maps were verified against surface hail reports and radar reflectivity data. The comparison showed that combining GEM with HAILCAST provided a powerful tool to predict maximum hail size with lead time of about 12 hours.

However, HAILCAST revealed some obvious shortcomings. A major difficulty was that it could not simulate the evolution of convective clouds. Secondly, it neglected to simulate the dynamic effects of the forming of precipitation. Moreover, effects of vertical wind shear on storm organization were excluded. The fundamental reasons responsible for these shortcomings were due mostly to the use of a steady-state cloud model. In HAILCAST, the parameters of updraft velocity, in-cloud temperature and

liquid water content in modeled cloud remain unchanged for infinite time, whereas a real convective storm evolves greatly in time. The evolutionary of storm parameters strongly affects hail growth (Cotton and Anthes 1989). Furthermore, as the steady-state cloud model produced long-live updrafts without death, it required an estimation of life duration of cloud updraft to supply input for hail growth. This requested more information to estimate the life cycle of cloud and it was often hard to get realistic estimations although the hail growth time and final hail size on the ground were sensitive to cloud life cycle and cloud intensity (Foote 1984, Henry 1993, Hand and Conway 1995). In addition, the updraft velocity at the cloud base for the steady-state cloud model in HAILCAST had to be assumed artificially.

Time-dependent, multi-dimensional convective cloud models can realistically simulate a convective storm, and the trajectory of growing hailstones as Lagrangian functions can be computed to predict maximum hail size on the ground. They have contributed greatly to our current understanding of hail growth mechanisms (Xu 1983, Farley 1987, and Kubesh et al 1988). Obviously, the advantage of using a time-dependent multi-dimensional convective cloud model coupled with a hail growth model is expected to have high accuracy based on more physically realistic storm simulation.

However, some other questions challenge the employment of this approach. First of all, it demands excessive computational resources in terms of computer core memory storage and computing time (Brooks, 1992). Secondly, it has very high demand on time-dependent multi-dimensional model initial data for temperature, humidity and wind. It is quite difficult to obtain atmospheric data significant for storms on the horizontal grid-points spanning merely one or two hundred meters as the values of model initialization. The multi-dimensional models are often used in designated field experiments limited to relatively small areas. Access to the model's output is available only to a selected group of researchers (Brooks, 1993). It is also hard to choose which trajectory is the best for maximum hail growth in multi-dimensional domain.

To avoid these shortcomings, it is hoped to find an alternative approach to numerically simulate hail growth and predict maximum hail size on the ground. The expected approach not only has the ability to realistically simulate the physical features of hail growth zone (HGZ) of storm clouds, but is also efficient in terms of consuming computer power, and easy to be initialized as well. For the eventual objective of operational usage, both the accuracy and efficiency of the approach should be taken into consideration together. It is expected that the new coupled model technique will definitely contribute to the forecasting of maximum hail size on the ground in operational application.

1.3 Theory of hail growth and growth environment

1.3.1 Hail growth microphysics

Hailstones grow when hail embryos accrete supercooled water droplets and ice crystals in convective clouds with strong updrafts (Garcia and List, 1992). The hail embryos typically vary between hundreds of microns to thousands of microns in diameter (Macklin, 1977), and they may be in the form of frozen drops or graupel particles (Keight, 1978; Federer and Waldvogel, 1978; Knight, 1981).

The presence of water substances in cloud involving liquid water droplets and ice particles is a critical factor influencing hail growth, as the cloud water affects the hail mass change and heat balance through the process of collection or accretion and latent heat release. Most of hail growth occurs in the region of storm cloud between the 0°C and – 40°C levels, where the cloud water consists in the majority of supercooled water droplets. Above the – 40°C level, the cloud water is usually in the form of ice crystals only (Vali and Stansbury, 1965). Hailstones within this region grow by accreting ice crystals, but only slowly, due to the small ice-ice collection efficiency. Obviously, the changing of the profile of water substances with time in storm cloud influences the hail growth.

The rate of hail growth depends on its heat budget: the rate of release of latent heat as accreted supercooled water droplets freeze on the hailstone surface, versus the rate at which this latent heat is transferred away from its surface. The surface temperature of a growing hailstone is typically a few degrees warmer than the in-cloud temperature. The in-cloud temperature profile plays a significant role in the decrease of hailstone surface temperature by the evaporation of water from the surface of the hail and the conduction of heat. Below the level of in-cloud temperature 0°C, the hailstone's temperature is colder than the surrounding temperature. Melting of the hailstone usually occurs below the freezing level due to warm surrounding temperature. Consequently, the profile of in-cloud temperature and its time evolution affect the hail growth. Fluctuation of the height of freezing level and magnitude of averaged temperature below the freezing level influence the hail melting before it reaches to ground surface.

There are two primary growth regimes for hailstones depending on the rate of heat transfer to and from the hailstone. If the rate of release of latent heat on a hailstone due to accretion of cloud water exceeds the rate of heat transfer away from the hailstone surface due to conduction, evaporation and sublimation, the hailstone's temperature rises rapidly to 0°C and it enters the so-called wet growth regime. During this situation, as the hailstone temperature is equal to 0°C, liquid water could exist on the surface of the hailstone. In the wet growth regime, any intercepted ice crystals are accreted, as they easily "stick" to the hailstone's wet surface (English, 1973). Depending on the ambient in-cloud temperature, cloud water mixing ratio and size of the hailstone, it may begin to shed some liquid water away from its surface (Levi and Lubart, 1998; Greenan and List, 1995) as the hailstone can not hold too much liquid water on its surface based on its surface area or hail size. This shedding process could be an important source of rain and new hail embryos in thunderstorms (Rasmussen and Heymsfield, 1987c; Kubesh et al., 1988). Simply, if the hailstone's surface temperature equals or exceeds 0°C on any altitude, the hailstone probably begins to melt.

If the rate of heat transfer away from the hailstone surface is sufficiently large, the hailstone's temperature remains below 0°C. This mode of hail growth is known as the dry

growth regime. During dry growth, since the surface temperature of the hailstone is now below 0°C, any accreted supercooled water droplets are frozen completely on to the hailstone's surface. However, only a small fraction of intercepted ice crystals are accreted, as they do not readily "stick" to the dry surface of the hailstone (English, 1973).

A cut hailstone often displays a number of concentric layers alternating between opaque and transparent ice (Macklin, 1977). These layers result from the hailstone undergoing wet or dry growth as it passes through regions of varying temperature and water mixing ratio in a cloud (Rogers and Yau, 1996). The white and opaque layer indicates the dry growth regime, during which the hail is consisted of a high concentration of small air bubbles trapped as the cloud water droplets rapidly freeze upon contact with the hailstone (Macklin, 1977). Conversely, mostly transparently layers are due to wet growth with a lower concentration of larger air bubbles present in the frozen water deposit. Figure 1.2 is a photo showing a cut sample of hailstone with different thin sections. We can see that the dry growth was in dominance, featuring in feather-like in dry growth regime. The wet growth was within most outside layers while possible frozen droplet embryo.

The rate of mass growth of a hailstone is governed by the process of continuous collection of cloud water. The instantaneous mass growth rate of a hailstone is proportional to its terminal velocity and the cloud water mixing ratio. It is also proportional to the cross-sectional area of the hailstone (perpendicular to the flow), and the net collection efficiency of cloud water. Obviously, the cloud situations as surrounding conditions for hail growth always significantly influence the hail growth both in the temperature changing and mass growth. Description of hail growth in terms of formulas will be discussed in detail in the next chapter.

1.3.2 The Hail Growth Zone (HGZ) in storm cloud

Field studies and numerical modeling of hail growth have shown that there is a preferential region within hailstorms where maximum hail growth rate occurs (English,

1973; Browning, 1977; Nelson, 1983; Foote, 1984; Miller et al., 1988). This region is called the hail growth zone (HGZ) and occurs at the in-cloud temperature from about – 20°C to – 40°C. There are three reasons for maximum hail growth occurring in the HGZ (Brimelow, 1999). The first one is that the maximum updraft is often located within the HGZ. And secondly, the in-cloud temperature as the ambient temperature for hailstones is low enough to facilitate dry growth of hailstone, which enables most or all of the accreted water to freeze on the hailstone's surface. Last, within the HGZ the cloud is composed of a mixture of supercooled water and ice crystals (Vali and Stansbury, 1965). A hailstone undergoing wet growth within this mixed-phase zone accretes ice crystals, in addition to supercooled water droplets, without adding heat to the hailstone. The collection of ice crystals thus allows the hailstone to grow larger than it would have been able to if all the available accreted mass were liquid (Nelson, 1983).

1.3.3 Storm scale features significantly affecting hail growth

The presence of hail embryos is a basic microphysical criteria required for hail growth in hailstorms. However, storm-scale features have strong influences on hail growth. For maximum growth, the growing hailstone must remain in the HGZ long enough to reach an appreciable size. This can only be realized if the hailstone's terminal velocity is almost balanced by the cloud updraft velocity as the stone grows within the storm (Browning, 1977). If the updraft is too strong, the hailstone is rapidly carried upward through the HGZ and ejected into the storm anvil. If the updraft is too weak, the hailstone will fall from the cloud before it attains an appreciable size. For the formation of severe hailstones with the diameter of 2 cm, maximum updraft velocity greater than $25\,ms^{-1}$ is usually required in the HGZ to support the large hail (Brimelow, 1999). As the residence time of hailstone in storm cloud is determined by the balance between the hailstone's terminal velocity and cloud updraft velocity, apparently, the changing of updraft velocity of evolving storm cloud and the cloud life cycle duration significantly influence the hail growth through affecting the residence time of hail in the HGZ.

The residence time of hail in storm cloud is also affected by the width of the updraft and strength of the horizontal storm relative winds (Nelson, 1983; Miller et al., 1988). A broad band of strong updrafts and light horizontal storm relative winds are beneficial to maximize the residence time of hail and increase the likelihood of severe hail reaching the ground surface.

Another important factor influencing final hail size is the amount of hail melting before the hail reaches the ground. The amount of melting depends on the hail size and its density below the freezing level (Rasmussen and Heymsfield, 1987b). On the one hand, the profile of in-cloud temperature, especially the altitude of freezing level strongly affects hail melting. The amount of melting increases as the height of freezing level increases and the mean temperature below the freezing level rises. On the other hand, fast going through the region below the freezing level to reach ground helps the hail be less melt. Hopefully, longer residence time in the HGZ supported by moderate to strong updraft preferentially balancing the hail terminal velocity and less time in melting layer below freezing level blown by downdraft are favorable conditions to produce large hail on the ground. As a request, providing realistic profiles of in-cloud temperature in addition to those of updraft/downdraft and cloud water mixing ratio is still another key factor for hail growth. Therefore, it is of significance to couple the time-dependent two-cylinder cumulus model with the hail growth model to forecast maximum hail size since the simulations of storm cloud using the time-dependent two-cylinder cumulus model provide physically realistic surrounding conditions for hail growth.

The trajectories most likely to produce large hails are those that entail a single ascent and descent through or around the main updraft (Nelson, 1983; Foote, 1984; Rasmussen and Heymsfield, 1987c; Miller et al., 1988 and Brandes et al., 1995). Recent modeling results also show that large hailstones do not undergo recirculation (Brimelow, 2002). Based on the findings from field experiments and modeling studies, the hail growth within a storm cloud consists of three stages (which we paraphrase from Brimelow, 1999):

(1) Hail embryos form in a broad region of weak to moderate updrafts upwind of the main updraft, where they have sufficient time to reach millimeter sized particles as they are advected towards the updraft core.

(2) When the particles enter the HGZ, they are several millimeters in diameter and have significant terminal velocity (>15 ms^{-1}) preventing them from being prematurely ejected into the anvil. Also, the low precipitation efficiency and entrainment commonly observed in the updraft core ensure liquid water contents close to their adiabatic values within and on the periphery of the main updraft (Bluestein et al., 1988). As a result, the hailstones experience rapid growth as they are advected across the updraft core by the storm relative inflow.

(3) When the terminal velocity of the hailstones exceeds that of the updraft, they begin descending and continue to grow until the onset of melting below the freezing level.

1.4 Statement of proposed research and thesis organization

We plan to couple a time-dependent, two-cylinder cumulus model with a time-dependent hail growth model to forecast maximum hail size on the ground. The proposed research consists of two major parts. Part one involves model coupling and case studies. In part two, the model verification in forecasting maximum hail size against observations and comparisons with other relevant model forecast techniques are investigated. The major issues to be dealt with in this thesis are:

1) Is it feasible to couple a time-dependent two-cylinder cumulus model including precipitation effects with a hail growth model to simulate hail growth and forecast maximum hail size on the ground?
2) What are effects of cloud evolution on hail growth?
3) What are the effects of precipitation on cumulus cloud and hail growth?
4) How accurate is the new model technique in forecasting maximum hail size on the ground against observations collected within the Alberta Hail Project (AHP)?
5) Does the inclusion of precipitation in the model cloud improve the predictive skills of forecasting peak hail size?
6) Is the new model better than previous models used to forecast maximum hail sizes for

Alberta hailstorms?

In conclusion, the method in the thesis is to develop a fast-running time-dependent two-cylinder cumulus model coupled with a hail growth model. It is expected that the coupled model technique should be suitable for investigating hail growth and forecasting maximum hail size on the ground. The final objective is expected to provide an assistant tool in forecasting maximum hail size for operational job.

The thesis is organized in seven chapters. Chapter 1 is the introduction. Chapter 2 provides a description of the model components and the issues involving coupling techniques. In chapter 3, some cases with severe hail and small hail observed in the AHP area are studied in detail. In chapter 4, various sensitivity experiments involving parameters about the cloud and hail are tested. Furthermore, effects of coupling technique on hail growth are investigated. Model investigations for the AHP data during three summers of 1983-1985 are carried out in chapter 5. Verification of the new model performance in forecasting maximum hail size for AHP data and comparisons with other model forecasting techniques HAILCAST and NOMOGRAM are calculated in chapter 6. Conclusions and some suggestions for future work are listed in chapter 7.

Chapter 2 MODEL DESCRIPTION

Our approach to model maximum hail size is to couple a time-dependent two-cylinder cumulus model with a time-dependent hail growth model. This combined model technique is expected to provide useful tools to issue severe weather warnings for large hail in an operational setting. This chapter describes the cumulus model, the hail growth model, and the coupling technique.

2.1 The time-dependent two-cylinder cumulus model

The time-dependent two-cylinder cumulus model used in this thesis has been adapted from the model code used by Yau (1980). The model is similar to that used by Chen (2002, 2004).

2.1.1 Basic equations of the cumulus model

The vertical momentum equation is given by

$$\frac{\partial w}{\partial t} = -\frac{1}{\rho_0}\nabla\cdot(\rho_0 w\vec{u}) + gB - g(q_c + q_r) \tag{2.1}$$

where $B=\frac{\theta_v - \theta_{v0}}{\Theta}$; θ_v virtual potential temperature, θ_{v0} basic state virtual potential temperature (horizontal averaged, basic state P_0, ρ_0, T_0 are hydrostatic), Θ vertically averaged constant potential temperature. q_c and q_r are cloud and rain water mixing ratio. $\vec{u}$ represents the wind velocity. The local tendency of vertical velocity is determined by the buoyancy force, water loading effects and advection/convection terms. In the derivation of the vertical momentum equation, a continuity equation for air based on a horizontally averaged density of environment ρ_0 has been used to filter out sound waves so that only gravity wave type motions will result from the buoyancy force. Here

the buoyancy force is formulated in virtual potential temperature, which has relations with virtual temperature (T_v) and vapor mixing ratio (q_v) in the following form.

$$\theta_v = T_v(\frac{P_{00}}{P})^{R/C_P} = \theta(1+0.6q_v).$$

The thermodynamic equation is given by

$$\frac{\partial\theta}{\partial t} = -\frac{1}{\rho_0}\nabla\cdot(\rho_0\theta\vec{u}) + S \tag{2.2}$$

where S represents diabatic heating/cooling terms due to condensation of water vapor and evaporation of cloud water and rain water. Conservation equations for water substances are given by

$$\frac{\partial}{\partial t}\begin{bmatrix} q_v \\ q_c \\ q_r \end{bmatrix} = -\frac{1}{\rho_0}\nabla\cdot\begin{bmatrix} \rho_0 q_v\vec{u} \\ \rho_0 q_c\vec{u} \\ \rho_0 q_r\vec{u} \end{bmatrix} + \begin{bmatrix} 0 \\ 0 \\ \frac{1}{\rho_0}\frac{\partial(\rho_0 V_r q_r)}{\partial z} \end{bmatrix} + \begin{bmatrix} EVPR + EVPC - COND \\ COND - EVPC - AC - CC \\ AC + CC - EVPR \end{bmatrix} / \rho_0 \tag{2.3}$$

where q_v vapor mixing ratio, q_c the cloud water mixing ratio and q_r is rain water mixing ratio, respectively. V_r is the terminal velocity of rain water which depends on the mixing ratio of rain water. The last terms on the right hand are attributed to vapor condensation, evaporation of cloud and rain water, auto-conversion and accretion of rain, which will be described in part of cloud microphysical parameterization scheme.

The model geometry consists of two concentric cylinders with inner and outer radii denoted by a and b, respectively. The basic equations can be changed for the usage of two-cylinder model. Following Asai (1967), the averaging operators for a variable A are defined using cylindrical coordinates (r, λ) in inner cylinder as

$$(\overline{A})_a = \frac{1}{\pi a^2}\int_0^{2\pi}\int_0^a Ardrd\lambda$$

$$(\tilde{A})_a = \frac{1}{2\pi}\int_0^{2\pi} A d\lambda \quad \text{at} \quad r = a$$

$$(A^*)_a = A - (\overline{A})_a$$

$$(A^{"})_a = A - (\tilde{A})_a$$

where the quantities with overbar (—) and overwave (~) represent averages over the inner cylinder cross-section area and along the boundary circle between inner and outer cylinders. a is inner cylinder radii. λ is azimuth angle in the cylindrical coordinate. The geometrics is shown in Figure 2.5.

Similarly, for the outer cylinder operators are cast as below using r from a to b,

$$(\overline{A})_b = \frac{1}{\pi(b^2 - a^2)}\int_0^{2\pi}\int_a^b A r dr d\lambda$$

$$(\tilde{A})_b = \frac{1}{2\pi}\int_0^{2\pi} A d\lambda \quad \text{at} \quad r = b$$

$$(A^*)_b = A - (\overline{A})_b$$

$$(A^{"})_b = A - (\tilde{A})_b$$

where the quantities with overbar (—) and overwave (~) represent averages over the outer cylinder cross-section area and along the outer boundary circle. b is outer cylinder radii.

Applying these operators to (2.1), (2.2), (2.3), equations for the inner column as cloud updrafts are cast as below.

$$\frac{\partial}{\partial t}\begin{bmatrix} w \\ \theta \\ q_v \\ q_c \\ q_r \end{bmatrix} = -\begin{bmatrix} ED_w \\ ED_\theta \\ ED_v \\ ED_c \\ ED_r \end{bmatrix} - \frac{1}{\rho_0}\frac{\partial}{\partial z}(\rho_0 \begin{bmatrix} ww \\ w\theta \\ wq_v \\ wq_c \\ (w - V_r)q_r \end{bmatrix}) + \begin{bmatrix} gB - g(q_c + q_r) \\ \alpha(COND - EVPC - EVPR) \\ (EVPR + EVPC - COND)/\rho_0 \\ (COND - EVPC - AC - CC)/\rho_0 \\ (AC + CC - EVPR)/\rho_0 \end{bmatrix} \tag{2.4}$$

And a continuity equation connecting the inner and outer cylinders is formulated as

$$ED_w + \frac{\widetilde{w}_{r=a}}{\rho_0}\frac{\partial}{\partial z}(\rho_0 w) = 0 \tag{2.5}$$

where $ED_i = \frac{2}{a}\widetilde{u}\cdot\widetilde{i}$, representing dynamic entrainment. $\alpha = L_v/(C_p\pi_0\rho_0)$ is a coefficient for thermodynamics. L_v: latent heat of evaporation. C_p: specific heat for constant pressure. $\pi_0 = (P_0/P_{00})^{R/C_P}$: the ratio of hydrostatic pressure via standard pressure. It is noticed that the denoted over bar for area averaged variables has been omitted. All quantities are valid for inner cylinder. Subscript a is dropped out. We can see that the local changes for area averaged variables representing the cloud five parameters are controlled by entrainment across inner boundary layer, convection terms, buoyancy force, water loading effects, and complex microphysical processes.

In deriving above equations (2.4) and (2.5), the following major assumptions have been made.

1) No large-scale forcing exists in the two cylinders and no inflow or outflow occurs at the out boundary layer.

2) The variable $\widetilde{i}$ in terms of dynamical entrainment is assumed to have the environment value. That is

$$\widetilde{A}_a = \begin{cases} A_a \cdots if \cdots \widetilde{u} > 0 \\ A_b \cdots if \cdots \widetilde{u} < 0 \end{cases}$$

3) The effects of lateral and vertical eddy fluxes are neglected as first approximation. Therefore all mixing effects are considered using the entrainment through the side of inner cylinder.

2.1.2 Warm precipitating parameterization scheme used in the cumulus model

The formation of cumulus cloud in nature is due to convection in conditionally unstable air. The upward motion lifts a parcel of moist air to reach its saturation and the vapor mixing ratio exceeding the saturated vapor mixing ratio is converted into cloud water causing diabatic heating due to condensation. A bulk-effect microphysical

parameterization scheme for a warm precipitating cloud, first suggested by Kessler (1969), is used. It consists of three categories of water substance: water vapor, cloud water and rain water (Figure 2.1). It is assumed that the cloudy air contains enough condensation nuclei that any vapor in excess of saturation is condensed. Cloud water and rain water are treated by the "bulk" technique, which means that the cloud water shares the motion of wind, whereas the rain water posses a finite terminal velocity relative to the air. The cloud water is depleted by collection of rain (CC) and by auto-conversion (AC). On the other hand, evaporation of cloud and rain water serves as sources for the water vapor in the air. The rain water fall downward with the mass-weighted terminal velocity and the water loading effects attenuate the cloud development dynamically. The rain water that reaches the ground surface eventually reduces the total content of water substances in the cloud. The surface rainfall rate quantifies the intensity of cloud convection to some extent. The evaporation of cloud water ($EVPC$) and rain water ($EVPR$) transform some of liquid water into vapor. As the evaporation of liquid water needs heat absorbed from the cloud, the processes of evaporation then attenuate the development of cloud in thermodynamics through cooling the in-cloud temperature.

Saturation mixing ratio with respect to liquid water can be estimated by

$$q_s = q_s(p,T) = (\frac{3.8}{p})10^{\left[\frac{7.5(T-273)}{(T-36)}\right]} \tag{2.6}$$

where q_s represents the saturation mixing ratio as a function of pressure p and temperature T.

When the moist air is in the state of super-saturation, (i.e. $q_v > q_s$), condensation occurs, and there is zero evaporation.

$$COND = \frac{q_v - q_s}{1 + \frac{L_v^2 q_s}{C_p R_v T^2}} \text{ , and } EVPC = 0,\ EVPR = 0 \tag{2.7}$$

If $q_v < q_s$, evaporation of cloud water occurs and there is zero condensation.

$$COND = 0 \qquad EVPC = \frac{-(q_v - q_s)}{1 + \frac{L_v{}^2 q_s}{C_p R_v T^2}} \tag{2.8}$$

In unsaturated air, rain water also (partially) evaporates but it takes time. Assuming a inversely exponential rain drop size distribution, Kessler's (1969) parameterization results in

$$EVPR = -4.3(q_v - q_s)(\rho_0 q_r)^{\frac{13}{20}} \tag{2.9}$$

The auto-conversion of vapor into cloud water is assumed to be given by

$$AC = AC(q_c, q_c^*) = MAX[0, K_{AC}(q_c - q_c^*)] \tag{2.10}$$

where K_{AC} is the auto-conversion rate with a constant value of $10^{-3} s^{-1}$, $q_c^* = \frac{A_u}{\rho_0}$ is a critical cloud water mixing ratio as the auto-conversion threshold. A_u is taken the value of 1 $\mathrm{g}m^{-3}$. The formula for accretion or collection of cloud water by falling rain is

$$CC = 928 q_c (\rho_0 q_r)^{\frac{7}{8}} (\frac{\rho_{00}}{\rho_0})^{\frac{1}{2}} \tag{2.11}$$

where ρ_{00} is the density at P_{00} (1000 hPa) and assumed to have the value of 1 kgm^{-3}.

Terminal velocity of rain water and rainfall rate at the ground surface are given by

$$V_r = 2864(\rho_0 q_r)^{\frac{1}{8}} (\frac{\rho_{00}}{\rho_0})^{\frac{1}{2}} \tag{2.12}$$

$$RFR_S = V_{rS} \rho_{0S} q_{rS} \tag{2.13}$$

where V_{rS}, ρ_{0S}, q_{rS} are the fall speed of rain water, basic state air density and rain water mixing ratio at surface, respectively. Multiply RFR_S with 3600 seconds, the

rainfall rate is then converted into millimeters per hour (mmh^{-1}). For more information about the warm rain parameterization see some chapters of Emanuel (1994).

2.1.3 Numerical methods for the cumulus model

The set of nonlinear partial differential equations is solved numerically by a finite difference scheme. To minimize truncation errors and to express the continuity equation in a more natural manner, a staggered grid system is used. Velocity fields are defined on the edges of grid box and all other variables are solved at the center of grid box (Figure 2.2). The equations involving vertical advections are written in conservation form. The solution is obtained by the modified upstream method (Soong and Ogura, 1973; Yau, 1980). This method is chosen to avoid unphysical negative values at a grid point.

The time staggering scheme is used. The velocity fields are calculated at half time steps and the resulting values are then used to compute the various quantities from time step n to $n+1$. Similarly, to calculate velocities at time step $n+\frac{1}{2}$ given at $n-\frac{1}{2}$, other variable values at time step n are used. Figure 2.3 shows the scheme of time staggering.

For boundary conditions, the vertical boundaries are rigid and free-slip, i.e., $w_a = w_b = 0$ at $z = 0$ and $z = H$. Also, the vertical gradient of all thermo dynamical variables and the mixing ratios at the top and bottom boundaries remain zero. The lateral boundary of outer annulus is closed while the inner lateral boundary between inner and outer columns is open for mixing caused by entrainment. A small perturbation near the cloud base level provides a trigger to start the convection tapping latent energy from a convectively unstable sounding.

In summary, the time-dependent two-cylinder cumulus model is composed of two concentric cylinders. An updraft prevails in the inner cylinder while a compensating downdraft fills the outer annulus. Complex interactions between dynamics, thermodynamics and microphysics are taken into account. This cumulus model captures

quite realistically the gross features of a cumulus life cycle consisting of evolving updraft-downdraft couplet. It allows modeling the evolutionary of precipitation and changing water loading effects. The model provides a time-height conditions for storm updraft, water vapor, in-cloud temperature, cloud water mixing ratio, and rain water mixing ratio etc, which then will be used as input for the hail growth model.

2.2 The time-dependent hail growth model

The time-dependent hail growth model is that used in HAILCAST by Brimelow (2002, 2005). The time evolution of hail is modeled along the hailstone's trajectory from its embryonic stage at cloud base to cloud top and then falling down to the ground. The governing equations are based on the conservation of water mass and energy, and include effects of accretion, dry growth, wet growth, melting, and shedding of excess liquid water.

The input data for the hail growth model are the values of vertical velocity, in-cloud temperature, mixing ratio of cloud water, and of rain water along the hailstone's trajectory. The amount of cloud ice is determined using the relation proposed by Vali and Stansbury (1965), which depletes the cloud water exponentially from near-adiabatic values at – 20°C to zero at – 40°C.

A spherical hail embryo is placed in the inner cylinder. We assume that the hail stone remains spherical and that its density remains uniform having a value of 0.9 gcm^{-3} (solid ice). The storm updraft supports or holds the growing hailstone which accretes supercooled cloud water droplets, rain water and ice crystals. The rate of accretion is determined by the mass and heat budgets of the hailstone, which depend on the hailstone's size and the in-cloud conditions, such as updraft velocity, temperature, and water substance mixing ratio. Also, depending on the heat transfer to and from the hailstone, the hail enters wet or dry growth regime. In the wet growth regime, excess water is shed if the mass of liquid water present on the hailstone's surface exceeds a critical limit determined using the empirically derived linear relationship of Rasmussen

and Heymsfield (1987a). In the dry growth regime, all accreted liquid water is frozen onto the hailstone's surface while some of the accreted ice is bumped away from the stone. Below the freezing level the ambient temperature is much warmer than that of hailstone. Therefore, the stone is usually melting and no more growth occurs within the region. The size (mass) of hailstone continues to change until it reaches the earth surface. However, the hailstone's temperature remains zero after the stone enters a region below freezing level. A detailed description of the hail growth model is given by Brimelow (1999).

Mass growth equations:

For a spherical hail, the rate of its mass change is attributed to the accretion of supercooled water droplets, rain water and ice crystals in ambience.

$$\frac{dM}{dt} = \frac{dM_w}{dt} + \frac{dM_i}{dt} = \frac{V_t \pi D^2}{4}[\chi_{cw} E_{cw} + \chi_{rw} E_{rw} + \chi_i E_i] \tag{2.14}$$

$$M = M_w + M_i = \frac{4\pi (D/2)^3}{3}\rho_h = \frac{\pi D^3}{6} 0.9$$

where M_w and M_i represent the mass of accreted liquid water and ice per unit time interval, respectively. V_t is the terminal velocity of hailstone with diameter of D. $\chi_{cw}, \chi_{rw}, \chi_i$ are concentrations of cloud water, rain water and ice in the unit of gcm^{-3}, which are approximately taken as the values of mixing ratios deprived from the cumulus model output. E_{cw}, E_{rw}, E_i are the collection efficiencies of the accreted cloud water droplets, rain drops and ice crystals. The relation $V_t \pi D^2 / 4$ represents the volume of a cylinder swept out per unit time interval by the hailstone.

Collection efficiencies of accreted water are assumed as $E_{cw} = 1.0$ (accreted cloud water) during wet or dry growth, while $E_{rw} = 0.1$ for accreted rain water. The collection efficiency for rain water is assumed much smaller because averaged rain drop size (2000 μm) is much bigger than that of cloud water droplet (20 μm), about one hundred times. Collection efficiency of ice crystal is set to $E_i = 1.0$ during wet growth

and $E_i = 0.21$ during dry growth. These values are motivated by Geresdi (1998) for the collection efficiency between hail and rimed ice particles. The increase in mass due to deposition is neglected as for particles larger than 100 μm the increase in mass due to accretion of supercooled water and ice crystals is much greater than that due to deposition (Dennis and Musil, 1973).

Heat balance equations:

The total heat exchange (Q_T) per unit time interval between the hailstone and its environment is given by

$$\frac{dQ_T}{dt} = \frac{dQ_K}{dt} + \frac{dQ_S}{dt} + \frac{dQ_W}{dt} + \frac{dQ_I}{dt} \tag{2.15}$$

The first term is convection and conduction of heat (Q_K) determined by

$$\frac{dQ_K}{dt} = 2\pi DcK(T_c - T_s) \tag{2.16}$$

where D is hail diameter, c denotes the ventilation coefficient, K is the thermal conductivity, and T_c and T_s are the ambient in-cloud temperature and the hailstone's surface temperature respectively. If $T_c > T_s$, conduction increases the hail temperature. Conversely, heat is transported from hail to the environment by conduction.

The heat exchange due to sublimation and evaporation is modeled by

$$\frac{dQ_S}{dt} = \begin{cases} -2\pi dcL_v D\Delta\rho \ldots\ldots\ldots for T_s \geq 0^0 C \\ -2\pi dcL_s D\Delta\rho \ldots\ldots\ldots for T_s < 0^0 C \end{cases} \tag{2.17}$$

where L_v latent heat of vaporization and L_s latent heat of sublimation, d diffusivity ($cm^2 s^{-1}$), $\Delta\rho = \rho_e - \rho_s$ the difference in vapor density between the hailstone surface (ρ_s) and the environment air (ρ_e).

The heat due to the freezing of accreted water is given by

$$\frac{dQ_W}{dt} = \frac{dM_w}{dt}\left[L_f - C_w(T_s - T_c)\right] \tag{2.18}$$

where L_f is the latent heat of freezing at 0°C, C_w specific heat of water and T_c in-cloud temperature. Apparently, high mixing ratio of water imposes strong influences on the heat budget as accreted liquid water per unit time interval is proportion to water mixing ratio.

The loss of heat due to the accretion of cloud ice is given by

$$\frac{dQ_I}{dt} = \frac{dM_i}{dt} C_i(T_c - T_s) \tag{2.19}$$

where C_i is the specific heat of ice.

Fraction of water (F_W) on the hail is described as follows.

During wet growth, the hailstone surface temperature T_s remains at 0°C. The time change of F_W is given by

$$\frac{dF_W}{dt} = -\frac{F_W}{M}\frac{dM}{dt} + \frac{1}{ML_f}\left[\frac{dQ_T}{dt}\right] \tag{2.20}$$

During dry growth $F_W = 0$, the change for surface temperature is given.

$$\frac{dT_s}{dt} = -\frac{T_s}{M}\left[\frac{dM}{dt}\right] + \frac{1}{MC_i}\left[\frac{dQ_T}{dt}\right] \tag{2.21}$$

Shedding scheme:

Assume a given ice core mass (M_i) of hail, the criteria mass M_{crit} for shedding is given after Brimelow (1999, 2002).

$$M_{crit} = 0.268 + 0.1389M_i \tag{2.22}$$

If the amount of water on the hail, determined from the product of $M \times F_W$, exceeds M_{crit}, the excess water ($MF_W - M_{crit}$) is shed away from the hail. Shedding happens only during wet growth.

Terminal velocity:

The terminal velocity is derived from the balance of dragging force and hail gravity force.

$$V_t^2 = \frac{4g\rho_h}{3C_d\rho_a}D$$

$$V_t = V_t(D) = V_t(M) \tag{2.23}$$

C_d is drag coefficient. Obviously, the terminal velocity is proportion to hail diameter and the hail density.

Kinetic energy of hailstone:

$$KE = \frac{1}{2}MV_t^2 = \frac{1}{2}(\rho_h\frac{\pi D^3}{6})(\frac{4g\rho_h}{3C_d\rho_a}D) = \frac{\pi g\rho_h^2}{9C_d\rho_a}D^4 \tag{2.24}$$

Position of hail:

$$Z = Z_{init} + (w - V_t)t \tag{2.25}$$

Z_{init} is initial height of hail embryo above ground level (AGL). w is vertical velocity deprived from cumulus model.

2.3 Coupling the cumulus model and the hail growth model

The numerical approach for modeling the maximum hail size is to couple the time-dependent cumulus model with the time-dependent hail growth model. An observed or prognostic sounding is planned to be used as input to initialize the cumulus model. The cumulus model outputs provide the conditions of storm cloud as the functions of time and height. The profiles of the cloud parameters are simulated at each time step of 5 seconds in the cumulus model. The hail growth model uses the time-dependent cumulus parameters as input to simulate a time series of hail size, hail temperature, and fraction of liquid water on the hail.

As the time step for hail growth is much shorter (0.1 seconds) than that for cumulus, a hail grows in a cloud with unchanged conditions for a time period of cumulus model time step (5 seconds). The hailstone is transported to a height determined by the difference of hailstone's terminal velocity and vertical velocity (updraft/downdraft). As the hail could be advected to any level in the cloud, the surrounding conditions at this height are spatially interpolated based on the values from two neighboring grid points in the cumulus model. The distance step for discrete grid points in the cumulus model is taken as Δz (100 meters) depicted in Figure 2.2.

The residence time of the hailstone in the air is a major factor controlling the hailstone size. It is determined by the hail size and the intensity of vertical velocity in storm cloud and the cloud life time. Longer residence time in the HGZ and short residence time in the melting region below the freezing level are optimum for large hail occurrence. The profile and time evolution of cloud updraft significantly influence the hail growth as they affect hail residence time in the HGZ and the time leaving the melting level. The time integration for the hail growth is terminated when the hailstone reaches the ground. The coupling procedure is one way nesting. All the computations are confined in the unit system of centimeter (cm), gram (g) and second (s). Figure 2.4 and 2.5 show the procedures and schematic diagram for the coupling techniques.

Chapter 3 CASE STUDIES

In this chapter, two cases will be studied using the cumulus model coupled with hail growth model. One case is a severe hail day observed in central Alberta on 11 July 1985. The other one is a case with small hail on 24 August 1983. For both cases, the upper air soundings released at 1715 local day time (LDT) from Penhold within the Alberta Hail Project (AHP) area were used as input to initialize the model running. Valid hail size data were observed within the area of 100 km around Penhold and within three hours of sounding release time. These criteria had been used before by many other researchers (Bremilow, 2002; Poolman, 1990). The model provides the evolution of cumulus cloud parameters involving updraft velocity, liquid water mixing ratio and in-cloud temperature. Time history of hail growth is simulated in detail. The maximum hail sizes for the cases are numerically 'forecasted' eventually. We also compare the new model simulation with those from HAILCAST for these two cases.

The main objective for this chapter is to examine whether it is feasible to couple the time-dependent two-cylinder cumulus model with the time-dependent hail growth model to simulate the hail growth and forecast maximum hail size. Furthermore, we will investigate whether the new time-dependent cumulus model approach is more realistic than the steady-state cumulus model approach used in HAILCAST.

3.1 Synoptic setting for 11 July 1985 and 24 August 1983 cases

On 11 July 1985 around 1600 LDT, several severe thunderstorms developed over the foothills north of Rocky Mountain House and began moving eastward onto the prairies (Figure 3.1a). The most intense radar reflectivity was 60 dBZ (Figure 3.1b). A total of 228 hail reports that were observed within the area with about 100 km distance around Penhold were received. There were eight separate reports of maximum hail size being that of golf-balls, approximately 4 cm in diameter.

Figure 3.2 shows the tephigram of the balloon sounding released from Penhold at 1715 LDT. The surface-based CAPE was $756\,Jkg^{-1}$. A stable layer with sudden reduced lapse rate was present at about 770 mb acting as a capping lid for accumulating convective potential energy near the ground. The large CAPE value suggested the potential for a strong convection once the capping lid was eroded and the convective instability would be released.

Smith and Yau (1993) conducted a detailed investigation of the outbreak of the convection for this case in terms of synoptic analysis. The favorable synoptic airflow and the large convective instability caused a hailstorm. The upslope warm moist low level air and cooling aloft with an approaching trough coincided with large amount of latent and sensible energy. This combination initiated and sustained vigorous convection by removing the capping lid present in the PBL with the trigger mechanism of upcoming aloft trough.

Brimelow (2002a) used HAILCAST to model the maximum hail size for this day. We will use the newly developed time-dependent two-cylinder cumulus model coupled with hail growth model to investigate the case for the aspects of convection and maximum hail size.

We thought that it would be instructive to examine how the new model technique would model a weak hailstorm. Therefore, we selected the second case of 24 August 1983, which had only small hail stones. Brimelow (1999) described this case in more detail. A multicell storm developed on the afternoon of 24 August 1983 along the foothills, west of Penhold. The cells moved eastward. Only ten hail reports were recorded in the Albert Hail Project area. The largest observed hail size was pea-sized hailstones with diameter (0.4~1.3 cm). Brimelow (1999) did synoptic analysis on the case of August 24 1983. He found that there was no significant upper-air trough presenting upstream of central Alberta. The wind on 500 mb was weak. In combination of 500-1000 mb thickness it hardly caused temperature advection onto central Alberta. Light north-

westerly winds also dominated the surface circulation, which was not helpful to transport warm moist air sourced from east in the low levels.

Figure 3.3 shows the sounding released from Penhold at 1715 LDT 24 August 1983. The atmosphere had a deep layer of convectively unstable air with big CAPE of $1060\,Jkg^{-1}$. The surface temperature was relative high with 22°C and surface dewpoint was 11°C. A capping lid existed at 615 mb. Despite the big amount of CAPE, the storm was rather short-lived as the storm environment lacked wind shear and low level moisture transport.

3.2 Model simulation of the 11 July 1985 hailstorm

The time-dependent two-cylinder cumulus model coupled with the hail growth model is used to simulate the storm cloud and hail growth. Figure 3.4 shows the time-height pattern of storm updraft, cloud water mixing ratio, and rain water mixing ratio. The storm cloud reaches a top height of about 8.5 km above ground level (AGL) with a lifetime of about 50 minutes. The strongest updraft speed reaches over 30 ms^{-1} at height of about 6 km AGL. The model storm showed cloud water mixing ratio values are slightly above $2\,gkg^{-1}$ between 4 and 6.5 km AGL and last for about 25 minutes (Fig 3.4b). The initiation of rain water mixing ratio occurred near the cloud top and gradually subsides to lower levels (Fig. 3.4c). The basic characteristic life cycle of model storm was similar to observed storm evolution (Fig. 3.1) and the model simulations of Yau (1980) and Chen (2002).

After 25 minutes of the cumulus model integration, the cloud top had reached a height over 5 km AGL. At this time a hail embryo with diameter of 0.03 cm was introduced at the cloud base of 2.3 km AGL. The time-dependent hail growth model then was run using parameters derived from the cumulus model as input. The changing parameters of cloud with time and height provided surrounding conditions for the hail growth. Figure 3.5 shows the profiles of storm cloud parameters used for the hail growth

at different times after the hail embryo is introduced at the cloud base. Considering complex microphysical processes involving mass change, heat budget, melting and shedding in the storm cloud conditions, the hail growth is simulated.

Figure 3.6 depicts the modeled hail growth history for the case of 11 July 1985. The hailstone takes 29 minutes to grow from its embryonic stage at cloud base to cloud top and then falling down to the ground, reaching a final size of 4.6 cm in diameter (i.e. golf-ball size). The hailstone growth regimes include dry growth, wet growth, melting, and shedding of excess water (Figure 3.6b). During the first 2 minutes the hail embryo experiences wet growth. Then it enters the dry growth regime. The hailstone is lifted close to the cloud top at about 9 minutes (Figure 3.6c). During this lift the hailstone's diameter stays below 0.5 cm (Figure 3.6a). After 10 minutes, the hailstone descends to the ground surface (Figure 3.6c). Within the Hail Growth Zone (HGZ) the hailstone grows rapidly by collecting the cloud water and ice. After 20 minutes the hail continues growing collecting cloud water (wet growth) and begins to shed excess water on the hailstone (Figure 3.6b). Due to the surrounding temperature increasing with the height decreasing and heats added to the hail by collected liquid water, the fraction of liquid water on the stone accumulates increasingly. At 27 minutes the hailstone reaches its peak size with a diameter of 5.5 cm at the height of about 3 km AGL, while the fraction of water on the hail is about 40%. When the hailstone falls beneath cloud base, the collection of cloud water ceases (Figure 3.6b). Shedding of liquid water reduces its size. As the hail stone falls below the cloud base, melting occurs. The final diameter is 4.6 cm and fraction of liquid water is 10%. Figure 3.6d shows the time evolution of the modeled hailstone's terminal velocity and its kinetic energy (KE). Within first 15 minutes the KE is quite small due to its small diameter (light mass). After 15 minutes, the KE increases rapidly. The final KE is about $17\,J$.

3.3 Model simulation of the 24 August 1983 hailstorm

Figure 3.7 shows the time-height pattern of storm updraft, cloud water mixing ratio and rain water mixing ratio for the 24 August 1983 case. The storm updraft reaches

its peak of about 20 ms^{-1} at about 20 minutes on the height of 3.2 km. The height of cloud top increases gradually, reaching its maximum height of about 9.7 km AGL at 70 min. Thereafter the cloud collapses within a few minutes. In contrast, the cloud of 11 July 1985 seemed like steady state before its dissipation. The cloud base almost doesn't change with time. On average, the updraft at the cloud base is about $5\,ms^{-1}$. As a result, the modeled storm cloud for the case of 24 August 1983 displays moderate updraft without long life duration.

The cloud water mixing ratio is mainly distributed in low levels and during early period of cloud life (Fig.3.7b). The middle and upper levels of the cloud have cloud water transforming into precipitation. The core of rain mixing ratio is not very high just on the height of 3.9 km AGL at 30 minutes (Fig. 3.7c). The maximum rain water mixing ratio is about $8\,gkg^{-1}$ and its location is descending gradually with time.

Figure 3.8 shows the hail growth history simulated for 24 August 1983. A hail embryo with diameter of 0.03 cm is introduced at the cloud base of 1384 m AGL after 25 minutes of cloud integration. It takes 22 minutes to be 1.1 cm on the ground surface (Fig. 3.8a). The hail spends 10 minutes to reach the level of 5.5 km AGL (Fig. 3.8b) and doesn't reside on this level for a short period of time but falls down to the earth's surface within 12 minutes. The hailstone is transported upward but never reaches the cloud top. Figure 3.9 shows the profiles of updraft, cloud water and rain water mixing ratio at specific time steps after hail model is executed. The updraft and cloud water, which together mostly affect the hail growth, are weaken with time

The hail experiences various growth regimes. Figure 3.8b shows that the hail grows first in wet regime and then in dry regime while it is going upward within first 10 minutes. After the hail begins to fall down toward to the ground, it is melting but without shedding between 10 to 12 minutes before a very short dry regime period. The reason is that at 10 min the hail diameter is only 0.5 cm. As the hail descends, the surrounding air temperature increases with low water mixing ratio conditions. After 13 min the hail

begins to melt. At 19 minute liquid water on the hail reaches 89%, and the hail is at its biggest stage with diameter of 2.5 cm. Excess water is shedding away from the hail, which results in a sudden reduction of hail size from 2.5 cm to 1.4 cm. At this time the hail is already below the cloud base, it doesn't grow except melting before landing on the surface. The final hail size is 1.1 cm with a vast fraction of liquid water as 50%. Figure 3.8d shows the hail terminal velocity and kinetic energy. Obviously, due to small hail size the KE is quite small all the time.

Table 3.1 lists main parameters based on observations and simulations for the two cases. We can see that aspects concerning cloud and hail are compared one by one. The simulated maximum updraft for 11 July 1985 is larger than that for 24 August 1983 although the CAPE deprived from sounding is relative smaller. In addition, the simulated hail cloud of 11 July lasts longer than the hail cloud of 24 August (60 min versus 35 min). As a result, the simulated maximum hail sizes are different. Figure 3.10 compares the hail growth. The smaller hail of 24 August had an apparent lower trajectory (Fig. 3.10c).

3.4 Comparisons with HAILCAST simulations

It is interesting to compare the model clouds and hail growth using the time-dependent two-cylinder cumulus model with the model results based on the steady-sate cloud model in HAILCAST. Does the time-dependent precipitating coupled model technique offer an improvement in 'forecasting' maximum hail size for the two cases compared with HAILCAST involving steady-state cloud and without precipitation effects? This section will deal with this issue.

Figure 3.11 shows the profiles of model cloud deprived from HAILCAST. As the cloud model used in HAILCAST is steady-state, the profiles of cloud parameter involving updraft and liquid water content (LWC) do not change with time. The updraft profiles for the two cases in HAILCAST are similar to those at maximum stage in the time-dependent coupled cumulus-hail model technique with precipitation (thereafter refer

to P) compared with Figure 3.5a and Figure 3.9a. The major shortcoming of the steady-state assumption of HAILCAST (thereafter refer to H) is that additional information is needed about the cloud life duration because this duration greatly impacts the hail growth.

In addition, the cloud water contents deprived from H and P have significant differences. The liquid water content (LWC) in H for two cases are bigger, and especially the maximum LWC presents at much higher level compared with P. The reason for the simulated different amount of cloud water is due to the simulated formation of precipitation in P, as precipitation falls out and collects cloud water.

Figure 3.12 compares the hail growth history for two cases using HAILCAST. For the large hail case (11 July), the simulated final hail size is 4.8 cm with growth time of 62 minutes (Figure 3.12a). For the small hail case (24 August), the simulated final hail size is 1.4 cm with growth time of 24 minutes. Compared with those simulated using P, the hail size, terminal velocity and kinetic energy match well among two model approaches H and P. However, the growth time and trajectory for the large hail case of 11 July are very different. The hail takes 62 minutes to grow in H but only 29 minutes (Figure 3.6c) in P. The reason is due to a long time residing on the cloud top (Figure 3.12c) for the hail growth in H. Furthermore, according to the method used for estimating the cloud life duration in H, the model cloud life in H for 11 July is assumed as one hour. In contrary, the hail growth time of 62 minutes is longer than the cloud life duration. This means that after the cloud has vanished the hail is reaching to the ground. Steady-state assumption for the cloud in H should be responsible for this anomaly. For the small hail case of 24 August, the hail growth in H and P is fairly similar, except of fraction of liquid water. The growth regimes in H and P display a little bit different histories with different quantities of final fraction water 29% for H, 49% for P (Figure 12b and Figure 3.10b).

Table 3.2 compares the main parameters of cloud and hail growth for the simulations H and simulations P for the two case study days of 11 July and 24 August. On the aspects of modeled cloud, the time-dependent precipitating coupled model

technique P and operationally used model H (steady-state cloud) both can simulate basic features of storm clouds for two cases, not only severe convection but also moderate convection. However, maximum values of updraft and water content in the model cloud are higher in simulation P than in simulation H. With respect to simulated hail growth, the results display significant differences. Although P produces stronger convection, the simulated final hail sizes in P are smaller than those in model simulations H. In addition, the hail growth time in P is shorter than that in H, particularly for the large hail day of 11 July 1985.

3.5 Summary and conclusions

Based on two case study days we conclude that the new model coupling a time-dependent cumulus model with a hail growth model can be used to simulate the cloud growth and hail growth. Furthermore, the new model incorporates the cloud life cycle and includes precipitation.

It is feasible to couple the precipitating cumulus model with the hail growth model to successfully forecast maximum hail size on selected cases involving large and small hails. Secondly, the computing time is very short, promising this model approach (P) suitable for operational use in assisting hail forecasts. Furthermore, the coupled cumulus-hail model realistically simulated the hail growth for two cases observed in central Alberta. It shows robust performance on the case studies compared with operationally used model technique, HAILCAST.

Admittedly, for future real application in operational work, it needs a variety of experiments to test the model sensitivity for changes of various conditions in order to find a set of optimum configurations. Also, there is a need to verify the model performance against observations with a wide range of hail size based on a vast amount of samples. Moreover, comparisons with other operational used methods in forecasting skills on samples will provide objective evaluations for the coupled model technique.

Chapter 4 SENSITIVITY EXPERIMENTS

4.1 Introduction

Sensitivity experiments with the coupled cumulus model-hail growth model are important to quantify the relationship between input variables and model parameters. In this chapter, sensitivity experiments are carried out based on the two case studies of 11 July 1985 and 24 August 1983. The focus is on the sensitivity of the model-derived cloud profiles of storm updraft, cloud water and rain water, and hail growth to changes in selected cloud and hail microphysical parameters. The main variables of interest for the simulated cloud and forecasted hail are maximum updraft velocity ($W_{\max}$), temperature ($T_{W\max}$) at the altitude of$W_{\max}$, cloud top height (Z_{top}), maximum cloud water and rain water ($Q_{c\max}, Q_{r\max}$), and cloud life duration (τ_C). Parameters related to hail growth are also discussed, which include hail diameter on the ground (D_f), the time when hail reaches the ground (τ_f), as well as fraction of water (F_W) and kinetic energy (KE) of hail.

The first experiment is to investigate precipitation effects on the model cumulus cloud and hail growth by using alternatively a no-precipitating cumulus model and a precipitating cumulus model. Next, control experiments are conducted on different conditions. The sensitivity of model cloud to the ratio between inner and outer cylinder radius is examined, as these radii determine the cloud structure. Moreover, the sensitivity of hail growth to microphysical parameters is tested, which involves effects of initial size of hail embryo and initial height of hail embryo on final hail size. As the present numerical algorithm to forecast maximum hail size is a coupled model method, finding the coupling technique affecting forecast hail growth is investigated. For example, the effects of introduction time of hail embryo into the model cloud on hail growth and influence of time interval of unchanged cloud parameters to the hail growth.

4.2 Sensitivity experiments on involving precipitation effects

Precipitation effects are tested first, as precipitation affects the model cloud in dynamics and thermodynamics through the water loading effects and partial evaporation of rain water. Additionally, these effects affect the hail growth causing different maximum hail sizes on the ground.

Figure 4.1 shows the model-derived vertical velocity and cloud water mixing ratio for the conditions of switched-off precipitation effects in the time-dependent two-cylinder cumulus model for the 11 July case. Comparing with Figure 3.4 derived from the time-dependent coupled cumulus model technique with precipitation (P), the time-dependent coupled cumulus-hail model without precipitation (hereafter refer to F) shows quite different behaviors. In Figure 4.1a the updraft prevails all the time, but no downdraft exists during the whole integration of the model cloud. The maximum updraft is slightly weaker (just about $30\,ms^{-1}$) but the depth of convection is similar to that of P. Model F has larger water mixing ratio with a maximum amount of $6\,gkg^{-1}$ than model P. The non-precipitating model cloud gradually increases in intensity with height with an abrupt decrease near cloud top, whereas the precipitating cloud has a smoother profile. The strong updraft (>25m/s) in F sustains about 40 min, while the same updraft magnitude in P lasts about 35 min. Simulation F has no downdraft in the inner cylinder during the whole integration. The non-precipitating cloud has a longer life time, higher cloud water mixing ratios, slightly weaker storm updraft and no storm downdraft. This is consistent with similar findings by Yau (1980) and Haines (1994) as the formation and fall-out of precipitation shorten the cumulus cloud life time.

The hail growth for non-precipitating cloud (simulation F) is depicted in Figure 4.2. The final hail diameter (D_f) in F is 5.1 cm, which larger than the final hail size of 4.6 cm for the precipitating cloud in simulation P (Fig. 3.6a). This forecasted hail diameter of 5.1 cm is still consistent with observations in terms of hail category as a large hail between 3.3 and 5.3 cm. The hailstone has spent about 30 minutes (τ_f) from the

cloud base going upward to the cloud top and then falling down to the earth's surface with the same final fraction of water (FW_f) in P and a little bigger final kinetic energy (KE_f).

Figure 4.3 shows the time-height pattern of the model run F for the non-precipitating cloud simulated with the 24 August 1983 case sounding. The non-precipitating model cloud has a cloud top of 7.0 km AGL. The maximum updraft velocity occurs at 23 min at the height of 4 km AGL. The stronger updraft core with velocity larger than $15\,ms^{-1}$ lasts about 40 min from 18 to 58 min within a relatively deep layer stretching from 2.1 to 4.5 km. The simulated storm cloud shows no downdraft (Fig. 4.3a). Cloud water mixing ratio hardly changes with time for a fixed height (Fig. 4.3b). The vertical gradient of cloud water mixing ratio just below the cloud top is quite large. Comparison of the non-precipitating cloud F (Fig. 4.3) with the precipitating cloud P (Fig. 3.7) indicates that the presence of precipitation causes an inner-cylinder storm downdraft.

Figure 4.4 depicts the hail growth history for the non-precipitating cloud F for 24 August. The final hail size (D_f) on the surface is much larger with diameter of 2.5 cm (Figure 4.4a) than that (1.1 cm) of P in Figure 3.8a. The simulated hail size based on the non-precipitating cloud F over-forecasted hail size for 24 August 1983. The hail growth time (τ_f) for simulations F and P are similar (22 minutes). The hail trajectory reaches much higher level in F. This results in a larger final hail size on the ground. The final fraction of water (FW_f) in F is smaller (15% in Figure 4.4b) compared to P (Fig. 3.8).

Our sensitivity experiments F with non-precipitating clouds suggest that the precipitation effects on hail growth are dramatic for the small hail case of 24 August (Table 4.1).

In summary, we find that after precipitation is switched off from the cumulus model, the simulated clouds indicate different features. Downdraft does not exist, cloud water mixing ratio rises much bigger. Updraft is elongated in terms of time duration but the intensity of updraft is relatively decreased in no-rain storm clouds. Consequently, the changed cloud parameters due to no consideration of precipitation must have affected the hail growth. Within a no-rain storm cloud, a hail needs a longer time to grow, and the final hail size typically is larger than that simulated using rain model technique P. Furthermore, precipitation sensitivity experiment for case of 24 August 1983 with small hail suggested that precipitation exerts much stronger impacts on hail growth in moderate cloud than in severe clouds. The precipitation switched-off model technique F tends to over forecast hail size after comparison with observations.

In comparison of no-rain cloud parameters in F with those from steady-state model HAILCAST, we can find that the time-dependent no-rain storm clouds have tendency to close to situations in H. The maximum updraft, cloud water content, and cloud top are very close to each other comparing Figure 4.1 and Figure 4.3 with Figure 3.11. On the aspects of hail growth, the final hail size is slightly bigger in F than H. The hail growth time is apparently shorter in the time-dependent cloud even without rain effects than in H. This still looks realistic due to consideration of time-dependent cumulus model in F. Therefore, it is very important to apply the time-dependent precipitating cumulus model coupled the hail growth model for simulating and forecasting maximum hail size.

The time-dependent two-cylinder cumulus model with precipitation captures gross features of storm clouds involving updraft-downdraft couplet and changing water loading effects. It provides quite realistic surrounding parameters for hail growth. Coupling the cumulus model with the hail growth model, the coupled technique P, supplies a promised tool to numerically forecast maximum hail size.

4.3 Sensitivity experiments for storm diameter

The geometric structure of the time-dependent cumulus model consists of two concentric cylinders. The inner cylinder essentially contains the storm cloud, whereas the outer cylinder contains the relatively quiescent environment. The inner cylinder with radius a represents the storm updraft while compensatory subsiding motion occurs in outer cylinder with radius b. Sensitivity experiments about a and b have been carried out to examine the geometrical factor influences on intensity and duration of cumulus cloud. It is found that, in general, when the ratio a/b becomes smaller, the simulated storm clouds become stronger in terms of updraft and cloud water mixing ratio. Furthermore, there exists a threshold for the ratio to produce convective clouds sensible for the hail growth, say that modeled cloud top should be higher than 5 km AGL with supportive updraft velocity >10 ms^{-1}. For the two case studies (11 July 1985 and 24 August 1983) the ratio a/b is required to be smaller than 0.3. This means that an updraft prevailing throughout the depth of inner cylinder column needs a vast compensatory subsiding motion in the immediate surrounding. Considering typical cumulus scale and in purpose to simulate maximum hail size, we assume the ratio as 0.1 for the inner cylinder with radius of 1.5 km. Due to assumption that the outer cylinder is closed, noted in chapter 2, there is no exchange with environment atmosphere across outer boundary layer. So there are no sources of heat and moisture from outside for the cumulus development. The only energy is derived within two cylinders. Hopefully, an assurance domain for hail growth is to assume a relatively broad outer cylinder for cumulus cloud production. Based on typical cumulus scales, an outer cylinder domain is set up with the radius of 15 km.

4.4. Sensitivity experiments for different hail embryo sizes

The next series of sensitivity experiments examines the effects of different initial hail embryo sizes. Table 4.2 compares five model experiments labeled D1 to D5. These experiments differ in terms of initial hail embryo diameters (D_i) that were introduced at the model cloud base (Z_0) at 25 minutes of cloud integration in P for cases 11 July 1985 and 24 August 1983. The final hail size (D_f) on the ground and correspondent hail

growth time (τ_f) are listed. For the 11 July case we find the following: As the initial hail size D_i increases, so does the final hail size D_f. However, the hail growth time τ_f becomes slightly shorter with increasing initial hail embryo size. Otherwise, the changes are rather small. Although the initial hail sizes increase 30 times from 0.01 to 0.3 cm, the final hail sizes on the ground are still close to one another. All the modeled final hail sizes initialized from different embryo sizes are well consistent with observations as large hailstones. These results are agreed well with those findings of English (1973) and Brimelow (2002a). They found that a wide range of hail embryo sizes could produce similar hail size. Figure 4.5 shows the hail growth history for different hail embryo sizes for the case of 11 July. The final hail sizes are quite similar (Fig. 4.5a) with almost the same final fraction of liquid water. Smaller initial hail embryos have longer trajectories.

Sensitivity experiments for the small hail case of 24 August confirm that initial hail embryo sizes have relatively little effect on final hail sizes. The final hail size decreases slightly with increase of initial hail embryo size, while the hail growth time is similar (Table 4.2). Figure 4.6 shows the hail growth time history for embryo sensitivity experiments for 24 August. The experiment D1 displays that a hail embryo with diameter of 0.01 cm is ejected from the cloud at 8 min and does not reach the ground surface. The other obvious feature is that the moderate updrafts to blow a larger hail embryo into higher altitude. So in Figure 4.6c, with the increase of embryo the height the embryo can reach decreases from D1 to D5. Simultaneously, the final fraction of water is becoming much bigger from 0 in D1 to 100% in D5 in Figure 4.6b.

4.5 Sensitivity experiments for different heights of initial hail embryos

The sensitivity of final hail size to initial height of hail embryo is examined by comparing model experiments H0 through H4 (Table 4.2.). Z_i represents the initial height above cloud base of hail embryo with size of 0.03 cm. The final hail size (D_f) on the ground and hail growth time (τ_f) are simulated for two cases using P.

For the 11 July 1985 case, the final hail size D_f on the ground reduces from 4.6 in H0 to 2.7 cm in H4 as the initial height (Z_i) of embryo increases from 0 to 2000 m above cloud base. The hail growth time τ_f increases from 29 to 47 minutes. These model findings seem reasonable because in the model cloud a hail embryo lifted from a higher initial position spends less time in reaching to the cloud top. As less traveling time from initial position to cloud top, the hail gets very small increases in size. Falling down from the cloud top it reenters the Hail Growth Zone (HGZ) with a comparatively small size. A smaller hail stone collects less cloud water while falling down to the ground. Therefore, an embryo lifted from higher initial position lands on the surface with smaller final size. The smaller hail stone tends to reside longer in the storm cloud supported by updraft for a longer time. Consequently, although an embryo lifted from a higher position has a longer growth time history, its final size actually is becoming smaller.

Figure 4.7 shows the time history of simulated hail sizes for the 11 July case using different initial positions of the initial hail embryo of diameter 0.03 cm. Clearly, different initial positions of embryo result in different hail trajectories, final hail sizes, and hail growth times.

For the 24 August case, only the hail embryos lifted from 0 and 500 m above cloud base (ACB) can grow and land on the ground surface. Others initialized from altitudes higher than 1000 m ACB are ejected out the clod top. Figure 4.8 compares the time history of hail growth for the 24 August case. In experiment H1, the hail embryo lifted from 500 m ACB grows into 1.7 cm eventually on the ground. Compared with H0, the final hail size is bigger obviously while growth time is same for two different embryo initial positions. The hail embryos lifted from levels over 1000 m above cloud base are above the moist cloud water region and they can not grow into a significant size to overcome the moderate storm updraft. The small hail stones are ejected out from the cloud top before returning to fall down to the ground. The embryo lifted from 1000m ACB is ejected out at 7 minutes with size of 0.24 cm at cloud top. Embryos from 1500m

and 2000m ACB are ejected out at 5 and 4 minutes with size of 0.1 cm at clod top, respectively. In conclusion, in a shallow storm cloud with moderate convection, embryos initially lifted from cloud base have more possibility to grow and land on the ground compared with others.

4.6 Sensitivity experiments for different model coupling strategies

Testing the sensitivity of maximum hail size to the method of coupling the time – dependent cloud model with the hail growth model is important. Sensitivity experiments were made to test the impact of at which time the hail growth model is started relative to the cloud model. In other words, the test examined the sensitivity of final hail size to the introduced time of initial hail embryos in the cloud. In addition, sensitivity experiments were made to test the effect of time span of constant cloud parameters as surrounding conditions for hail growth on final hail size.

Table 4.3 lists the results of these sensitivity experiments. τ_i denotes the introduction time of hail embryo into the model cloud, whereas τ_d is the time span of cloud parameters, which provides surrounding conditions for hail growth. This means that within a time span of cloud parameters for hail growth, the profiles of cloud parameters do not change with time. For example, if τ_d is 5 minutes, it means that a hail grows within a model cloud which remains steady for 5 minutes. After five minutes, new profiles of cloud parameters deprived from time-dependent cumulus model replace old ones (profiles of cloud parameters) for further 5 minutes used as new surrounding conditions with time forwarding for hail growth. Obviously, in HAILCAST, it is equivalent that the steady-state cloud model provides profiles of cloud parameters for hail growth for just one time span. However, even for longer τ_d as 5, 10, or 15 minutes, the time-dependent cumulus model provided 6, 3, or 2 different cloud profiles for hail growth if assumed the hail growth time is about 30 minutes.

Experiments T1 to T5 represent model simulations in which the hail embryo (of size 0.03 cm) is entered at cloud base at different τ_i time, varying from 20 to 60 min. For the 11 July 1985 case, the final hail size D_f on the ground decreases with the postponement of hail embryo introduction time. The modeled hail size is reduced from large hail (4.9 cm) to small one (1.3 cm). Moreover, the hail growth time is becoming shorter with the delay of introduction time of hail embryo. These results are attributed to the fact that the simulated precipitating cloud lasted about 60 minutes from 20 to 80 minutes displayed in Figure 3.4a. If the introduction time of hail embryo is postponed, which is equivalent to the situation that hail embryos present too late in a storm cloud in nature, the gradually decreasing updraft in intensity has no strong capability to uphold the hail in the cloud for a long time period. In addition, decreasing cloud water mixing ratio with time (Figure 3.4b) means that there is less cloud water collection for hail growth. Otherwise, the fraction of water on the hail becomes much bigger with the reduction of hail size because smaller hails are more vulnerable to melt below the freezing level. Especially, if the final hail size is smaller than 3 cm, the final fraction of water increases quite obviously with reduction of hail size (Figure 4.9b). Time histories of hail growth for different introduction times are depicted in Figure 4.9. Apparently, with delay of introduction time of hail embryo into model cloud, the final hail size becomes smaller quickly. Growth time becomes shorter and trajectory becomes lower. In conclusion, for our purpose of modeling maximum hail size, it is determined that once the top of modeled cloud is over 5 km AGL, a hail embryo is introduced at the cloud base. The statistical time to introduce hail embryo at cloud base is assumed at 25 minutes after beginning of cumulus model integration.

For the case of 24 August, the sensitivity experiments T1 to T5 show similar results. In T1, when a hail embryo is introduced on the cloud base at 20 minutes, it goes up to cloud top in 8 minutes and is ejected out of cloud with size of 0.5 cm. The updrafts in Figure 3.7a support this result. It is clear that between 20 to 30 minutes in Figure 3.7a the updrafts are stronger with speed over 15 ms^{-1} but cloud top is not very high (below 6.5 km AGL). The other situation is that when the hail embryo (0.03 cm) is introduced

on the cloud base at 60 minutes, the updrafts can not uphold the hail due to too weak updraft velocity around the cloud base (Figure 3.7a). The hail embryo falls downward to melt and vanish in 10 minutes. Figure 4.10 shows the time history of hail growth on introduction time sensitivity experiments for the case of 24 August 1983. The most obvious feature is that T1 is blown out of cloud top while T5 falls down directly from cloud base. In conclusion, with delaying introduction time of hail embryo the final hail size becomes smaller and the hail takes less minutes to grow due to decaying of cloud updraft. Suitable introduction time of hail embryo into the cumulus cloud is the moment when the modeled cumulus begins to develop into its mature stage.

The time step for the two-cylinder cumulus model integration is 5 seconds while in hail growth model the time step is set as 0.1 second. Outputs from the cumulus model provide surrounding conditions for hail growth. These cloud parameters involving updraft velocity, cloud water mixing ratio, rain water mixing ratio, and the in-cloud temperature etc are functions of height and time. Coupling the cumulus model with the hail growth model provides a numerical technique to forecast maximum hail size. As a result, the time intervals or time spans of cloud parameters in coupling techniques influence the hail growth. Five sensitivity experiments, labeled C0 through C4, are compared in Table 4.3. The model time intervals for cloud parameters are 0.5, 1, 5, 10, and 15 min from C0 to C4, respectively. For the 11 July case, with the increase of time span forecasted hail size rises slightly from 4.6 cm in C0 to 5.0 cm in C4 and the hail growth time becomes longer very slightly from 29 to 31 minutes. For the case of 24 August 1983, same rising tendency happens in hail size but hail growth time keeps almost same.

Figure 4.11 shows time histories of hail growth on experiments C0 to C4 for 11 July 1985. It is easy to find that for different time spans of cloud simulated hailstones are close to each other in size (Fig. 4.11a). Hail growth time does not increase vastly with the increase of time span from 0.5 to 15 min. Consequently, fraction of liquid water, terminal velocity and kinetic energy do not have big discrepancy. However, hail growth trajectories display different patterns for different time spans of cloud parameters (Fig.

4.11c). The experiment C0 and C1 are very similar, based on time spans of 0.5 and 1 min, respectively. With the increase of time span, the period of time the hail resides on the cloud top becomes obviously longer. For example, C4 in Figure 4.11c has more than 10 minutes from 3 to 15 minutes to stay on the cloud top when using time span of cloud as 15 minutes

Figure 4.12 shows the time history of hail growth in experiments of C0 to C4 for the case of 24 August 1983. First, due to increase of time span of cloud profiles, the simulated hail size on the ground becomes larger from 1.1 to 2.1 cm gradually while the growth time does not change greatly. However, the fraction of liquid water and kinetic energy do not display big discrepancy as the simulated hail stones remain small. The results suggest that using a shorter time span for time changing cloud profiles is better.

In general, it is found that the simulated hail size on the ground increases with the increase of time span of cloud profiles. On the other hand, the hail growth time is not very sensitive to the time span of cloud profiles based on these two studies. Therefore, it is beneficial to use more frequent time changing cloud profiles as surrounding conditions for hail growth to forecast maximum hail size. Actually, we select 0.5 minute as time span for changing cloud profiles.

4.7 Summary and conclusions

Based on two different hail cases, sensitivity experiments have been conducted to investigate the sensitivity of coupled model technique in forecasting maximum hail size to changes of various parameters. These parameter changes for sensitivity experiments involve three aspects in the coupled model technique, which are cloud parameters concerning precipitation effects and ratio between inner and outer cylinder radius, microphysical parameters for hail growth and those for coupling schemes, respectively.

The model cloud is sensitive to precipitation effects. If precipitation is switched off in the cumulus model, the maximum updraft velocity ($W_{\max}$) of cloud becomes

weaker by about 5 % and the cloud top is lowered by about 15%. Also, the model cloud without precipitation in F has no downdraft, but last longer. For maximum hail growth, the non-precipitating cloud produces a larger hail size but using a longer time. On the weak hail case (24 August 1983), the model cloud produces larger hail with diameter of 2.1 cm, significantly larger than reported observation. Precipitation effects in the coupled model have strong impacts on the modeled hail growth, since the precipitation significantly influences the cloud dynamics and thermodynamics through changing water loading effects and partial evaporation of precipitation. This proved that the time-dependent two-cylinder cumulus model with precipitation (P) is able to capture basic features of cumulus cloud with updraft-downdraft couplet, changing water loading effect. Coupled with hail growth model, the new model technique P realistically simulated and forecasted maximum hail size on both studied cases.

Sensitivity of maximum hail growth to hail embryo initial size is tested. It is found that the hail growth is not very sensitive to changes of hail embryo initial size. A wide range of initial embryo size can produce almost same size hails on the surface. This result is consistent with previous studies (e.g. Brimelow 2002). The initial altitude of hail embryo has strong influences on hail growth. Increasing initial height of embryo results in smaller hail and increases hail growth time.

The hail growth is found to be sensitive to introduction time of hail embryo into the cloud model. With delay of introduction time, the hail size becomes smaller and hail growth time becomes shorter. If the introduction time is too late, the model cloud updraft can not uphold the embryo. Hence, the embryo falls downward directly from the cloud base to the ground.

In conclusion, this chapter has focused on sensitivity of model cloud and hail growth to changes in key microphysical parameters and important coupling techniques. Based on the sensitivity experiments for all considered parameters, it is found that precipitation and the time changing of cloud parameters are two critical factors influencing storm cloud characteristics and hail growth. Furthermore, the impact of initial

altitude of hail embryo on modeled hail growth is also a major factor to determine maximum hail size on the ground. By comparing the simulated results with observations for two cases, it is suggested that coupling the time-dependent two-cylinder precipitating cumulus model with hail growth model (P) provides a promising numerical technique to simulate the hail growth and forecast maximum hail size. Of course, evaluations for the technique performance are needed based on verifications against observations in a large amount of samples. The following chapters deal with these issues.

Chapter 5 MODEL VERIFICATION USING ALBERTA HAIL PROJECT DATA

5.1 Introduction

In previous chapters, we reported on hail growth model simulations using the new coupled time-dependent cumulus model-hail growth model. We focused on two case study days. Sensitivity experiments for different model parameters were made for these two cases. The case study simulations suggest that the time dependent precipitating cloud model has advantages compared to the steady state, non-precipitating cloud model used in HAILCAST. However, there is still the issue of how well the new coupled model is based on many cases and how the model forecasts compare with observations of hail size. The verification statistics of such model-observation comparisons might point to the usefulness of considering the new time-dependent coupled model as forecasting tool for issuing severe weather warnings of large hail. For such a model-observation comparison of maximum hail sizes it is crucial to have good hail size observations and good proximity soundings required for model initialization. In this chapter, we describe the observational data set of the Alberta Hail Project (AHP). Numerical simulations of these data will then be carried out using different coupled model techniques, which involve precipitating cumulus model coupled with hail growth model (P) and non-precipitating cumulus model coupled with hail growth model (F). Moreover, traditionally and operationally used methods to forecast maximum hail size, NOMAGRAM (N) and HAILCAST (H) are also used to forecast hail size for the same data set. Finally, comparisons among their forecasting performances based on verifications against observations will provide primary analysis on model's advantages and disadvantages.

5.2 The Alberta Hail Project (AHP) data

To evaluate the coupled model technique's performance in forecasting maximum hail size on the ground, the Alberta Hail Project (AHP) data for three summers of 1983 to

1985 will be used to verify the model abilities. The AHP was a field program designed to examine hailstorms and also to test the possibility of hail suppression by glacier generic seeding using aircraft. The AHP target area covered approximately 48,000 km^2 with a center located at radar site in Penhold, near Red Deer. Hail size was reported mainly by farmers. Hail report cards were mailed to 19,464 farmers living in AHP area in each spring (Renick, 1983). On any given day in summer, about 10% to 20% of farmers reported the occurrence and peak size of hail on their property. This yielded a high resolution hail observation network with an average of one observer per 12~24 km^2. The hail data reported by farmers included observed largest hail size, time of the onset of hail and exact location of hail occurrence. Moreover, telephone surveys were conducted to verify radar observed storm clouds during the summer, yielding higher observation densities. Only a very small percentage of hails reaching on the ground were undetected. As a result, the AHP hail data are ideal to evaluate numerical techniques in forecasting maximum hail size. The observed maximum hail size was classified into six categories, each of which was referred to familiar sizes such as grape size, walnut size, pea size, etc. (Table 5.1).

Upper air soundings were released from Penhold twice daily at 0615 and 1715 local day time (LDT). As most thunderstorms occur in the late afternoon in central Alberta (Smith, 1998), the afternoon observations were used as proximity soundings for the thunderstorm environment. The thermodynamic soundings released at 1715 LDT from Penhold were used as initial conditions for the two-cylinder cloud model. The observed maximum hail size data collected between 1415 and 2015 LDT within 100 km of Penhold was used to verify the model forecast maximum hail size on the ground. This criterion has been used by Moor and Pino (1990) and Brimelow et al. (2002). Figure 5.1 and Figure 5.2 depict the AHP area and the hail observation network, respectively. The area of hail collection network for verification is about one fourth of the total AHP area. However, since most farmers inhabit central Alberta, the density for hail observations is relatively higher.

Following Brimelow et al. (2002) and Ranger (2003) we selected the three summers of 1983 to 1985. During this period there was good quality control over the accuracy of both the hail data and the sounding data. Based on the criteria of observed hails for verification of forecast hail size and the record quality of sounding data (for example, some data missing T or Td at any level etc), a total of 160 days are available during these three summers. This number of samples involves 20 days with large hail (representative diameter: RD$\geq$2.7 cm), 42 days with small hail (RD$\leq$1.7 cm), and 98 days with no hail. The diversity of observed hail events is helpful to test model techniques in forecasting the occurrence of hail and distinguishing maximum hail size.

For the coupled cumulus-hail model technique, two situations will be investigated. The first one is to include precipitation effects in the cumulus model, while the other one is to exclude precipitation effects. Totally, four methods, P, F, H and N will be employed to investigate the AHP data. At last comparing the coupled model techniques P and F with operationally used model techniques, H and N helps to find out the improvements in forecasting maximum hail size on the ground. Definitely, the same AHP data during three summers of 1983 to 1985 must be used for various model technique investigations so that objective comparable evaluations for different techniques can be obtained.

5.3 Time-dependent cloud model – hail model simulations using AHP data

In this section, forecast maximum hail size using the model techniques P and F is verified against observations of maximum hail size within designated district in the AHP area. Model forecast hail size on the ground for each sounding data is placed against representative diameter (RD) of observation. Finally, a distribution of forecast hail size against observations is obtained.

Figure 5.3 shows the distributions of forecast hail size based on the coupled cumulus-hail model technique considering precipitation effects (P) plotted against hail

observations from the AHP data. D_O denotes the representative diameter of observed maximum hail size. D_f represents model forecasted maximum hail size on the ground based on available sounding data. In the diagram, the line in orange color represents the perfect hitting between forecast hail size and observation. The dashed lines in magenta color represent lower and upper limits for hail representative diameter. These two dashed lines composite a hitting strip for forecast hail size D_f.

Overall, it is found that the coupled cumulus-hail model technique P poses an ability to forecast maximum hail size. Most of forecasted hail sizes are within the hitting strip of representative diameter of observed hail size organized by two dashed lines. Furthermore, the forecasted hail size distributed in category is basically matched well with the category of observed hails. It means that for observed hail size classified into a specific hail category based on the criteria listed in Table 5.1, the forecasted hail size using the model technique P is almost within the same category. Particularly, for the cases with relatively small maximum hail size (RD$\leq$1.7cm) the forecasted hail size is closer to the representative diameters of observed maximum hailstones. On the other hand, for the days with maximum hail diameters larger than golf ball size (RD=4.3 cm), the model technique predictions are distributed sparsely around the hitting strip for large hail categories. The distributions reveal that the forecast misses several large hail events. For no hail days of observation, the distribution shows that there are some of forecasted hails. Apparently, those days without observed hails are falsely forecasted. On the contrary, some of observed hails are missed by forecast.

To examine the precipitation effects on the hail growth and maximum hail size forecast, the same coupled model technique but precipitation scheme being switched-off in the time-dependent two-cylinder cumulus model is employed to investigate the AHP data. Finally, it is convenient to figure out the precipitation effects by analyzing and comparing the model P and F performances based on the large amount of same sample data.

Figure 5.4 also shows the distributions of forecasted hail size against observations like that in Figure 5.3, but the coupled cumulus-hail model technique, F used to forecast hail size did not include precipitation effects in the cumulus model. It is found that many forecasted hail sizes were above the upper limit dashed line of representative diameter for observations. For the observed no hail days, some forecasted hail size is badly exaggerated. The most seriously false-forecasted hail size for observed no hail days reaches about 6 cm. In general, the distribution reveals that the model technique F poses a tendency to over-forecast hail size for many cases, especially for observed no hail days (false alarm) and small hail days (over-forecast). Otherwise, although the technique F displays the strong tendency to over-forecast observed hails, there still exist some miss forecasts.

Apparently, switched-off precipitation effects in the time-dependent two-cylinder cumulus model are responsible for this deficiency. As indicated from case studies and sensitivity experiments in previous chapters, if precipitation is not taken into consideration in the cumulus model, there is no formation of a storm downdraft in the non-precipitating model cloud. The long lasting updraft is preferred to uphold the hail in the storm for much longer time. Consequently, there is the tendency to produce large hailstones and false alarms in the model simulation and prediction compared with observations. The model F obviously makes over-forecasts for many of observed hails in addition to some of seriously false forecasts for observed no-hail days. This suggested that it is necessary to take precipitation effects into consideration when the time-dependent coupled model technique is used to simulate the hail growth and forecast hail size, as precipitation profoundly affects the storm clouds in dynamics and thermodynamics through changing water loading effects and partial evaporation of rain water. As a result, the precipitating cumulus model involving updraft and downdraft couplet, changing water loading effect and formation and evaporation of precipitation in the coupled model technique P provides more physically realistic surrounding conditions for hail growth. Consequently, the forecasted maximum hail size on the ground using model technique P is expected to be more accurate than using F.

5.4 Investigations for the AHP data using HAILCAST with a steady-state cloud model

The newly coupled model techniques P and F have been employed to investigate the AHP data. It is revealed that the model technique P displays better performance in forecasting maximum hail size based on the analysis of distributions of forecasted maximum hail size against observations. Furthermore, we hope to find out if the new model technique can improve in forecasting maximum hail size through comparison with other numerical algorithms. For this purpose, operationally used hail forecast model technique, HAILCAST (H), and another traditional algorithm NOMOGRAM (N) are employed to carry out investigations on the AHP data. The technique H developed by Brimelow et al. (2002) is a numerical method to forecast maximum hail size by coupling a steady-state one-dimensional cloud model with a time-dependent hail growth model. Likewise, the algorithm N used by Renick and Maxwell (1977) forecasts maximum hail size by relating the expected maximum hail size in the form of hail category to maximum updraft velocity and the temperature at the height of maximum updraft (Fig. 5.8). The maximum updraft velocity and its corresponding temperature required to determine the hail size category for the usage of algorithm N are obtained from the steady-state one-dimensional cloud model output in HAILCAST.

Figure 5.5 shows the distributions of forecast hail size plotted against observations using H. We can see that many observed hail days are correctly forecasted. For extremely large hail days (RD$\geq$4.3 cm), the model technique H looks fairly robust. The scatter plot suggests that technique H tend to over-forecast some of hail days. Particularly, the over-forecasted hails using H are mainly concentrated on many days with relatively small hails in observation. On the issue of false-alarms, the model H false-forecasted a few of observed no hail days as hail events. The most seriously false alarm predicts a hail with size of 4.8 cm. Miss forecast still exists for each category of observed hail days.

The last algorithm used to investigate the AHP data is NOMOGRAM (N). The forecasted hail size is classified into various categories based on the classification criteria used in AHP (listed in Table 5.1). The forecasted hail representative diameter using N is depicted in Figure 5.8, which is based on the maximum updraft velocity and its correspondent temperature deprived from each sounding.

Figure 5.6 shows the distributions of forecasted hail size using NOMOGRAM (N) against observed maximum hail size. As the algorithm of NOMOGRAM is an empirical relationship between hail size and maximum updraft velocity, it forecasted hail size within six categories rather than in any decimals produced in previous models P, F and H. Clearly, many forecasted hail sizes are overlapped in Figure 5.6. We can see that on overall the technique N tends to under-forecast hail size for a few of hail days as many of forecasted hail sizes are located below the hitting strip. In particular, the distributions show that the algorithm N has poor ability to forecast hail size for extremely large hail days (RD$\geq$4.3 cm) because no forecasted hail size is within the hitting strip of observed representative diameter (RD) larger than 4.3 cm. The reason for this under-forecast is that the occurrence of large hail size is correlated to very strong storm updraft velocities (> $40 ms^{-1}$) in NOMOGRAM. On the other hand, it is quite easy to produce updraft velocity over $10 ms^{-1}$ using the steady-state cloud model in HAILCAST. The NOMOGRAM assumed that once the maximum updraft velocity is larger than 10 ms^{-1} hails will occur (depicted in Figure 5.8). This assumption caused many false forecasts for observed no hail days in N. Actually, the observed data suggest that most of the storm days had these updrafts but not produced hails. Complete neglect of cloud development process and hail growth microphysics in the algorithm N is responsible for this shortage of false forecast for observed no hail days and excessive under-forecast for observed large hail days.

5.5 Inter-comparison among different model techniques P, F, H, N

Furthermore, the coupled cumulus-hail model technique (P, F) performance in forecasting maximum hail size on the ground are compared with those of operationally used model techniques H and N.

Figure 5.7 depicts an inter-comparison among the model approaches P, F, H and N in the forecasting of maximum hail size for the AHP data. It is evident that the distributions of forecasted hail size using the coupled cumulus-hail model technique with precipitation effects (P) indicated as blue circles in Figure 5.7 are located much more close to the hitting strip compared with those using other algorithms. The another feature in the distributions is that corresponding to specific hail categories of observations, the forecasted hail sizes derived from F and H display many over-forecast cases, which are indicated by light blue diamonds for F and red triangles for H. Moreover, for observed hail category with representative diameter of larger than 2.7 cm the algorithm N under-forecasts some large hail days. Overall, although these four techniques all show their primary ability to forecast maximum hail size based on their investigations for the AHP data, the inter-comparisons reveal that the coupled cumulus-hail model with precipitation effects P displays much better distributions of forecasted hail size than the others. For more objective evaluation of model performance in forecasting maximum hail size on the ground, various forecasting skill scores are needed to calculate. These forecasting skill scores will provide more detailed information to asses the model performance on its every aspect.

5.6 Summary and conclusion

The investigations on the AHP data using different model techniques were discussed in this chapter. The distributions of forecasted hail size against observations were studied for each method. Finally, inter-comparisons of forecasted hail size distribution for different model techniques were carried out. As a result, on overall, these four methods P, F, H and N all display their basic ability to forecast maximum hail size based on their AHP data investigations. After comparison, the new coupled numerical model technique P looks in advance primarily in forecasting performance. Calculating

various statistical forecasting skill scores in next chapter is expected to prove these confirmations in further.

Before verifications for the model performance through calculating skill scores in next chapter, distinctive features and configurations for different model techniques are listed below. The summary of features of different model techniques would provide insights to help find the causes why different technique has different performance in forecasting maximum hail size. Logically, more complex technique makes advancements and improvements gradually from N, H, F to P.

Discussion of features and configurations of four model techniques listed in table 5.2.

Technique P: coupling a time-dependent two-cylinder cumulus model with precipitation scheme and a time-dependent hail growth model. The simulation of evolution of cloud and rain effects on the storm dynamics provides physically realistic surrounding conditions for hail growth, which includes detailed hail growth microphysics.

Technique F: also coupling the time-dependent two-cylinder cumulus model but no-considering precipitation effects with the time-dependent hail growth model. As rain effects are switched off, cloud parameters, especially cloud water mixing ratio and updraft velocity are strongly affected. Consequently, changed storm cloud without rain water produces different hailstones compared with rain storm cloud. Therefore precipitation effects on cloud and hail can be investigated through F.

Technique H: coupling a steady-state one-dimensional cloud model with the same hail growth model used in F and H. The evolution of cloud is not simulated. Rain effects on cloud and hail growth are ignorant. Relatively high simplification of cloud model provides coarse surrounding conditions involving profiles of cloud parameters, updraft velocity, cloud water content and in-cloud temperature for hail growth. So, the cloud evolutionary, rain effects on hail and other configurations like cloud life cycle and the velocity at cloud base are excluded.

Technique N: an empirical relation of maximum hail size on the ground to the maximum updraft velocity and the temperature at the altitude of maximum updraft. It completely neglects cloud development process and hail growth microphysics.

Apparently, after the description of each model technique, it is clear to understand the improvements of model techniques from N to P in forecasting maximum hail size. Model investigations on the AHP data are expected to prove these improvements.

Chapter 6 MODEL VERIFICATION AGAINST OBSERVATION AND INTER-COMPARISON AMONG DIFFERENT MODEL TECHNIUQES

6.1 Introduction

In chapter 5 we compared different model configurations to forecast maximum hail size for AHP soundings observed during the summers of 1983, 1984 and 1985. The forecast hail sizes were compared against maximum hail size observations for each day. To quantify the skills of the different model techniques it is useful to compute statistical forecasting skill scores for the observed maximum hail sizes. The verification provides objective evaluations for the coupled model technique in forecasting maximum hail size and how its forecasting skill compares to the older models.

6.2 Statistical methods used to evaluate the model performance

To evaluate the model performance, various statistical skill scores were needed to calculate. A 2×2 contingency table was constructed between forecasted hail size and observed hail size for three summers of 1983-1985 in order to determine these forecasting skill scores (Table 6.1). We use the following terminology: A hit (HT) constitutes correctly forecasting the occurrence of an event. A miss (MS) is recorded when the event is observed but not forecasted. A false alarm (FA) is recorded when the event is forecasted but not observed. A correct null (CN) is recorded when no event is observed and no event is forecasted. Based on the contingency table, the following skill scores are calculated: Probability of Detection (POD), False Alarm Ratio (FAR), Heidke Skill Score (HSS), Critical Success Index (CSI), Bias (B) and Reliability (R). The detailed definition and calculation formulas for these skill scores are listed in Table 6.2. The POD and FAR vary between 0 to 1. Combining higher POD and lower FAR scores provides a believable forecast. However, the POD and FAR give no credit for correct null

forecasts. The CSI measures overall performance with values ranging from 0 to 1. High score means good performance.

The HSS is the most popular skill score for forecast verification because it takes all values in the contingency table into account. Thus, the HSS is considered a measure of the true skill of a forecast. The value of HSS varies between -1 for absolutely no forecast skill and 1 for a perfect forecast skill. Generally, the HSS with a value of greater than 0.4 is considered good.

The B indicates the tendency of observed events is over-forecasted or under-forecasted. The B score of 1 indicates that a particular event is equally over-forecast and under-forecast (not over and under forecast, perfect). The B scores less than 1 and larger than 1 indicate a tendency to under-forecast and over-forecast an event, respectively. The R provides a creditability of the model forecast. The value of R ranging from 0 to 1 suggests the creditability of the model forecast from none to a completely reliable.

6.3 Model P evaluation and comparison with F

To quantify the model forecasting skills for maximum hail size prediction, various forecasting skill scores listed in Table 6.2 were calculated based on the 2×2 contingency Table 6.1 for the coupled model technique P. Various skill scores would provide objective evaluations on the model technique performance in forecasting hail size from global aspects.

For the purpose of evaluation and considering the importance of hail size to hail damage, all various hail sizes are summarized into three categories purposely for model evaluation, rather than very detailed category used in the AHP (Table 5.1). Large hails are those events with hail size larger than 2.7 cm in representative diameter as the hails with diameters larger than 2 cm pose significant damage to their targets. Small hails are those with hail size diameter less than 1.7 cm in representative diameter. Days without recorded hail fall are referred to as no hail days.

Figure 6.1 shows the model technique P forecasting skill scores for different hail events. For all hail days, the technique P was skillful with high POD of 0.6 and low FAR of 0.24. The HSS and CSI both reached over 0.5. Theses skill scores indicated that the technique P is capable of forecasting hail days and no hail days. For small hail days, the POD is 0.61 and the FAR is 0.25. The HSS and CSI are 0.59 and 0.51, respectively. It shows that the P has relatively stronger ability to forecast small hails. For large hail days, the technique P demonstrates relatively poor skills in forecasting large hails (RD>2.7 cm) due to the POD of 0.4, the FAR of 0.43, the HSS of 0.39 and CSI of 0.29. In general, the model P under-forecasted hail events as the B for different hail size is approximately 0.8.

Figure 6.2 shows reliabilities of the model P forecast for hail size categories classified into no hails, small hails and large hails. Model P provides high reliability for no hail and small hail forecasting as the reliability is 0.79 and 0.71, respectively. The reliability for large hail is weaker with the value of 0.49. On overall, it shows that the model P is able to forecast different hail sizes. Based on the analysis of Figure 6.1 and 6.2, it is concluded that the coupled numerical technique P is skillful to forecast the occurrence of hail and to predict hail size.

In chapter 5, analysis of distributions of forecasted hail against observations has revealed that switched-off precipitation effects in the time-dependent two-cylinder cumulus model caused many over-forecast, especially for observed small hail days. Moreover, some of no hail days were falsely forecasted. The forecasting skill scores will now provide objective evaluations for the performance of technique F. And the comparison of skill scores for P and F could help figure out the precipitation effects on hail forecasting.

Forecasting skill scores for model technique P and F are compared in forecasting all hail days, which are depicted in Figure 6.3. It is found that F has slightly higher POD and larger FAR. Consequently, for true skill HSS and reliability R, the technique P displays advanced performance. Bias of technique F is bigger than that of P mainly due to

many over-forecasts. It is suggested that the technique P is more skillful to forecast the occurrence of hail although the F still demonstrates its ability. Therefore, it is better to consider precipitation effects in the time-dependent two-cylinder cumulus model. The technique P is proved to have first priority in purpose of forecasting hail occurrence. Further comparisons discussed in the next section 6.4 would provide more solid proofs to support the technique P.

6.4 Inter-comparison of models P, F, H, and N

Figure 6.4 shows the different model technique forecasting skill scores for all hail days. We can see that the NOMOGRAM has highest POD with the value of 0.69, while the other three techniques have almost same POD of 0.61. For the value of FAR, the technique P has smallest amount of 0.23. However, the FAR increases apparently for other techniques, F with 0.26, H 0.32 and N 0.39. For the true skill score HSS and overall performance index CSI, the P and F are located clearly in the leading position. The HSS for P and F are 0.51 and 0.5, while H and N have just 0.41 and 0.4, respectively. The highest values of HSS and CSI prove that P is the best among the four techniques to forecast hail occurrence. On the other hand, for the values of B, the technique P has the lowest amount about 0.8 but N has the largest value of 1.13. According to the definition of bias listed in table 6.2, the high B large than 1 means N over-forecast some of hail days. In contrary, P, F and H have under-forecasts. Comparatively, technique P has most serious under-forecast rate due to lowest B of 0.8.

Further evaluations on the model skills to forecast different hail size are carried out using the following figures. Figure 6.5 shows different model technique forecasting skill scores for small hail days. The most distinctive feature in Figure 6.5 is that the B for N is pretty large with the value of 1.21. This suggests that the tendency of over-forecast of N was caused mainly by over-forecasting small hail sizes. The skill scores on small hail stones have different tendency for different techniques. For POD, N and P have high values of 0.69 and 0.61, while H and F have low values of 0.5 and 0.6. The tendency of FAR for the four techniques keeps almost same as that for all hails (Figure 6.4). N has

biggest FAR of 0.42 and P has smallest of 0.26. On most popular skill scores of HSS and CSI, P is still at the first position with the value of 0.6 and 0.51. The method F is second. The N is third and H is last. The comparison proved that for the prediction of small hails, the technique P and F are still at the leading positions.

Figure 6.6 shows different model technique forecasting skill scores for large hail days. We see that all models have relative poor skills to forecast days with large hail sizes. We can see that H has highest POD of 0.61; N has poorest POD of 0.22. The technique P and F are in the middles with values of 0.4 and 0.42 between N and H. H and F have biggest values about 0.61 of FAR for large hails. The P and N have FAR of 0.41 and 0.45. For true skill score HSS and overall performance score CSI, P has the value of 0.39 and 0.28, while H has 0.35 and 0.3. Although the HSS and CSI for all techniques are low, the technique P is still in superior relative to the other techniques. For days with large hails (Fig. 6.6), models H and F showed a distinctive high B. The values of 1.85 and 1.3 of B respectively for H and F mean that these two kinds of techniques seriously over-forecast large hail days. On the other hand, the smallest bias (about 0.5) of N means that the algorithm N seriously under-forecasted large hails because N has poorest ability to forecast large hails discussed in Chapter 5. Likewise, the value of 0.8 of B for the technique P means that it also under-forecasted large hails. Anyway, the technique P still displayed ability to forecast large hails although the skills were not very good due to relative under-forecast and miss forecast.

The technique P and F displayed competitive high forecasting skill scores based on the analysis of skill scores for days with small and large hail sizes. They were proved of skillful to distinguish hail size. As a result, the technique P showed its prominent skills on overall to forecast the occurrence of hail and determine hail size category sensible for hail damage warnings.

Figure 6.7 shows the reliabilities of category forecasts using different model techniques. It is clear that for no hail and days with small hail sizes, the new model technique P and F have high reliabilities with the value of more than 70%. However,

when the new model P forecasts the occurrence of large hails, we need to pay some cautions as the reliability of large hail forecast is not very high. Probable causes responsible for the relative low reliability of large hail forecast will be discussed in part of miss forecast of next section.

6.5 Conclusions and discussions

6.5.1 Conclusions

In this chapter, various forecasting skill scores were calculated to evaluate the technique performance in forecasting maximum hail size based on the investigations for the AHP data. Precipitation effects on hail forecast were also examined using the time-dependent two-cylinder cumulus model without precipitation parameterization coupled with hail growth model (F). The performance of new technique P was compared with those of operationally used technique H and N. The evaluation and the inter-comparisons among the different model technique performance revealed a few of significant findings.

1) The new model technique of coupling the time-dependent two-cylinder precipitating cumulus model with the time-dependent hail growth model method P is skillful to forecast the occurrence of hail and also the maximum size of hail.

2) The forecasting skill of the new technique of coupling a time-dependent precipitating cloud model with a hail growth model (P) was superior to the HAILCAST model, which is based on a steady-state cloud model without precipitation. The forecasting improvement can be attributed to the more realistic finite life cycle of the evolving cloud and also to the presence of precipitation.

3) The comparison between the model P (that allowed for precipitation) and model F (that had only cloud water but no rain) showed that the distribution of the rain water affected the life cycle of the storm cloud. In particularly, the water loading of the precipitation reduced the low-level storm updraft and caused the formation of a

downdraft. The downdraft diminished the vapor available for condensation and thereby shortened the duration of the cumulus cloud. Partial evaporation of the rainwater beneath the cloud base intensified the downdraft

4) The forecasting skill of the new technique of coupling a time-dependent precipitating cloud model with a hail growth model (P) was superior to NOMOGRAM technique. This shows that modeling the cloud dynamics, thermodynamics, cloud microphysics, and hail physics together add predictive value which is above the statistical empirical relationship of hail size with Convective Available Potential Energy (CAPE) as given in the hail NOMOGRAM.

5) The time-dependent cumulus model provided a natural life-cycle of the hailstorm, whereas using a steady-state cloud model required additional information about the duration of the storm updraft. This duration was difficult to estimate, but the hail growth and its final size were very sensitive to the storm duration. Moreover, the new model technique P avoided the issue that the updraft velocity at cloud base had to be assumed artificially in HAILCAST.

Based on these findings we suggest that it worthwhile to consider exploring whether the new model should be used as an operational tool to forecast hail size.

Clearly, some caveats still exist in the model technique. For example, the new technique P made a number of false forecast (alarm) and miss forecast. It is these bad forecasts which negatively affect the model performance. If the numbers of these two types of bad forecast could be reduced, it could be expected that the technique would have more excellent performance. The problems concerning the miss forecast and false alarm are discussed specifically in the next.

6.5.2 Discussion of false alarm and miss forecast

a. False alarm

As mentioned in definition, a false alarm (FA) is recorded when the event is forecasted but not observed. In previous sections, the forecast evaluation revealed that a number of cases of observed no hails were falsely forecasted as hails using different model techniques. When using model technique P, 11 observed no hail days out of 98 were forecasted as hails depicted in Figure 5.3, while for F the false alarm number was 13 in Figure 5.4. For H and N, the falsely forecasted cases were 15 depicted in Figure 5.5 and 26 showed in Figure 5.6 (most were overlapped), respectively. Obviously, the numbers of false alarm displayed a tendency to rise greatly with the simplification of model techniques from P to N. In comparison, the technique P considers cloud microphysics, precipitation parameterization schemes and detailed hail growth microphysics, while F is same as P except switched-off precipitation effects. On the other hand, the technique H is a method to couple a steady-state one-dimensional cloud model with a hail growth model. It does not include cloud microphysics and has no ability to provide time-changing cloud profiles for hail growth. The last and simplest technique N is just relationship among hail size on the ground with cloud maximum updraft velocity and the temperature on the altitude of maximum updraft velocity. N neither considers cloud microphysics nor hail growth processes. From Figure 5.8, it is easy to find that as long as the maximum updraft velocity is bigger than $10\,ms^{-1}$ above the level of 0°C, hails are definitely produced. Lack of considering cloud development and hail growth microphysics is responsible for many false alarms in N. Conversely, the technique P indicated its strong advantages and great improvements in performance of hail forecast through including the cloud development and hail growth processes.

For the 11 cases falsely forecasted by using technique P, weather conditions at that time were examined. Although sufficient moisture and warm surface temperature were optimum, thunderstorms were prevented from developing due to lack of trigger mechanism (Mueller et al. 1993). According to conceptual models for outbreaks of severe thunderstorms in central Alberta suggested by Smith and Yao (1993), the interaction of synoptic and meso-scale environments played a key role in triggering severe convections. They found that upper-air (500 hPa) trough and ridge were main factors to trigger whether the occurrence of hail or not even if sounding profiles presented potential for

thunderstorm outbreak. In their findings, 94% of all severe hail days were associated with an upper-air trough upwind of central Alberta. On the contrary, 71% of no-hail days had an upper-air ridge over Alberta. The present numerical technique P to forecast maximum hail size used just observed soundings as input to initialize the model running. In the conditions of sounding favorable for deep convections but ridge prevailing over Alberta, it still could have forecasted hails for observed no hail days. Therefore, it requests to combine synoptic analysis when the technique is used in forecasting maximum hail size. If synoptic background presented a favorable pattern for thunderstorm, and moisture and convective instability were sufficient deprived from sounding data, running the model would provide efficiency assistance in forecasting hail size. Anyway, even though synoptic conditions did not look like favorable for thunderstorms, the model forecast was still valuable in providing an alert of hail for weather forecasters.

On the other hand, a very small percentage of hail reaching on the ground was undetected due to strong localization of hailfall. So, in theory, the false alarms of model forecast hail should be further smaller if undetected hailfall was considered. Moreover, we can find in Figure 5.7 that the utmost falsely forecasted hail size was lest in comparison with other model techniques in addition to the smallest numbers of false alarm using P. The falsely forecasted hail sizes using P were all less than 2.7 cm in diameters. However, the other model techniques falsely forecasted many no hail cases as large hail size. For example, the largest falsely forecasted hail size using F was 6.1 cm. H and N forecasted no hail days with largest false alarm of 4.7 and 4.3 cm (Figure 5.7), respectively. On this aspect, it is also proved that the technique P has stronger ability to distinguish hail and no hail events compared with other techniques. The fundamental reason is attributed to considering time-dependent cloud development with precipitation parameterization and hail growth processes in P.

b. Miss forecast

When the numerical techniques were used to investigate the AHP data, some observed hails out of total 62 hail days were incorrectly forecasted as no hails. The amounts of miss forecast were 24, 23, 24 and 19 using P, F, H and N, respectively.

Relatively, the traditional algorithm N had lowest miss forecast since it was based just on the maximum updraft velocity and temperature on the height of maximum updraft. As long as the maximum updraft velocity of storm cloud was larger than 10 ms^{-1} and presented above freezing level, N must have forecasted hail occurrence. In reality of storm clouds, these criteria were not difficult to satisfy, but not all moderate or even weak thunderstorms complied with theses conditions could have produced hails. The model H forecasted maximum hail size on the ground according to surface based convective instability. It calculated steady-state one-dimensional updraft profile for hail growth using increased surface temperature and dew point through ensemble method. However, it still made the same number of miss forecast as P. For techniques P and F, due to consideration of cloud development involving time changing updraft/downdraft couplets and liquid water mixing ratio, hails were produced only within those modeled storm clouds with supportive updraft velocity and abundant cloud water content. These scenarios for hail growth in P looked more physically reasonable. After compared with other techniques on miss forecast, the new technique did not display serious disadvantages. However, the miss forecast was still a problem.

The issue of these miss forecasts (for P) was mostly attributed to three reasons. Firstly, too low surface temperature and dew point, probably contaminated or modified by precipitation, were responsible. For example, six large hail days listed in Table 6.3 had obviously low surface temperature below 19°C and dew point below 11°C at 1715 LDT. It was hard to initialize a deep convection using the very low observed surface temperature and dew point although sounding data indicated abundant moisture and potential convective instability. Otherwise, using convective temperature and modified low level lapse rate below 850 hPa based on mid-afternoon (14 LDT) surface temperature observation for late afternoon soundings (1715 LDT) probably provides an alternative way to initiate the model running.

Another reason responsible for miss forecast maybe concerned proximity of soundings. As previously mentioned, the observed maximum hail size was collected between 1415 to 2015 LDT in the area centered at Penhold with 100 km of radius. For

some cases if the location of hailfall was far away from the sounding site of Penhold, or the occurrence time of hailfall was leading (backing) much earlier (later) than the sounding release time, using the distanced and relatively 'not actual' sounding data had proximity problems to represent real in situ hailfall atmospheric conditions. Hailfalls associated with severe thunderstorms were meso-scale weather events. They had very strong localization features and often lasted a short period of time. For the model configurations, the outer cylinder radius was taken as 15 km. In theory, the hail growth in the modeled cloud is within this area. Correspondingly, collected hail data used for verification should be within this domain. Alternatively, using prognostic soundings deprived from numerical weather prediction (NWP) with high resolution in horizontal and densely produced on time scale is expected to provide effective methods to solve the problem.

The last cause resulting in miss forecast should be attributed to incomplete of model techniques. Adding the bulk effects of vertical wind shear into the model technique P is hopeful to reduce the rate of miss forecast and improve accuracy of forecast. The energy of instability determines the intensity of storm cloud, while the vertical wind shear strongly influences the cloud structure and lasting time. Tilt of cloud caused by wind shear helps hail to spend longer time in HGZ and less time to fall down to the ground because of tilted separation of updraft and downdraft. There could be more chances for hail to grow within a tilted storm cloud. As a result, it is expected to reduce the number of miss forecast.

Chapter 7 CONCLUSIONS AND SUGGESTIONS FOR FUTURE WORK

7.1 Introduction

This thesis addresses the problem of forecasting maximum hail size on the ground. Our approach is to couple a time-dependent two-cylinder cumulus model with a time-dependent hail growth model to forecast maximum hail size. The cumulus model includes a bulk-water parameterization scheme of cloud water and rain water. Therefore, the effects of the precipitation on the storm dynamics and thermodynamics are included.

In the thesis research, a number of sensitivity experiments have been carried out to determine the sensitivity of the modeled hail growth to changes of some of cloud and hail key parameters. The skillfulness of the new model technique in forecasting maximum hail size was examined by comparing model prediction with Alberta Hail Project (AHP) observations of maximum hail diameter. The new model technique was compared with other hail forecasting techniques. Major findings from the all thesis research are summarized as below in this chapter.

7.2 Conclusions

First we find that it is feasible to couple the time-dependent two-cylinder cumulus model with the time-dependent hail growth model to forecast maximum hail size. We improved and modified microphysics for cumulus model and adopted most of numerical code for hail growth model developed by Brimelow (2002). Coupling technique was finely designed in the convenience of reviewing cloud parameters changing with time and height. The new coupled model technique is quite thrifty on computing consumption. We found that coupling the time-dependent cumulus model with the time-dependent hail growth model actually added some computational time when compared to the operationally used HAILCAST, which coupled a steady-state cloud model with the time-

dependent hail growth model. However, the new model technique (P) was found to be still efficient computationally. It promises to assist in issuing hail warnings in operational work in terms of implementation.

Sensitivity experiments revealed that some changes of cloud and hail parameters have strong influences on hail growth. Precipitation is a major factor in affecting storm cloud and hail growth. In the examined cases, if precipitation is switched off in the cumulus model, the maximum updraft velocity (W_{max}) of cloud becomes weaker approximately by 6%. The altitude of cloud top is lowered about by 16%. However, the maximum cloud water mixing ratio is increased two to three times due to no conversion of cloud water to rain water. Moreover, the model cloud has no downdraft but has longer life duration. The modeled cloud without precipitation produces a little bigger hail size but using a relatively longer time compared with its counterpart of precipitating storm.

The ratio between radius of inner and outer cylinders significantly influences the model cloud intensity. The maximum updraft velocity (W_{max}) is increased with the decrease of radius ratio. This means that a deep and strong convection is companied by a vast compensatory subsiding motion in the immediate surrounding. Typically, the radius ratio is taken as 0.1 when outer cylinder radius is assumed as 15 km.

The changes of microphysics also influence the hail growth. Changing hail embryo initial size has less influence on hail growth and its final size. However, increasing initial height of hail embryo results in smaller hail on the ground and profoundly increases hail growth time.

As the present technique is to combine two time-dependent models together, the introduction time of hail embryo into the cumulus model influences the hail growth. The final hail size becomes smaller and hail growth time becomes shorter with delay of introduction time.

The hail growth is sensitive to the coupling technique. The cloud parameters as the function of height and time derived from cumulus model output provided surrounding conditions for hail growth. The time interval of the cloud condition supplied for hail growth model affected hail growth. It is found that the shorter the time span of cloud profiles used as surrounding conditions for hail growth, the better to simulate hail growth and forecast maximum hail size. The time interval less than 1 minute displayed very good performance. For model investigations on the AHP data, the profiles of cloud parameters used as hail growth surrounding conditions were changed every half minute.

More importantly, the coupled cumulus-hail model technique was used to investigate the AHP data, which had a wide range of hails in diameter. Various statistical forecasting skill scores were calculated to evaluate the model performance. Precipitation effects on hail forecasting performance were also investigated. Comparisons of the new model technique performance with those of operational methods proved great improvements in forecasting maximum hail size.

Coupling the time-dependent two-cylinder precipitating cumulus model with the time-dependent hail growth model is skillful to forecast the hail occurrence and distinguish the hail size. Furthermore, including the effects of precipitation in the cumulus model improves the performance of forecasting maximum hail size. This is attributed that the evolutionary of rain water field impacts on spatial and temporal distributions of the water loading, which feed back into the cloud dynamics. Evaporation of partial rain water also affects the storm dynamics.

The new technique P displayed improvement in forecasting of maximum hail size on overall compared with the operational HAILCAST, which was based on a steady-state one-dimensional cloud model. The main reasons are attributed to the employment of the time-dependent cumulus model, which is able to simulate the evolutionary of cloud and precipitation effects. The time-changing profiles of cloud parameters involving vertical velocity (updraft and downdraft), water mixing ratio, and the in-cloud temperature provided physically realistic inputs for the hail growth model.

Using the time-dependent coupled cumulus-hail model technique P greatly improved the forecasting of hail size compared to traditional NOMOGRAM algorithm. This showed that modeling microphysics and cumulus dynamics is of worthy in forecasting hail size.

Finally, there is no extra need to calculate the time duration of updraft and the vertical velocity at the cloud base as the time-dependent cumulus model provided a natural life-cycle of the hailstorm, whereas using a steady-state cloud model in HAILCAST required additional information about these cloud parameters.

In conclusion, it is proved that coupling the time-dependent two-cylinder cumulus model with the hail growth model is a robust numerical technique to forecast maximum hail size. For the purpose to assist operational job, it is expected to provide a useful tool in helping issue hail warnings for weather forecasters.

The maximum hail size forecast using the new coupled model technique depends on accurate proximity soundings that serve as initial data for the cloud model. In future applications of the model technique to assist in issuing hail warnings in operational work, prognostic soundings deprived from regional numerical weather prediction (NWP) models should be used. The newer operational NWP models have spatial resolutions of about ten kilometers. Running the new hail forecasting at each grid point of the NWP model would provide a good coverage of hail fall prediction. A contour map of forecasted maximum hail size on the ground could be obtained. This approach will help forecasters to identify quickly the locations most at risk for hail and to provide an estimate of maximum hail size on the ground. Moreover, it is available to access the prognostic sounding valid for the afternoon, but deprived from outputs of NWP in the morning. Running the hail forecast model in the morning to forecast hail size often occurring in mid to late afternoon is of great significance in alerting forecasters and disseminating severe weather warnings with sufficient lead time in advance of upcoming storms. Sufficient lead time of hail warnings with about 12 hours could be reached by

using prognostic soundings. Combing the model technique with regional NWP soundings would significantly benefit the prevention of hail damage.

7.3 Suggestions for future work

This thesis research addressed the issue of coupling a time-dependent two-cylinder cumulus model with a time-dependent hail growth model forecast maximum hail size at ground. The coupled numerical technique is consisted of three main complementary components. The first is the time-dependent two-cylinder cumulus model, which was the main focus of this thesis study. And the second is the microphysical hail growth model. The last is the coupling of two models, which involves various coupling parameters, for example, time interval of profiles of cloud parameters provided as surrounding conditions for hail growth, and introduction time of hail embryo into the cumulus model, etc. Definitely, there is room for improvements in each of the three parts of the coupled model technique in forecasting maximum hail size.

The first part of incompletes is found in the time-dependent two-cylinder cumulus model. An apparently urgent improvement is to add the tilting effect of wind shear on the storm structure. The present cumulus model used upright two concentric cylinders to represent the updraft and downdraft couplet. However, considering the bulk effect of vertical wind shear and incorporating this effect into the present coupled model technique would produce more realistic representations of storm cloud parameters, which would be benefit for the simulation of hail growth. Typically, the convective available potential energy (CAPE) of instability determines the intensity of storm cloud. However, the vertical wind shear strongly influences the cloud structure and the life duration of cloud. The tilted updraft and downdraft within a wind sheared cloud caused a tilted hail growth trajectory. As a result, the hail growth will be profoundly affected along its tilted trajectory as the hail probably spends more time in updraft and less time in downdraft compared to that in the upright updraft and downdraft storm. Furthermore, the life duration of storm cloud is likely to be longer due to strong vertical wind shear. This still impacts on hail growth.

The microphysics in the time-dependent hail growth model in the coupled model technique includes the assumption that the simulated hail density keeps constant and uniform as the value of $0.9\,gcm^{-3}$. Actually, hailstones generally exhibit a layered structure with transparent or opaque. The different layers represent different growth regimes that the hail enters during its evolution (Macklin, 1977). Investigations have shown that different hailstone layers have different densities that generally fall within the range 0.82 gcm^{-3} and 0.917 gcm^{-3} (List et al., 1970; Prodi, 1970). If these density variations during different growth regimes are incorporated into the hail growth microphysics, the effects of a varying hailstone density on model output parameters can be investigated. Definitely, the mass budget of hail growth will be affected due to changing hail density. As a result, the heat balance of the hail growth could be influenced as the changing of mass budget.

The cumulus model and the hail growth model are coupled by means of a group of parameters, which include introduction time of hail embryo into the cumulus model, initial position in the cumulus cloud, etc. We have found that hail growth is sensitive to these parameters. For example, if a hail embryo is introduced into the cumulus at very early or very late time, it is hard to produce severe hails because insufficient updraft has poor ability to uphold the hail in the hail growth zone for enough growth time. A possible method is to take the updraft velocity at cloud base and the height of the cloud top into consideration together. If these two parameters are complied with particular criteria at a specific time, a hail embryo will be introduced into the storm cloud. Proposed another method is that a hail embryo could be introduced into the storm cloud after the beginning of cumulus model integration at every five minutes. The eventually simulated biggest hail size out of those from different introduction times is selected as forecasted maximum hail size at surface. Admittedly, this execution would definitely increase the computational time for each individual hail case.

REFERENCES

Anthes, R. A., 1977: A cumulus parameterization scheme utilizing a one-dimensional cloud model. *Mon. Wea. Rev.,* **105**, 270-286.

Asai, T., and A. Kasahara, 1967: A theoretical study of the compensating downward motions associated with cumulus clouds. *J. Atmos. Sci.*, **24**, 487-496.

Barge, B. L., and G. A. Isaac, 1973: The shape of Alberta hailstones. *J. Rech. Atmos.*, **7**, 11-20.

Betts, A. K., 1982a: Cloud thermodynamics models in saturation point coordinates. *J. Atmos. Sci.*, **39**, 2182-2191.

Betts, A. K., 1982b: Saturation point analysis of moist convective overturning. *J. Atmos. Sci.*, **39**, 1484-1505.

Bluestein, H. B., E. W. McCaul Jr., G. P. Byrd, and G. R. Woodall, 1988: Mobile sounding observations of a tornado storm near the dryline: The Canadian, Texas storm of 7 May 1986. *Mon. Wea. Rev.*, **116**, 1790-1804.

Boatman, J. F., and A. H. Auer Jr., 1983: The role of cloud top entrainment in cumulus clouds. *J. Atmos. Sci.*, **40**, 1517-1534.

Brandes, E. A., J. Vivekanandan, J. D. Tuttle, and C. J. Kessinger, 1995: A study of thunderstorm microphysics with multiparameter radar and aircraft observations. *Mon. Wea. Rev.*, **118**, 1640-1644.

Brimelow, J. C., 1999: Numerical modelling of hailstone growth in Alberta storms. M.Sc. Thesis, University of Alberta, 153 pp.

Brimelow, J. C., and G. W. Reuter, 2002a: Modeling maximum hail size in Alberta thunderstorms. *Wea. Forecasting,* **17**, 1048-1062.

Brimelow, J. C, T. W. Krauss and G. W. Reuter, 2002b: Operational forecasts of maximum hailstone diameter in Mendoza, Argentina. *J. Wea. Mod.,* **34** 8-17.

Brimelow, J. C, G. W. Reuter and R. Goodson, T. W. Krauss, 2005: Spatial forecasts of maximum hail size using prognostic model soundings and HAILCAST. (*In press*).

Brooks, H. E., C. A. Doswell III, and R. A. Maddox, 1992: On the use of meso-scale and cloud-scale models in operational forecasting. *Wea. Forecasting,* **7,** 120-132.

Brooks, H. E., C. A. Doswell III, and L. J. Wicker, 1993: STORMTIPE: A forecasting experiment using a three-dimensional cloud model. *Wea. Forecasting,* **8,** 352-363.

Brooks, H. E., C. A. Doswell III, and J. Cooper, 1994: On the environments of tornadic and nontornadic mesocyclones. *Wea. Forecasting,* **9,** 606-618.

Browning, K. A., 1977: The Structure and Mechanisms of Hailstorms. *Meteor. Monogr.*, No. 38, Amer. Meteor. Soc., 1-43.

Browning, K. A., and J. G. D. Beimers, 1967: The oblateness of large hailstones. *J. Appl. Meteorol.*, **6**, 1075-1081.

Browning, K. A., and G. B. Foote, 1976: Airflow and hail growth in supercell storms and some implications for hail suppression. *Quart. J. Roy. Met. Soc.*, **102**, 499-533.

Chen, S. H. and W. Y. Sun, 2004: An explicit one-dimensional time-dependent tilting cloud model. *J. Atmos. Sci.*, **61**, 2797-2816.

Chen, S. H. and W. Y. Sun, 2002: A one-dimensional time dependent cloud model. *J. Meteor. Soc. Japan,* **80,** 99-118.

Cheng, L., and D. C. Rogers, 1988: Hailfalls and hailstorm feeder clouds – an Alberta case study. *J. Atmos. Sci.*, **45**, 3533-3545.

Cotton, W. R., and A. A. Anthes, 1989: Storm and cloud dynamics. Academic press. 883 pp, 540-577.

Dennis, A. S., and D. J. Musil, 1973: Calculations of hailstorm growth and trajectories in a simple cloud model. *J. Atmos. Sci.,* **30,** 278-288.

Doswell, C. A., III, J. T. Schaefer, D. W. McCann, T. W. Schlatter, and H. B. Wobus, 1982: Thermodynamic analysis procedures at the National Severe Storms Forecast Center. Preprints, *Ninth Conf. on Weather Forecasting and Analysis*, Seattle, WA, Amer. Meteor. Soc., 304-309.

Edwards, R. and R. L. Thompson, 1998: Nationwide comparisons of hail size with WSR-88D vertically integrated liquid water and derived thermodynamic sounding data. *Wea. Forecasting*, **13**, 277-285.

Emanuel, Kerry A, 1994: Atmospheric convection. Oxford university press. 588 pp, 281-324.

Eng Young, R. G., and K. A. Browning, 1967: Wind tunnel tests of simulated spherical hailstones with variable roughness. *J. Atmos. Sci.*, **24**, 58-62.

English, M., 1973: Alberta Hailstorms. Part II: Growth of large hail in the storm. *Meteor. Monogr.*, No. 36, Amer. Meteor. Soc., 37-98.

Farley, R. D., 1987: Numerical modeling of hailstorms and hailstone growth. Part III: Simulation of an Alberta hailstorm - natural and seeded cases. *J. Climate Appl. Meteor.*, **26,** 789-812.

Federer, B., J. Jouzel, and A. Waldvogel, 1978: Hailstone trajectories determined from crystallography, deuterium content and radar backscattering. *Pageoph.*, **116**, 112-129.

Foote, G. B., 1984: A study of hail growth utilizing observed storm conditions. *J. Climate and Appl. Meteor.*, **23**, 84-101.

Garcia-Garcia, F., and R. List, 1992: Laboratory measurements and parameterizations of supercooled water skin temperatures and bulk properties of gyrating hailstones. *J. Atmos. Sci.*, **49**, 2058-2073.

Geresdi, I., 1998: Idealised simulation of the Colorado hailstorm: Comparison of bulk and detailed microphysics. *Atmos. Res.*, **45**, 237-252.

Greenan, B. J., and R. List, 1995: Experimental closure of the heat and mass transfer theory of spheroidal hailstones. *J. Atmos. Sci.*, **52**, 3797-3815.

Guan, S., and G. W. Reuter, 1996: Numerical simulation of an industrial cumulus affected by heat, moisture and CCN released from an oil refinery. *J. Appl. Meteor.*, **35**, 1257-1264.

Haines, P. A., and W. Y. Sun, 1994: A convective cloud model for use in a cumulus parameterization scheme. *Mon. Wea. Rev.*, **122,** 165-182.

Henry, S.G., 1993: Analysis of thunderstorm lifetime as a function of size and intensity. Preprints, *26th Conf. on Radar Metero.,* Norman, OK, Amer. Meteor. Soc., 138-140.

Heymsfield, A. J., A. R. Jameson, and H. W. Frank, 1980: Hail growth mechanisms in a Colorado storm. Part III: Hail formation processes. *J.Atmos. Sci.*, **37**, 1789-1807.

Http://datalib.library.ualberta.ca/AHParchive/

Joe, P., D. Burgess, R. Potts, T. Keenan, G. Stumpf, and A. Treloar, 2004: The S2K severe weather detection algorithms and their performance. *Wea. Forecasting,* **2,** 43-63.

Kessler, E., 1969: On the distribution and continuity of water substance in atmospheric circulation. *Meteor. Monogr.,* Amer. Meteor. Sco., **32,** 84 pp.

Kitzmiller, D.H., W.E. McGovern, and R.F. Saffle, 1995: The WSR-88D severe weather potential algorithm. *Wea. Forecasting,* **4**, 141-159.

Knight, C. A., and N. C. Knight, 1970a: Hailstone Embryos. *J. Atmos. Sci.*, **27**, 659-666.

Knight, C. A., and N. C. Knight, 1970b: Lobe Structures of Hailstones. *J. Atmos. Sci.*, **27**, 667-671.

Knight, C. A., and N. C. Knight, 1978: Cylindrical ice accretions as simulations of hail growth: II. The structure of fresh and annealed accretions. *J. Atmos. Sci.*, **35**, 1997-2009.

Knight, N. C., 1981: Climatology of hailstone embryos. *J. Appl. Meteor.*, **20**, 750-755.

Krauss, T. W., and J. D. Marwitz, 1984: Precipitation processes within an Alberta supercell hailstorm. *J. Atmos. Sci.*, **41**, 1025-1033.

Kubesh, R. J., D. J. Musil, R. D. Farley, and H. D. Orville, 1988: The 1 August 1981 CCOPE storm: Observations and modeling results. *J. Appl. Meteor.*, **27,** 216-243.

Lenning, E., H.E. Fuelberg, and A.I. Watson, 1989: An evaluation of WSR-88D severe hail algorithms along the northeastern gulf coast. *Wea. Forecasting,* **3**, 1029-1045.

Lesins, G. B., and R. List, 1986: Sponginess and drop shedding of gyrating hailstones in a pressure-controlled icing wind tunnel. *J. Atmos. Sci.*, **43**, 2813-2825.

Levi, L., and L. Lubart, 1998: Modeled spongy growth and shedding process for spheroidal hailstones. *Atmos. Res.*, **48**, 59-68.

List, R., J.-G. Cantin, and M. G. Ferland, 1970: Structural Properties of Two Hailstone Samples. *J. Atmos. Sci.*, **27**, 1080-1090.

List, R., B. J. W. Greenan, and F. García-García, 1995: Surface temperature variations of gyrating hailstones and effects of pressure-temperature coupling on growth. *Atmos. Res.*, **38**, 161-175.

Macklin, W. C., 1977: The characteristics of natural hailstones and their interpretation. *Hail: A Review of Hail Science and Hail Suppression Meteor. Monog., No. 38*, Amer. Meteor. Soc., **16**, 65-88.

Matson, R. J., and A. W. Huggins, 1980: The direct measurement of the sizes, shapes and kinematics of falling hailstones. *J. Atmos. Sci.*, **37**, 1107-1125.

Miller, L.J., J.D.Tuttle, and C.A. Knight, 1988: Airflow and hail growth in a severe Northern High Plains supercell. *J. Atmos. Sci.,* **45,** 736-762.

Miller, L. J., J. D. Tuttle, and G. B. Foote, 1990: Precipitation production in a large

Montana hailstorm: Airflow and particle growth. *J. Atmos. Sci.*, **57**, 1619-1646.

Moore, J. T., and J. P. Pino, 1990: An interactive method for estimating maximum hailstone size from forecast soundings. *Wea. Forecasting,* **13**, 1078-1092.

Mueller, C.K., J.W. Wilson, and N.A. Crook, 1993: The utility of sounding and mesonet data to nowcast thunderstorm initiation. *Wea. Forecasting*, **8**, 132-146.

Murphy, A.H., 1993: What is good forecast? An essay on the nature of goodness in weather forecasting. *Wea. Forecasting,* **8**, 281-293.

Murphy, A.H., 1991: Forecast verification: its complexity and dimensionality. *Mon. Wea. Rev.,* **119,** 1590-1601.

Murphy, A.H., and Winkler, R., 1987: A general framework for forecast verification. *Mon. Wea. Rev.* **115,** 1330-1338.

Musil, D. J., 1970: Computer modeling of hailstone growth in feeder clouds. *J. Atmos. Sci.*, **26**, 474-482.

Nelson, S. P., 1983: The influence of storm flow structure on hail growth. *J. Atmos. Sci.*, **40,** 1965-1983.

Orville, H. D., and F. J. Kopp, 1977: Numerical simulation of the life history of a hailstorm. *J. Atmos. Sci.*, **34**, 1596-1618.

Ranger, C. G., 2003: Numerical modeling of the evolution of oblate hailstones in Alberta thunderstorms. M. Sc. Thesis, University of Alberta, 151pp.

Rasmussen, R.M., and A.J. Heymsfield, 1987a: Melting and shedding of graupel and hail. Part I: Model physics. *J. Atmos. Sci.,* **44,** 2754-2764.

Rasmussen, R.M., and A.J. Heymsfield, 1987b: Melting and shedding of graupel and hail. Part II: Sensitivity study. *J. Atmos. Sci.,* **44,** 2764-2782.

Rasmussen, R.M., and A.J. Heymsfield, 1987b: Melting and shedding of graupel and hail. Part III: Investigation into the role of shed drops as hail embryos in the 1 August CCOPE serer storm. *J. Atmos. Sci.,* **44,** 2783-2830.

Renick, J.H., and J.B. Maxwell, 1977: Forecasting hailfall in Alberta hail. A review of hail science and hail suppression. *Meteor. Monogr.,* No. 38, Amer. Meteor. Sci., 145-151.

Reuter, G. W. and S. Guan, 1995: Effects of industrial pollution on cumulus convection rain showers: a numerical study. *Atmospheric Environment*, **29**, 2467-2474.

Rogers, R. R. and M. K. Yau, 1989: A short course in cloud physics, 3rd Ed. Butterworth-Heinemann, 290 pp, 235-268.

Sanders, F., and A. J. Garrett, 1975: Application of a convective plume model to prediction of thunderstorms. *Mon. Wea. Rev.*, **103**, 874-877.

Simpson, J., and V. Wiggert, 1969: Models of precipitating cumulus towers. *Mon. Wea. Rev.*, **97**, 471-489.

Smith, S. B., and M. K. Yau, 1993a: The causes of severe convective outbreaks in Alberta. Part I: A comparison of a severe outbreak with two nonsevere events. *Mon. Wea. Rev.*, **121,** 1099-1125.

Smith, S. B., and M. K. Yau, 1993b: The causes of severe convective outbreaks in Alberta. Part Π: Conceptual model and statistical analysis. *Mon. Wea. Rev.*, **121,** 1126-1134.

Smith, S. B., G. W. Reuter and M. K .Yau, 1998: The episodic occurrence of hail in central Alberta and the Highveld of South Africa. *Atmos. Ocean*, **36**, 169-178.

Soong, S. T., 1974: Numerical simulation of warm rain development in an axisymmetric cloud model. *J. Atmos. Sci.*, **31**, 1262-1285.

Soong, S. T., and Y. Ogura, 1973: A comparison between axisymmetric and slab-symmetric cumulus cloud model. *J. Atmos. Sci.*, **30**, 879-893.

Srivastava, R. C., 1967: A study of the effect of precipitation on cumulus dynamics. *J. Atmos. Sci.*, **24**, 36-45.

Vali, G., and E.J. Stansbury, 1965: Time-dependent characteristics of the heterogeneous nucleation of ice. Sci. Rep., MW-41, McGill University, Montreal, 31 pp.

Wisner, C., H. D. Orville, and C. Meyers, 1972: A numerical model of a hail-bearing cloud. *J. Atmos. Sci.*, **29**, 1160-1181.

Witt, A., M. D. Eilts, G. J. Stumpf, J. T. Johnson, E. D. Mitchell, and K. W. Thomas, 1998: An enhanced hail detection algorithm for the WSR-88D. *Wea. Forecasting*, **13**, 286-303

Xu, J. L., 1983: Hail growth in a three-dimensional cloud model. *J. Atmos. Sci.*, **40**, 185-203.

Yao, M. K., 1980: A two-cylinder model of cumulus cells and its application in computing cumulus transports. *J. Atmos. Sci.*, **37**, 2470-2485.

Yao, M. K., 1980: The effects of evaporation, water load and wind shear on cloud

development in a three-dimensional numerical model. *J. Atmos. Sci.*, **37**, 488-494.

Yao, M. K., 1979: Perturbation pressure and cumulus convection. *J. Atmos. Sci.*, **36**, 690-694.

Yao, M. K., and P. M. Austin, 1979: A model for hydrometeor growth and evolution of raindrop size spectra in cumulus cells. *J. Atmos. Sci.*, **36**, 655-668.

Appendix A: List of used symbols

Symbol	meaning
a	radius of inner cylinder
A	any variable
b	radius of outer cylinder
B	buoyancy
c	ventilation coefficient
C_d	dragging coefficient
C_i	specific heat of ice (cal g^{-1} K^{-1})
C_p	specific heat at constant pressure
C_w	Specific heat of water (cal g^{-1} K^{-1})
d	diffusivity
D	hail diameter (cm)
D_f	final hail diameter on the ground (cm)
D_i	initial size of hail embryo
D_0	observed hail size
E_i	collection efficiency of the accreted ice crystals
E_{cw}	collection efficiency of the accreted cloud water
E_{rw}	collection efficiency of the accreted rain water
g	gravitational acceleration
H	extent of vertical boundary
$\tilde{i}$	cloud parameters ($\tilde{w}, \tilde{\theta}, \tilde{q}_v, \tilde{q}_c, \tilde{q}_r$) at inner boundary layer
K	thermal conductivity
K_{AC}	Auto-conversion rate
L_f	latent heat of freezing at 0°C
L_s	latent heat of sublimation
L_v	latent heat of evaporation.
M	Mass of hailstone
M_i	mass of accreted ice per unit time interval
M_w	mass of accreted liquid water per unit time interval
P_0	basic state pressure
q_c	cloud water mixing ratio
q_r	rain water mixing ratio
q_v	water vapor mixing ratio

q_s	saturation mixing ratio respect to liquid water
R	idealized gas constant
S	heating and cooling terms
t	time
T	temperature
T_c	in-cloud temperature
T_s	hailstone's surface temperature
T_v	virtual temperature
$\vec{u}$	three-dimensional velocity vector
$\tilde{u}$	radial velocity at the edge of the inner cylinder
V_r	terminal velocity of rain water
V_t	terminal velocity of hailstone
w	vertical velocity
z	vertical coordinate
Z	height position of hailstone
π_0	nondimensional pressure
ρ_0	basic state density of air
ρ_{00}	air density at standard pressure P_{00} (1000 hPa) 0.001 gcm^{-3}
θ	potential temperature
θ_v	virtual potential temperature
θ_{v0}	basic state virtual potential temperature
Θ	vertically averaged constant potential temperature
τ_C	cloud life time
τ_f	hail growth time
τ_i	introduction time of hail embryo into the model cloud
τ_d	time interval for the profiles of cloud parameters

Appendix B: Equations for outer cylinder

The cumulus model consists of tow concentric cylinders in geometrics. Prevailing updraft in inner cylinder is compensated by the down draft in outer cylinder. Appling average operators concerning cross-section area for outer cylinder and along the boundary layers to vertical velocity equation and water substance conservation equations, the equations for outer cylinder can be obtained. All quantities are horizontal averages. Like wisely described for inner cylinder, the overbar will be dropped.

$$\sigma^2 w_a + (1-\sigma^2) w_b = 0,\ \sigma = \frac{a}{b}$$

$$\frac{\partial \theta_b}{\partial t} - \frac{2a}{(b^2-a^2)} \tilde{u}_a \tilde{\theta}_a + \frac{1}{\rho_0}\frac{\partial}{\partial z}\rho_0 \theta_b w_b = \alpha [COND - EVPC - EVPR]_b$$

$$\frac{\partial q_{vb}}{\partial t} - \frac{2a}{(b^2-a^2)} \tilde{u}_a \tilde{q}_{va} + \frac{1}{\rho_0}\frac{\partial}{\partial z}\rho_0 q_{vb} w_b = \frac{1}{\rho_0}[EVPC + EVPR - COND]_b$$

$$\frac{\partial q_{cb}}{\partial t} - \frac{2a}{(b^2-a^2)} \tilde{u}_a \tilde{q}_{ca} + \frac{1}{\rho_0}\frac{\partial}{\partial z}\rho_0 q_{cb} w_b = \frac{1}{\rho_0}[COND - AC - CC - EVPC]_b$$

$$\frac{\partial q_{rb}}{\partial t} - \frac{2a}{(b^2-a^2)} \tilde{u}_a \tilde{q}_{ra} + \frac{1}{\rho_0}\frac{\partial}{\partial z}\rho_0 q_{rb}(w_b - V_{rb}) = \frac{1}{\rho_0}[AC + CC - EVPR]_b$$

To distinguish variables valid for inner and outer cylinders, sub-denotes a and b are used to represent the quantities for inner and outer cylinders. In comparison, variables used for inner cylinder in equation (2.4) and (2.5) omitted all subscripts.

Appendix C: Modified upstream method

The modified upstream method was used to discrete the cumulus equations. This method is available to avoid unphysical negative values at a grid point without resorting to other techniques like 'hole-filling'.

On the equations with the form $\frac{\partial Q}{\partial t}+\frac{2}{a}\tilde{u}\tilde{Q}+\frac{1}{\rho_0}\frac{\partial}{\partial z}(\rho_0 wQ)=S$, which are equations for potential temperature, water vapor mixing ratio, cloud water and rain water mixing ratio listed in (2.4), the finite difference scheme for grid volume j is written as

$$\frac{\partial Q}{\partial t}=(Q_j^{n+1}-Q_j^n)/\Delta t$$

$$\frac{2}{a}\tilde{u}\tilde{Q}=\frac{2}{a}\tilde{u}_j^{n+\frac{1}{2}}Q_j^n$$

$$\frac{1}{\rho_0}\frac{\partial}{\partial z}(\rho_0 wQ)=\frac{1}{\rho_{oj}}(\rho_{0j+\frac{1}{2}}w_{j+\frac{1}{2}}^{n+\frac{1}{2}}Q^*_{j+\frac{1}{2}}-\rho_{0j-\frac{1}{2}}w_{j-\frac{1}{2}}^{n+\frac{1}{2}}Q^*_{j-\frac{1}{2}})/\Delta z$$

$$S=S_j^n$$

The rules for evaluating $\tilde{Q}_j^n$, $Q^*_{j+\frac{1}{2}}$, $Q^*_{j-\frac{1}{2}}$ are:

If $\tilde{u}_j^{n+\frac{1}{2}}\le 0$, $\tilde{Q}_j^n=(Q_b)_j^n$

If $\tilde{u}_j^{n+\frac{1}{2}}>0$, $\tilde{Q}_j^n=(Q_a)_j^n$

If $w_{j+\frac{1}{2}}^{n+\frac{1}{2}}\le 0$, $Q^*_{j+\frac{1}{2}}=Q_{j+1}^n$

If $w_{j+\frac{1}{2}}^{n+\frac{1}{2}}>0$, $Q^*_{j+\frac{1}{2}}=Q_j^n$

For the vertical velocity equation in inner cylinder, the formation in (2.4) is rewritten as below format

$$\frac{\partial w_a}{\partial t}+\frac{2}{a}\tilde{u}_a\tilde{w}_a+\frac{1}{\rho_0}\frac{\partial}{\partial z}(\rho_0 w_a w_a)=g(\frac{\theta_{va}-\theta_{v0}}{\Theta}-q_{ca}-q_{ra})$$

The following form of the finite difference analog will be used to march from $w^{n-\frac{1}{2}}$ to $w^{n+\frac{1}{2}}$ (subscript dropped):

$$\frac{w^{n+\frac{1}{2}}_{j+\frac{1}{2}}-w^{n-\frac{1}{2}}_{j+\frac{1}{2}}}{\Delta t}+\frac{2}{a}\tilde{u}^{n-\frac{1}{2}}_{j+\frac{1}{2}}\tilde{w}^{n-\frac{1}{2}}_{j+\frac{1}{2}}+\frac{1}{\rho_{0j+\frac{1}{2}}}(\rho_{0j+1}w^{n-\frac{1}{2}}_{j+1}w^{*}_{j+1}-\rho_{0j}w^{n-\frac{1}{2}}_{j}w^{*}_{j})/\Delta z$$

$$=g(\frac{\theta^{n}_{v_{j+\frac{1}{2}}}-\theta^{n}_{v0_{j+\frac{1}{2}}}}{\Theta^n}-q^{n}_{c_{j+\frac{1}{2}}}-q^{n}_{r_{j+\frac{1}{2}}})$$

If a variable is not calculated explicitly at a point, a simple average will be used. For example,

$$w_j=\frac{1}{2}(w_{j+\frac{1}{2}}+w_{j-\frac{1}{2}}),\qquad Q_{j+\frac{1}{2}}=\frac{1}{2}(Q_j+Q_{j+1})$$

Furthermore,

$$w^{*}_{j+1}=w_{j+\frac{1}{2}}\qquad \text{if}\qquad w_{j+\frac{1}{2}}>0$$

$$w^{*}_{j+1}=w_{j+\frac{3}{2}}\qquad \text{if}\qquad w_{j+\frac{1}{2}}\le 0$$

The star * represents variables at the time step of n.

FIGURES

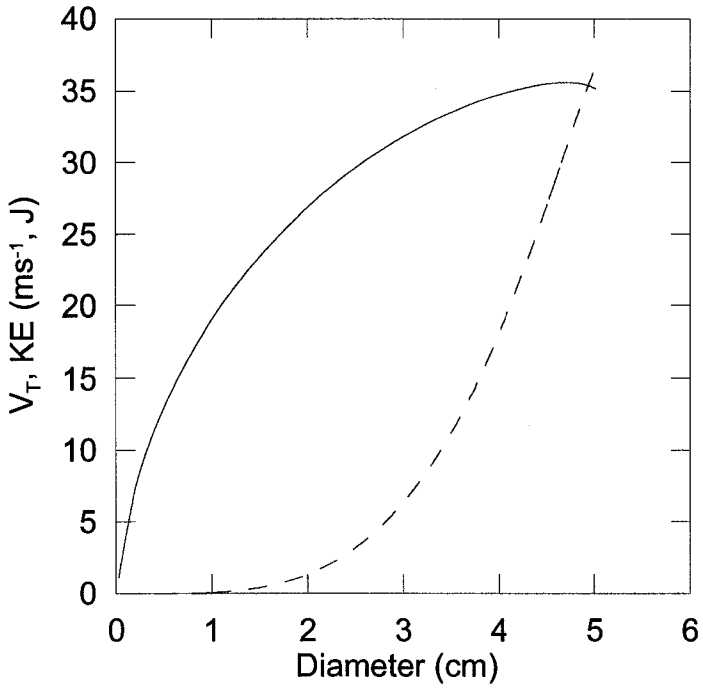

Figure1.1: A hailstone's kinetic energy (KE) denoted using dashed line and terminal velocity change with the hail diameter.

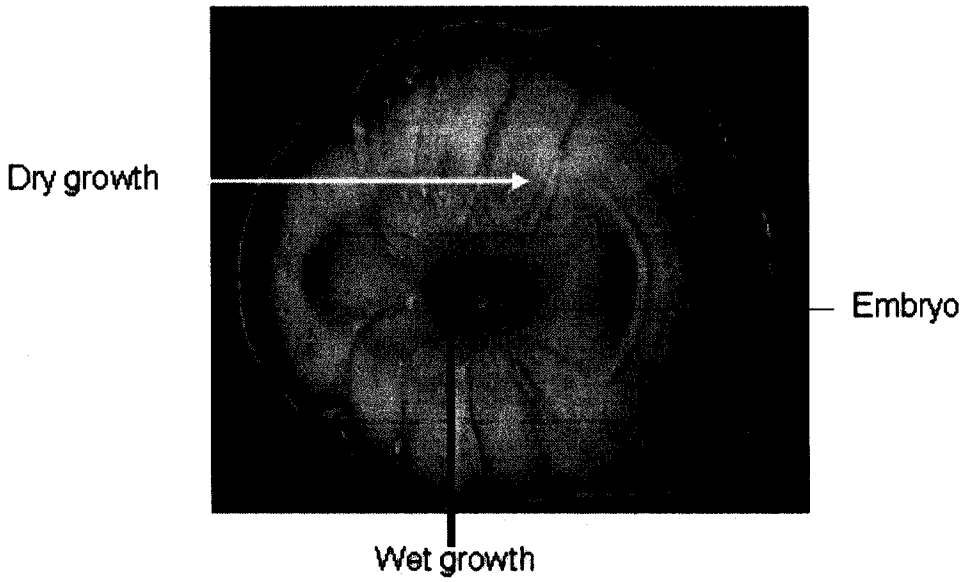

Figure 1.2: A cut sample of hailstone showing different thin sections. Note of Analysis: Dominance of dry growth, Feathering in dry growth regime. Wet growth within most outside layers, Possible frozen droplet embryo.

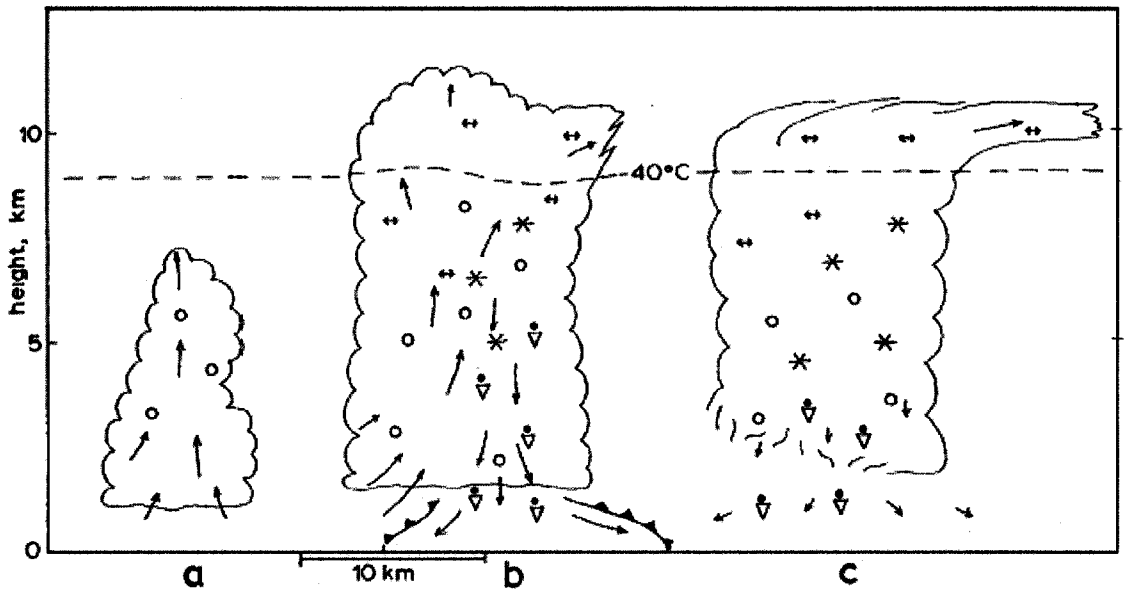

Figure 1.3: The life cycle of a local thunderstorm, showing different stages of development of a thunderstorm cell. Hail growth is affected by the cloud conditions and hail microphysics. → Wind, longer arrow for faster wind. ○ Cloud drops. ↔ Ice crystals. ∇ Rain drops. * Hail. ▲▲▲ downburst boundary. After Dusan Djuric (1994).

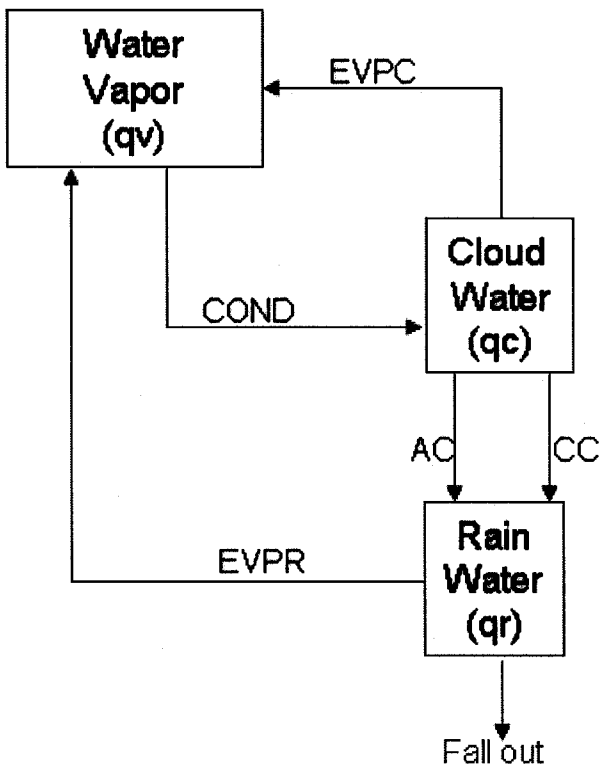

Figure 2.1: Schematic structures for basic microphysical processes in the cumulus model.

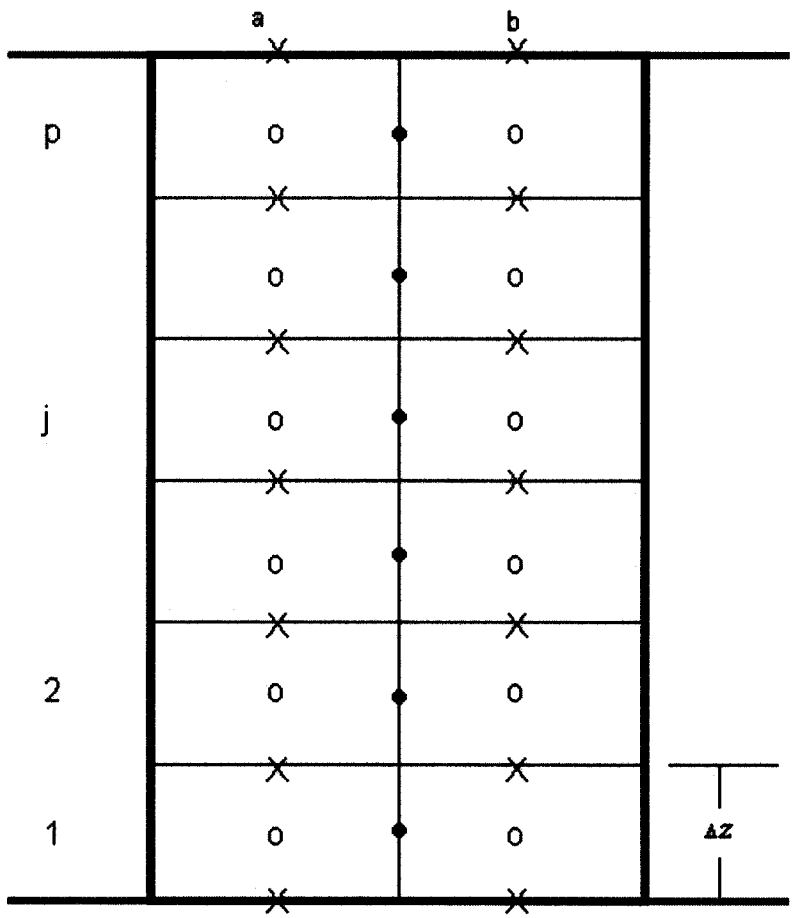

Figure 2.2: The schematic diagram for staggered grid points. There are p grid volumes numbered from 1 to p. This gives $\Delta z = H / p$. w is solved at the ×points, $\tilde{u}$ at the • points, and all other variables at the o points.

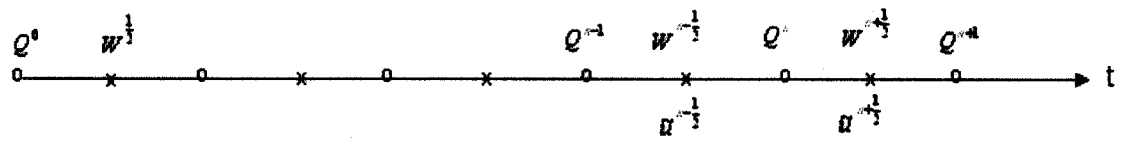

Figure 2.3: The schematic diagram for the time staggering. w and $\tilde{u}$ are calculated at a different time relative to other variables Q (θ, q_v, q_c, q_r).

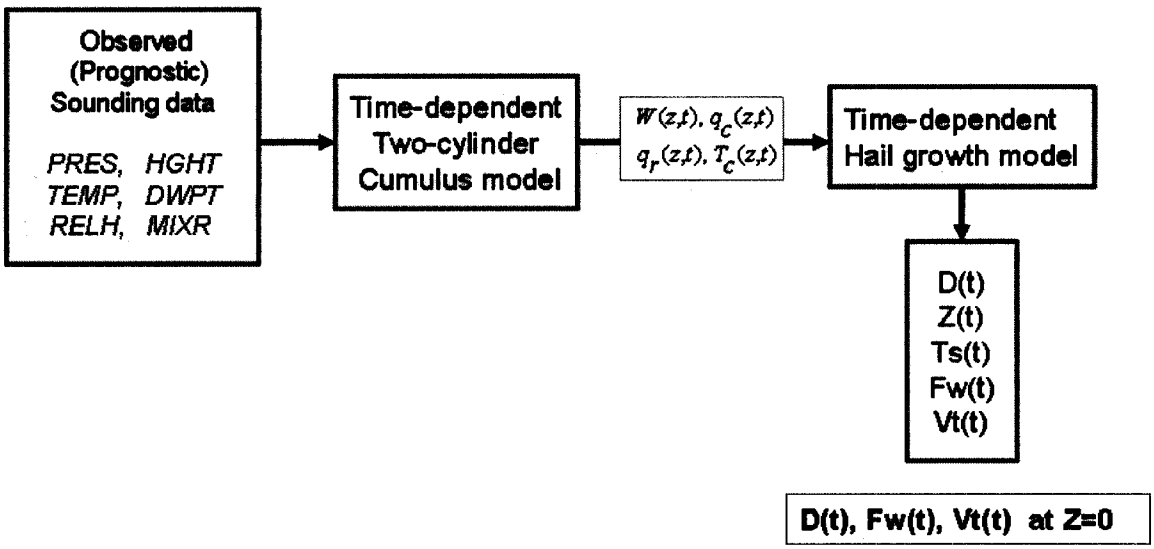

Figure 2.4: The schematic diagram for coupling procedure.

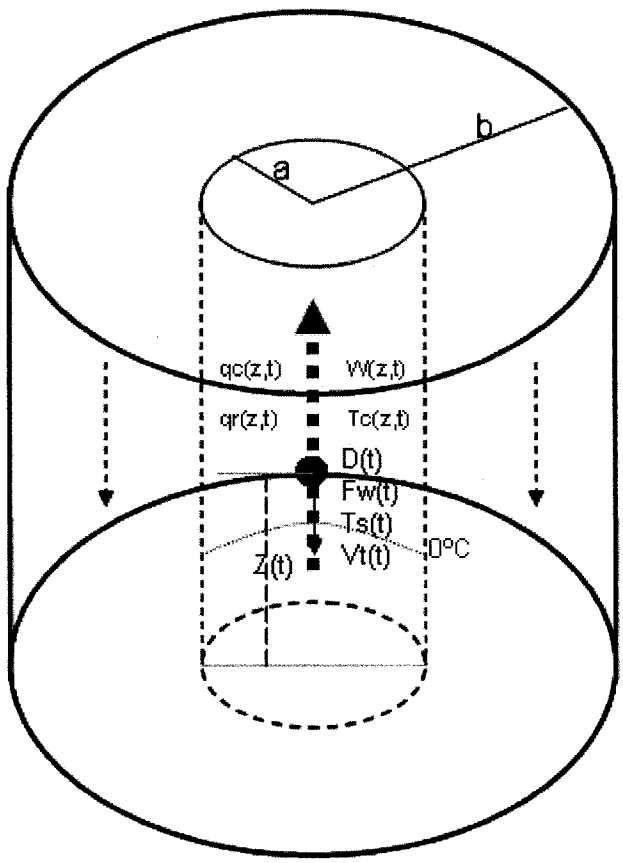

Figure 2.5: The schematic structure for coupling the cumulus model with hail growth model.

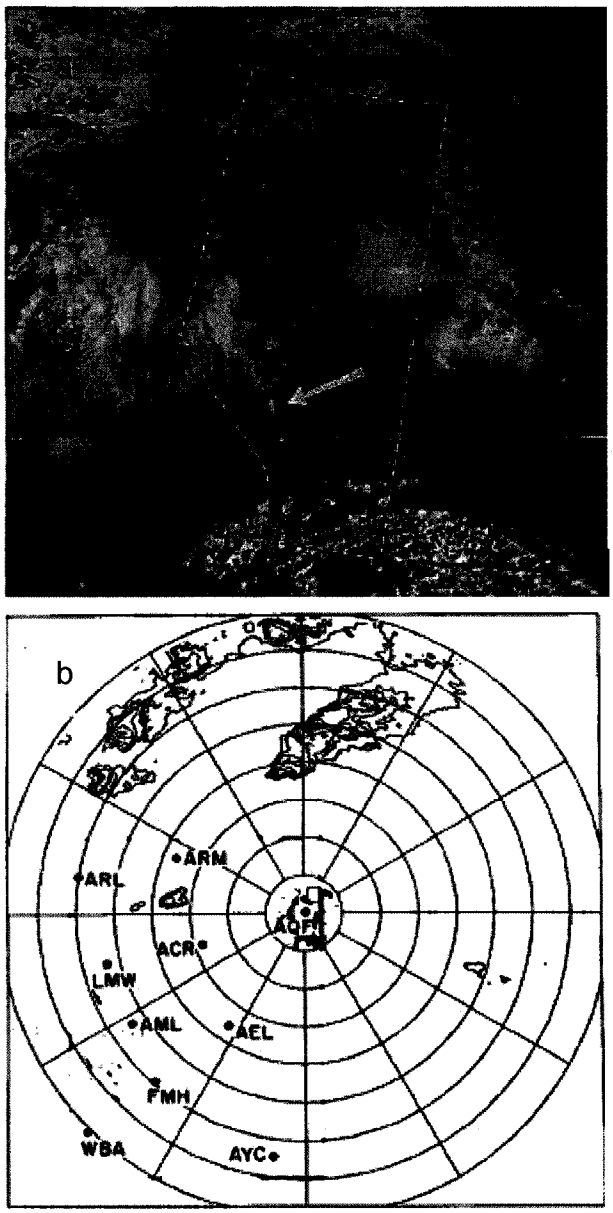

Figure 3.1: (a), infrared satellite imagine of Alberta taken from a NOAA polar-orbiting satellite at 1534 LDT 11 July 1985. White arrow indicates line of towering cumulus clouds that formed over the Alberta foothills. And (b), radar PPI observed from Red Deer (AQF) at 19 LDT for 11 July 1985. Range markers are spaced 20 km apart. Contours are of radar reflectivity with interval of 10 dBZ. Minimum contour is 20 dBZ. Elevation angle is 1.8°. The weak ground echoes near 240°, at a range of 120-140 km, are from the higher peaks in the Alberta foothills. Abbreviations like AQF, AYC etc represent mesoscale observation network stations for this year's experiment.

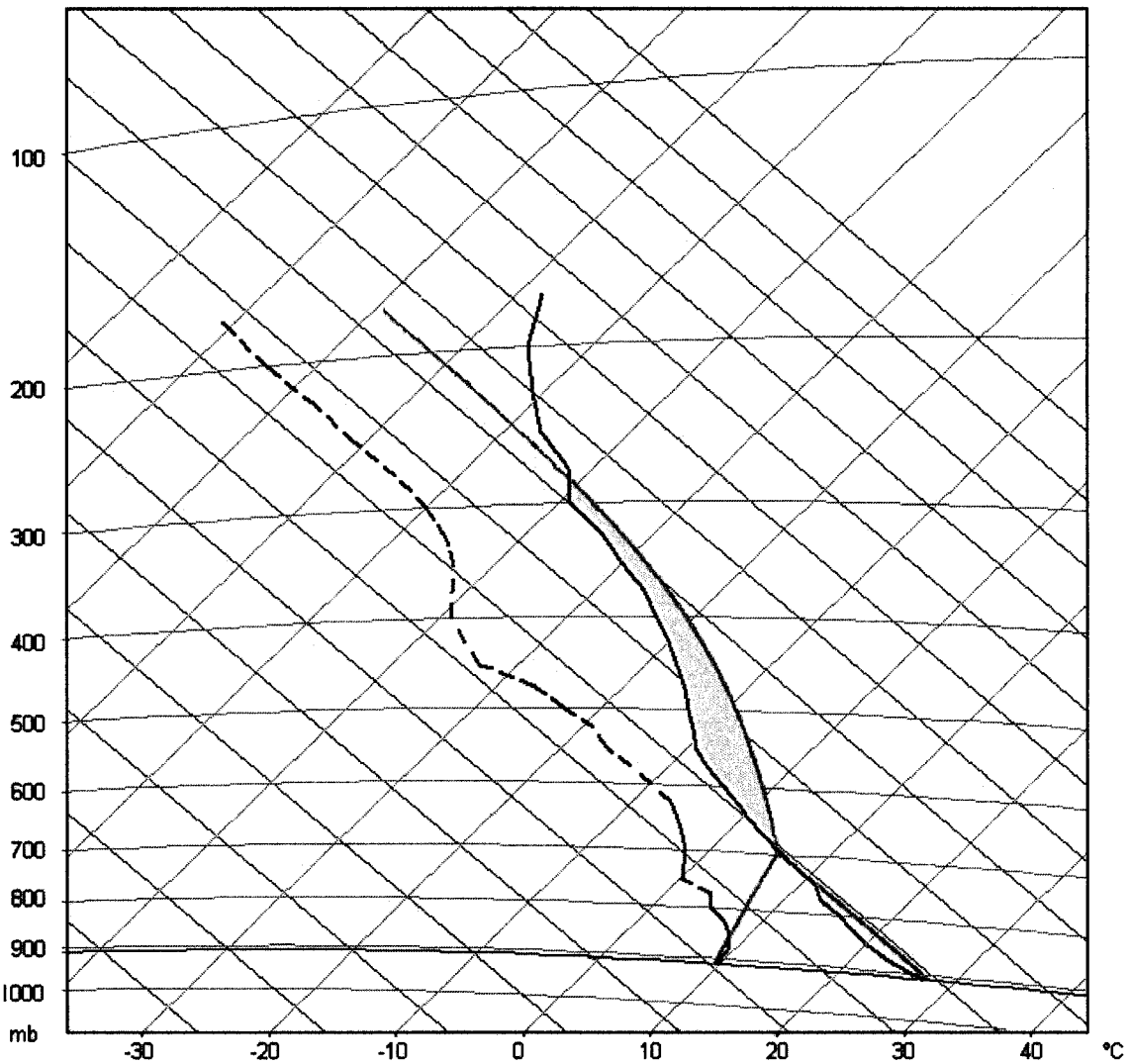

Figure 3.2: Upper-air sounding released from Penhold at 1715 LDT on 11 July 1985 plotted on a tephigram. The dashed green line represents the dew point profile, the solid red line is the environmental temperature, and the curved solid blue line denotes the pseudoadiabat based on the observed surface temperature and dew point. Pink area means the CAPE.

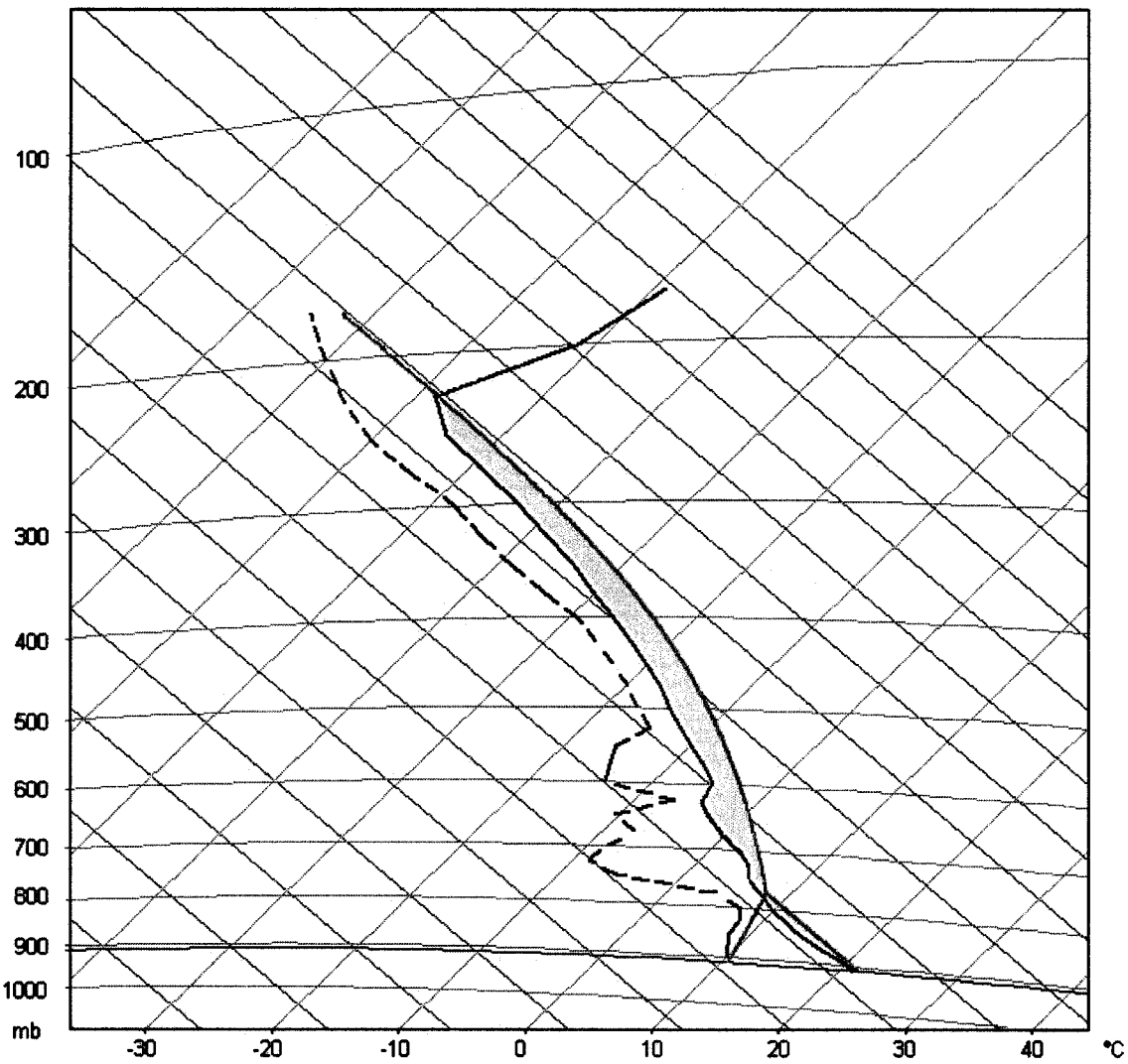

Figure 3.3: Upper-air sounding released from Penhol at 1715 LDT on 24 August 1983 plotted on a tephigram. The dashed green line represents the dew point profile, the solid red line is the environment temperature, and the curved solid blue line denotes the pseudoadiabat based on the observed surface temperature and dew point. Pink area means the CAPE.

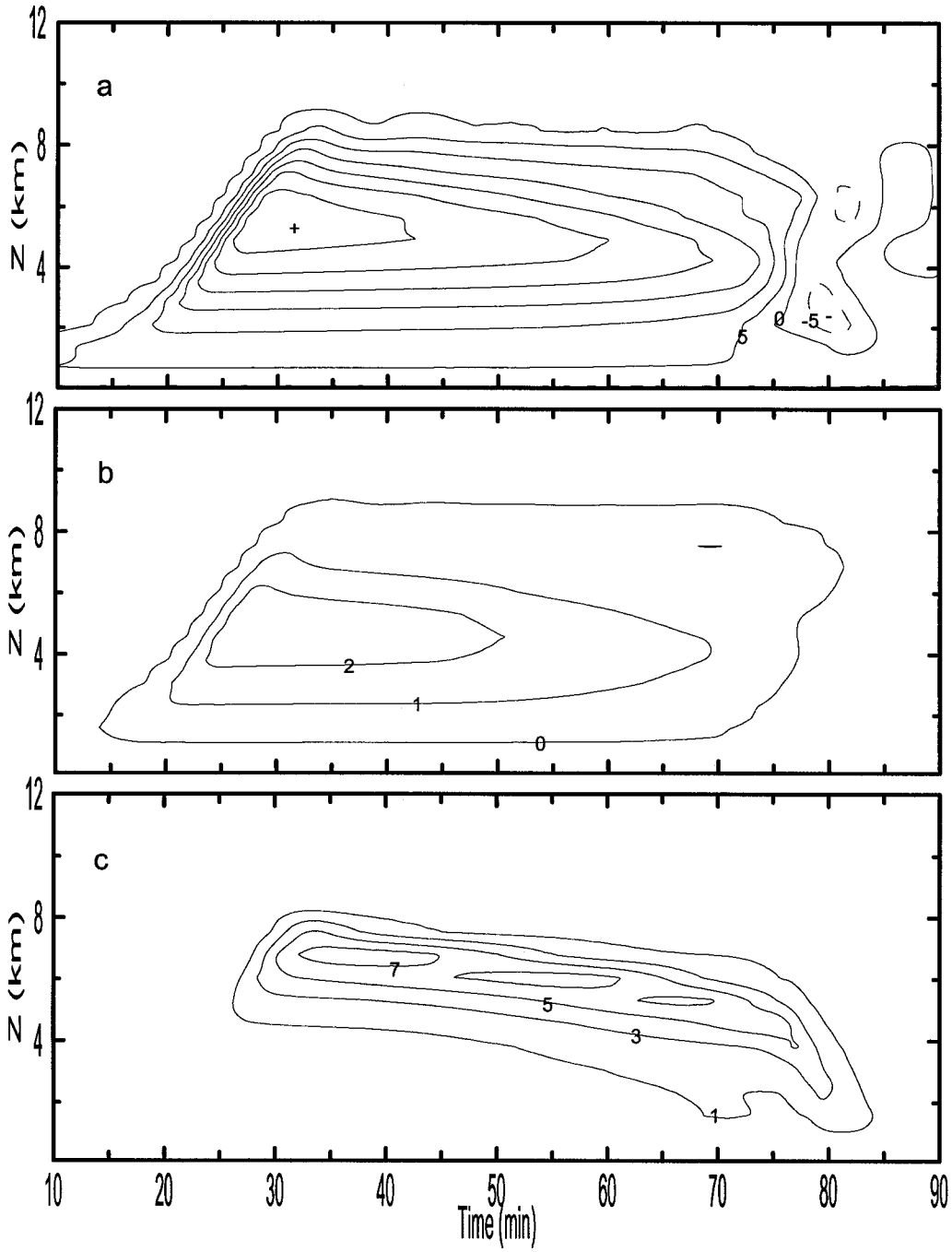

Figure 3.4: Model-derived cloud parameters plotted with height and time for the day of 11 July 1985. Contour maps: (a) Vertical velocity in ms^{-1} with interval of $5\,ms^{-1}$. Solid line and dashed line represent updraft and downdraft. Positive and negative signs denote updraft and downdraft cores. (b) Cloud water mixing ratio in gkg^{-1}. (c) Rain water mixing ratio in gkg^{-1}.

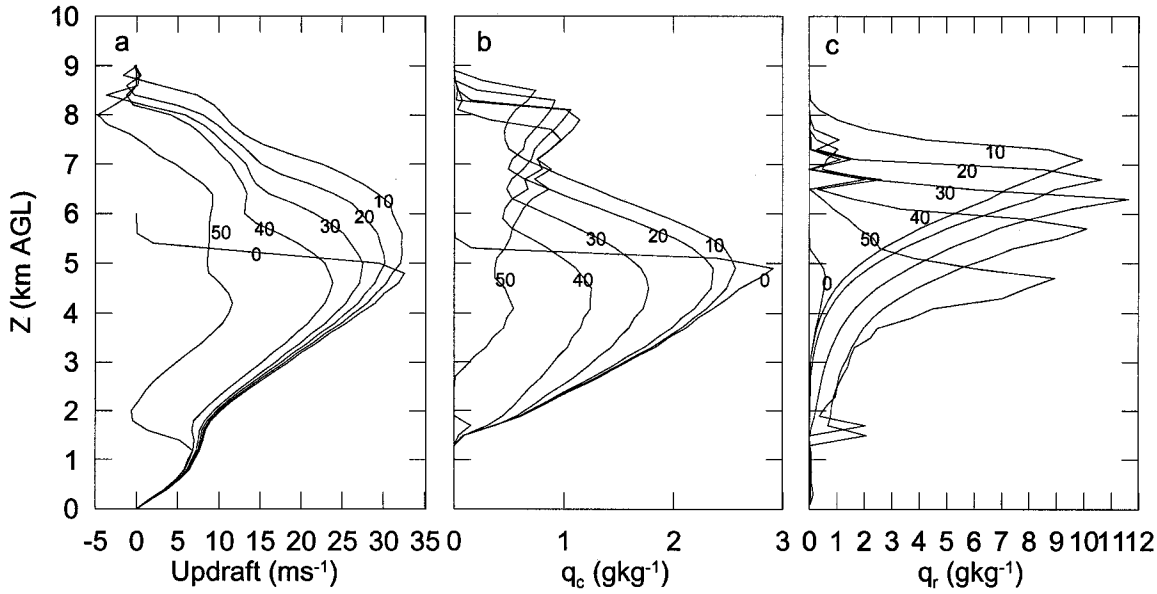

Figure 3.5: Profiles of cumulus cloud parameters used as surrounding conditions for hail growth at different time in the coupled model with precipitating effect for the case of 11 July 1985. (a) Updraft in m/s, (b) cloud water in g/kg, and (c) rain water in g/kg. Numbers on the lines represent the time in minute after the hail embryo is introduced.

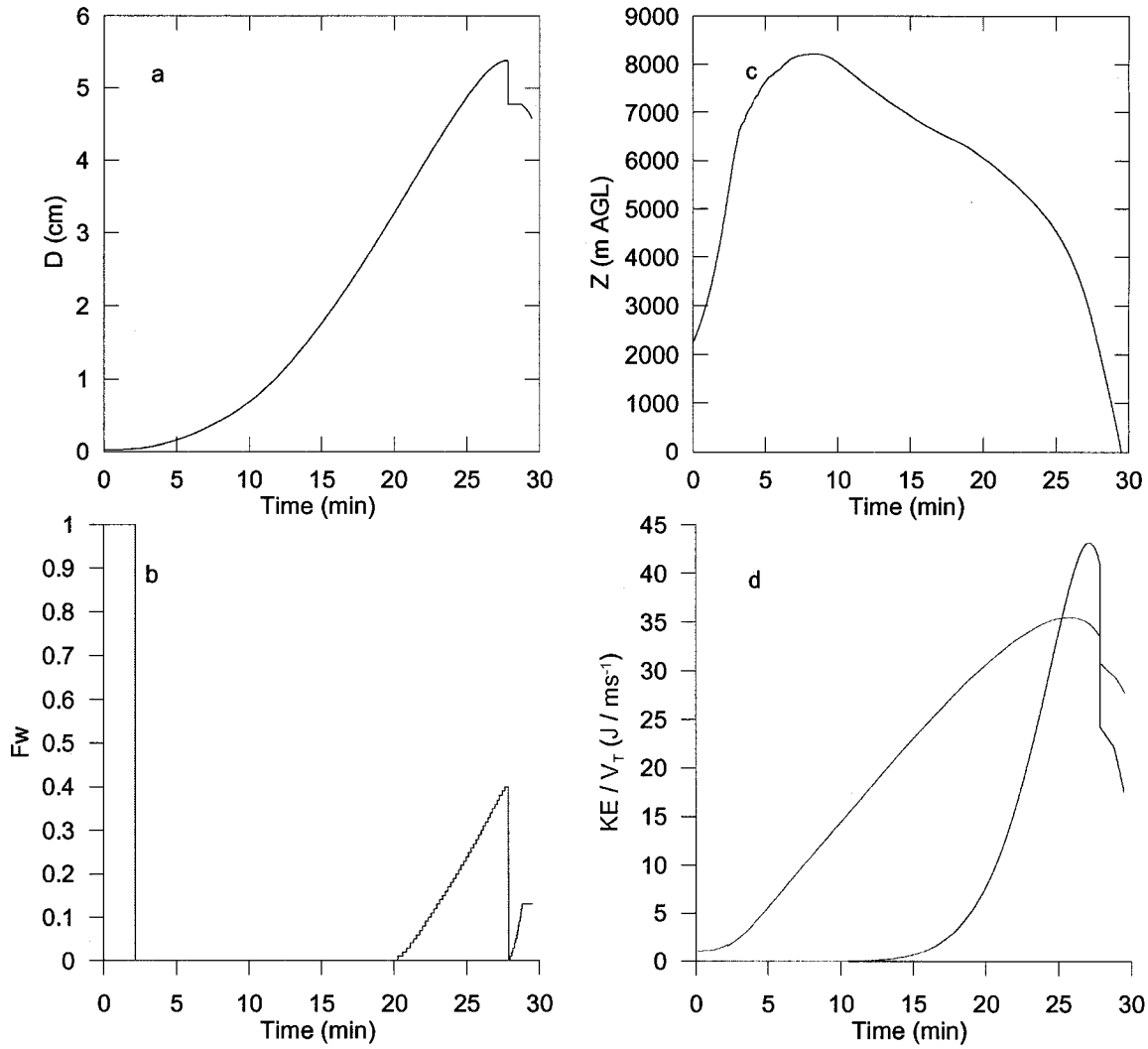

Figure 3.6: Growth time history of hailstone modeled using the coupled cumulus-hail model for the case of July 11 1985. Depicted figures are (a) hail diameter D, (b) fraction of water on the hail, (c) the height of hail, and (d) the terminal velocity V_T and kinetic energy KE (red) of hailstone.

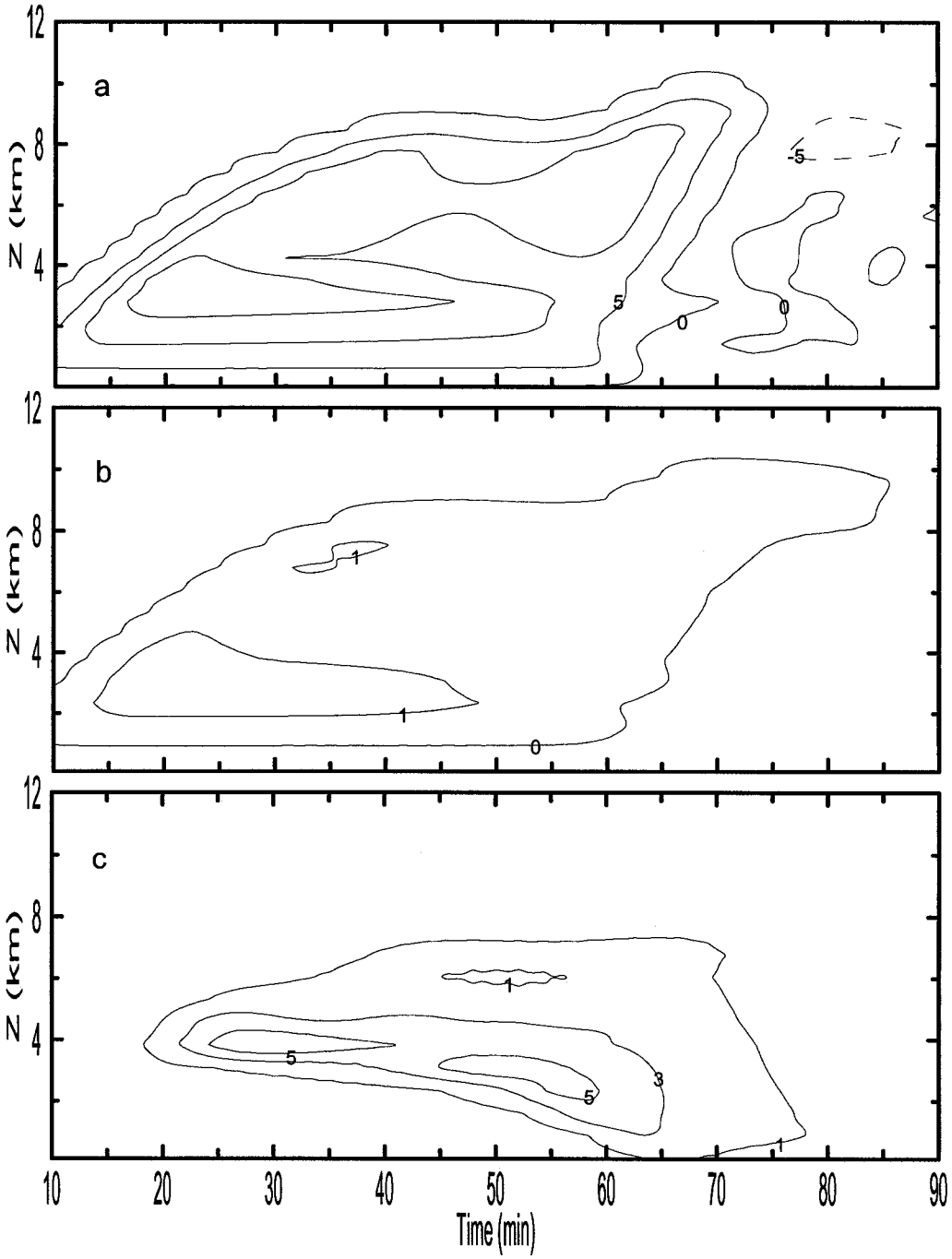

Figure 3.7: Model-derived cloud parameters plotted with height and time for the day of 24 August 1983. Contour maps: (a) Vertical velocity in ms^{-1} with interval of $5\,ms^{-1}$. Solid line and dashed line represent updraft and downdraft. (b) Cloud water mixing ratio in gkg^{-1}. (c) Rain water mixing ratio in gkg^{-1}.

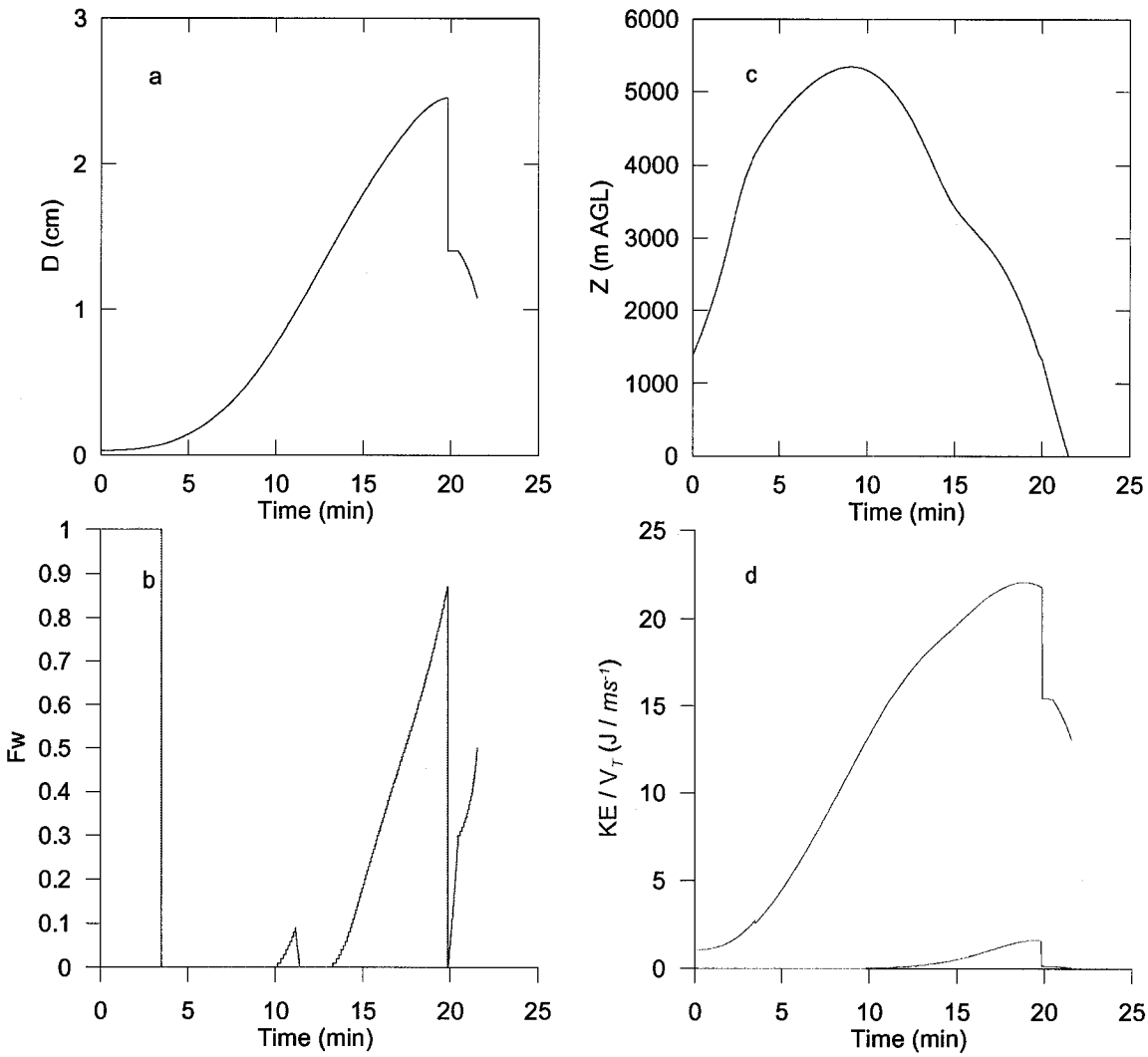

Figure 3.8: Hail growth history for the case of 24 August 1983.
($D_f = 1.1cm, \tau_f = 22\min$).

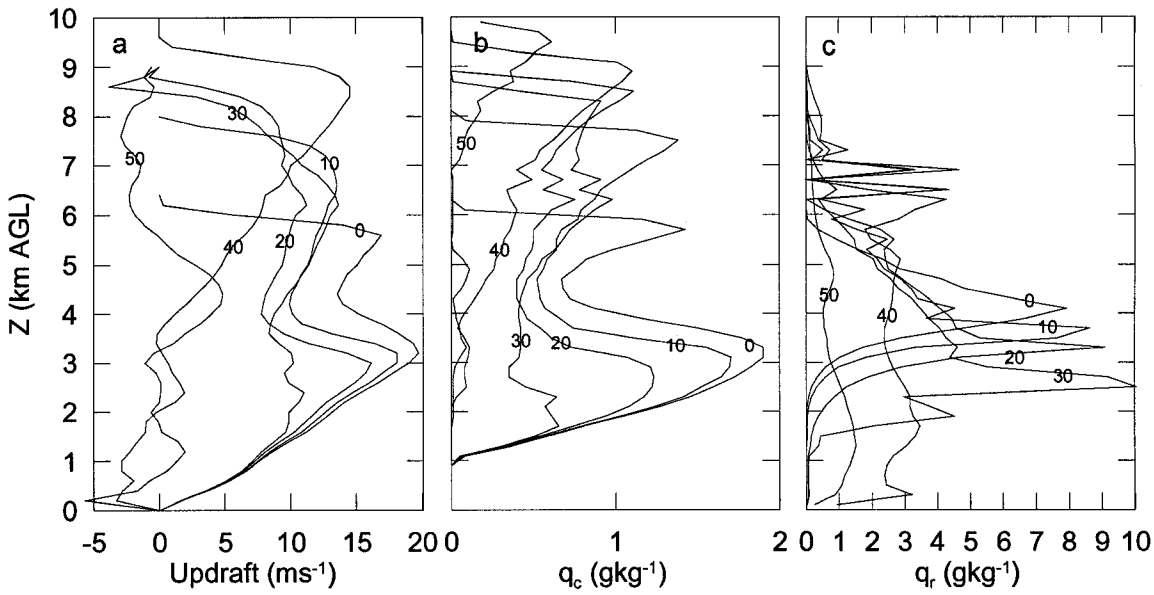

Figure 3.9: Profiles of cumulus cloud parameters used as surrounding conditions for hail growth at different time in the coupled model with precipitating effect for the case of 24 August 1983. (a) updraft in ms^{-1}, (b) cloud water in gkg^{-1}, and (c) rain water in gkg^{-1}. Numbers on the lines represent the time in minute after the hail embryo is introduced.

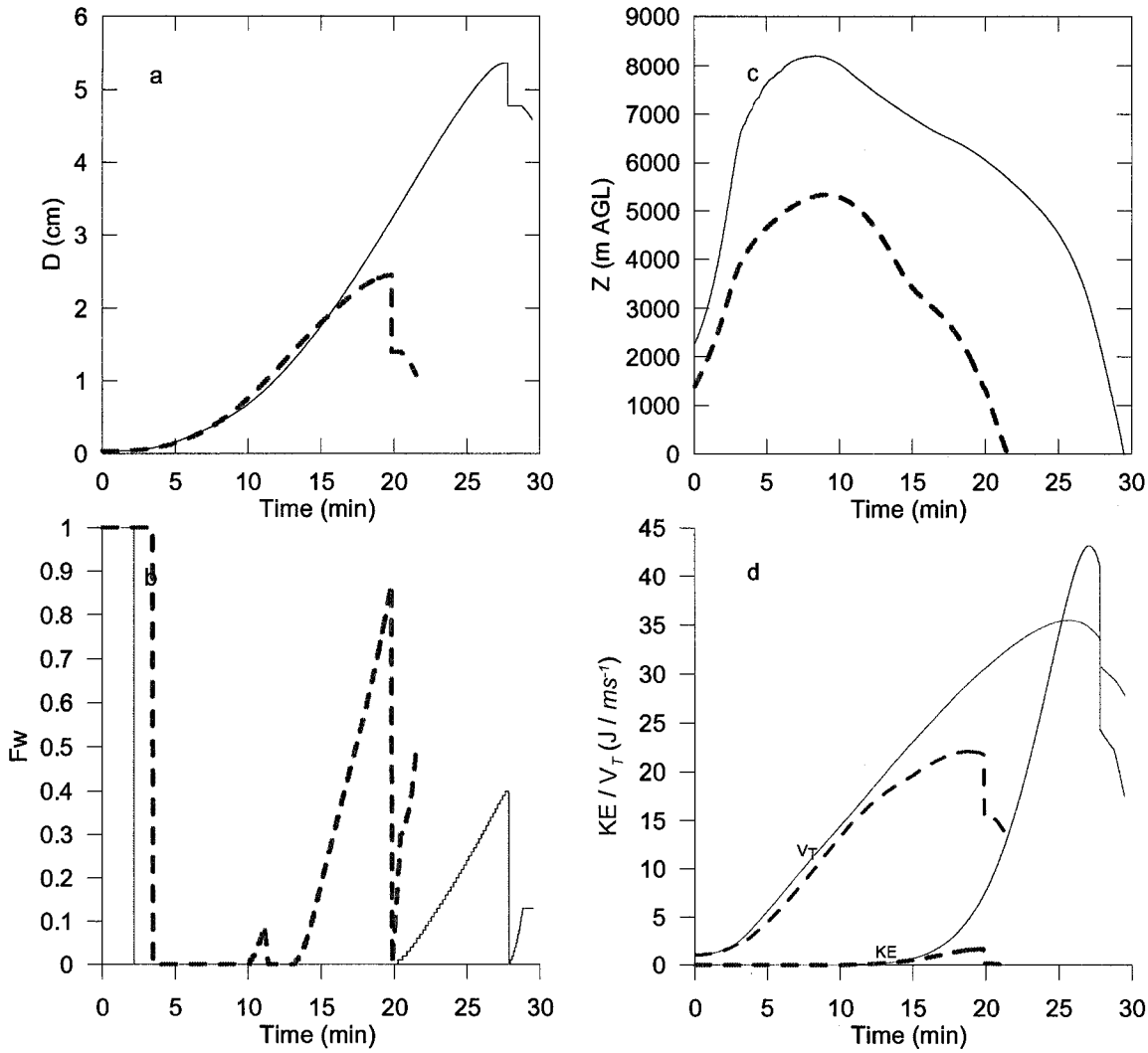

Figure 3.10: Comparison between two cases of 11 July 1985 and 24 August 1983 (dashed lines) using the time-dependent coupled cumulus-hail model technique considering precipitation effects.

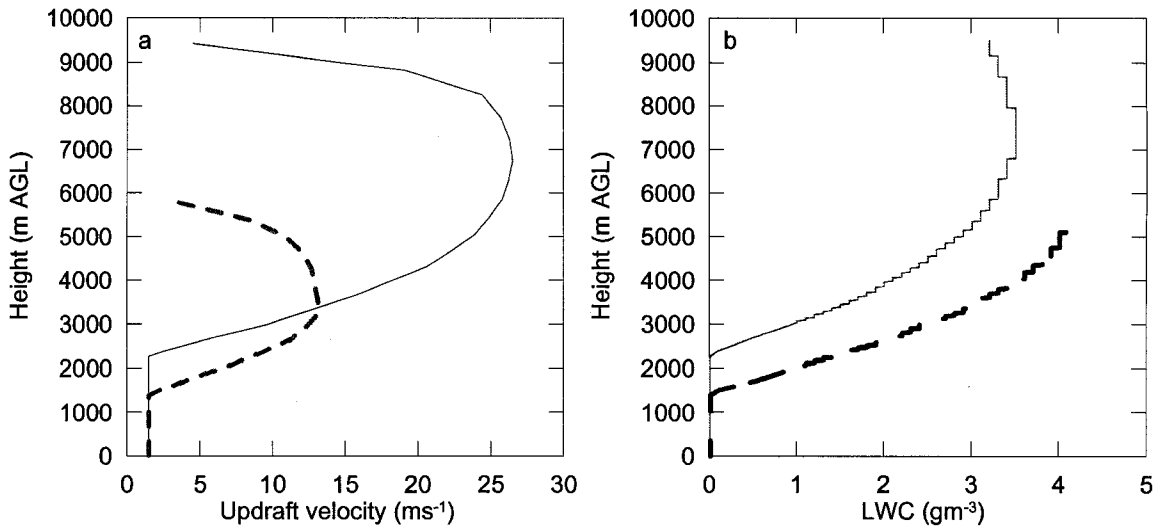

Figure 3.11: HAILCAST model-derived profiles of (a) updraft velocity and (b) liquid water content (LWC) for the cases of 11 July 1985 and 24 August 1983 (dashed lines).

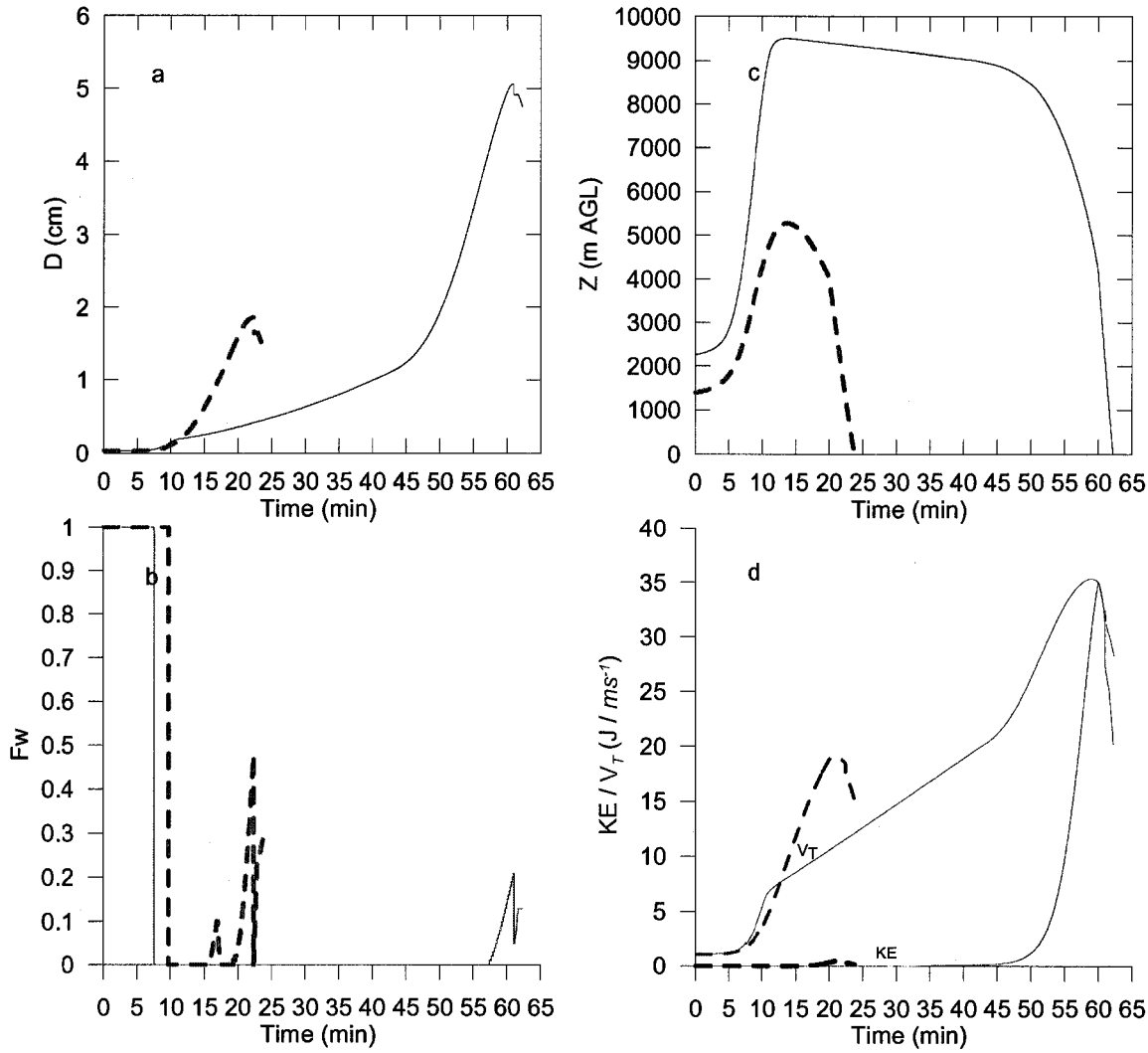

Figure 3.12: Hail growth history simulated using HAILCAST. (a) hail size D, (b) fraction of water, (c) trajectory of hail height Z, and (d) terminal velocity and KE for the cases of 11 July 1985 and 24 August 1983 (dashed lines).

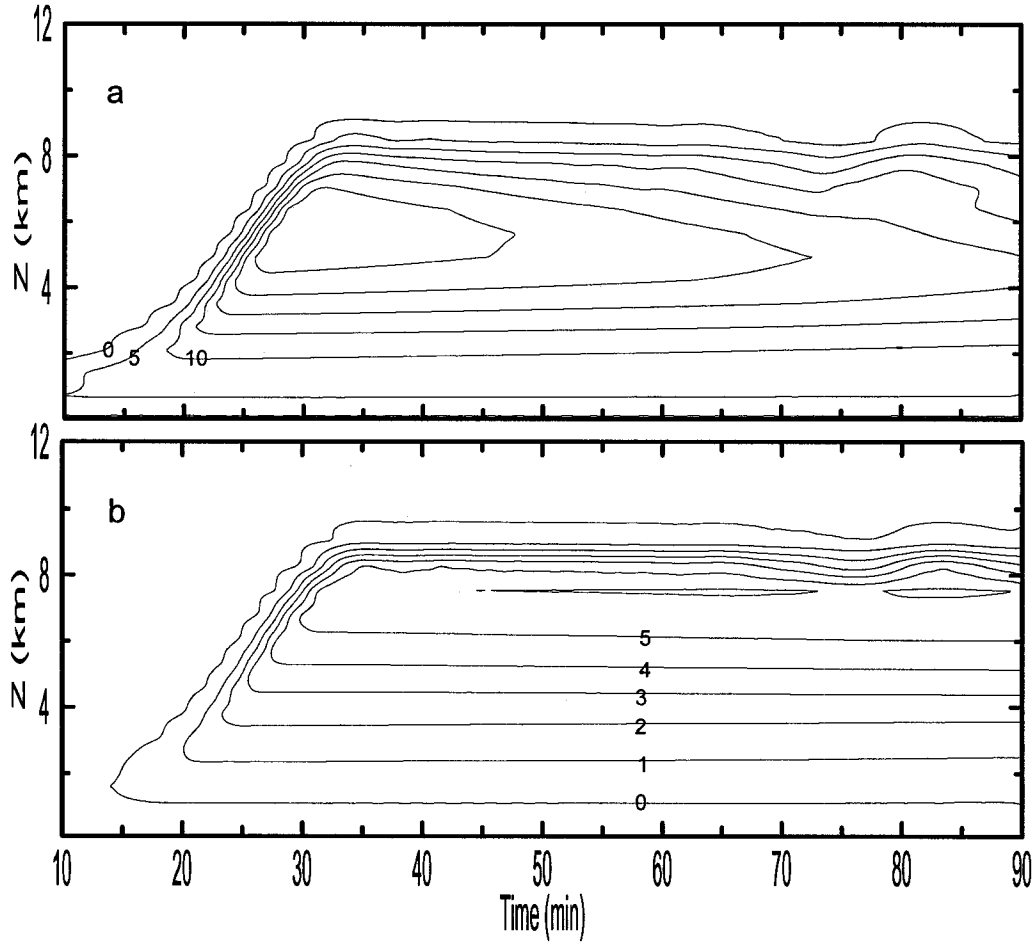

Figure 4.1: Model-derived cloud parameters plotted with height and time for the case of 11 July 1985, precipitation effects were switched off in the model running of F. (a) Vertical velocity in ms^{-1} with the interval of $5\,ms^{-1}$ beginning from zero, and (b) Cloud water mixing ratio in gkg^{-1}.

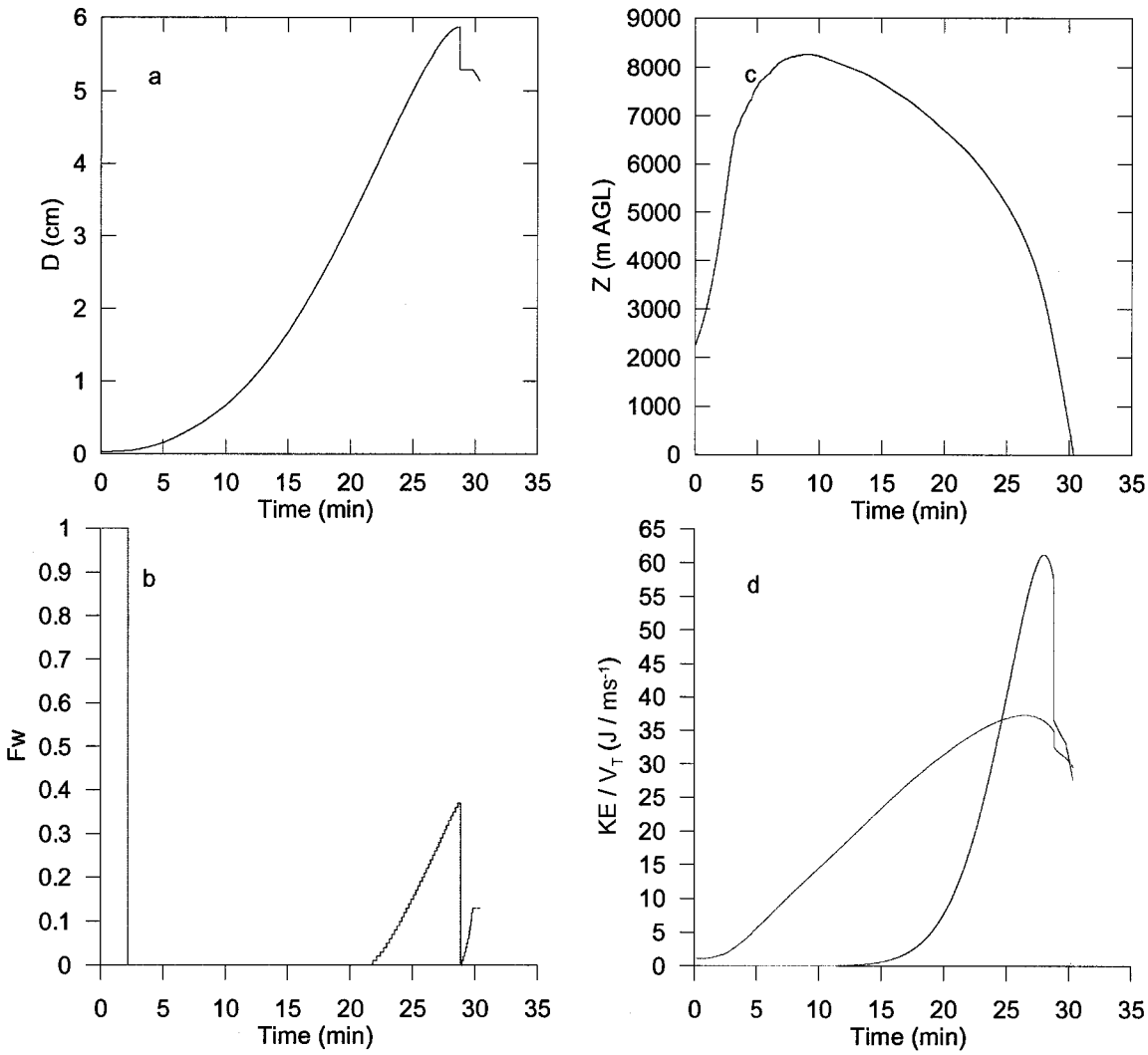

Figure 4.2: Hail growth history simulated using F without precipitation for the case of 11 July 1985. (D_f=5.13 cm, τ_f=30 min).

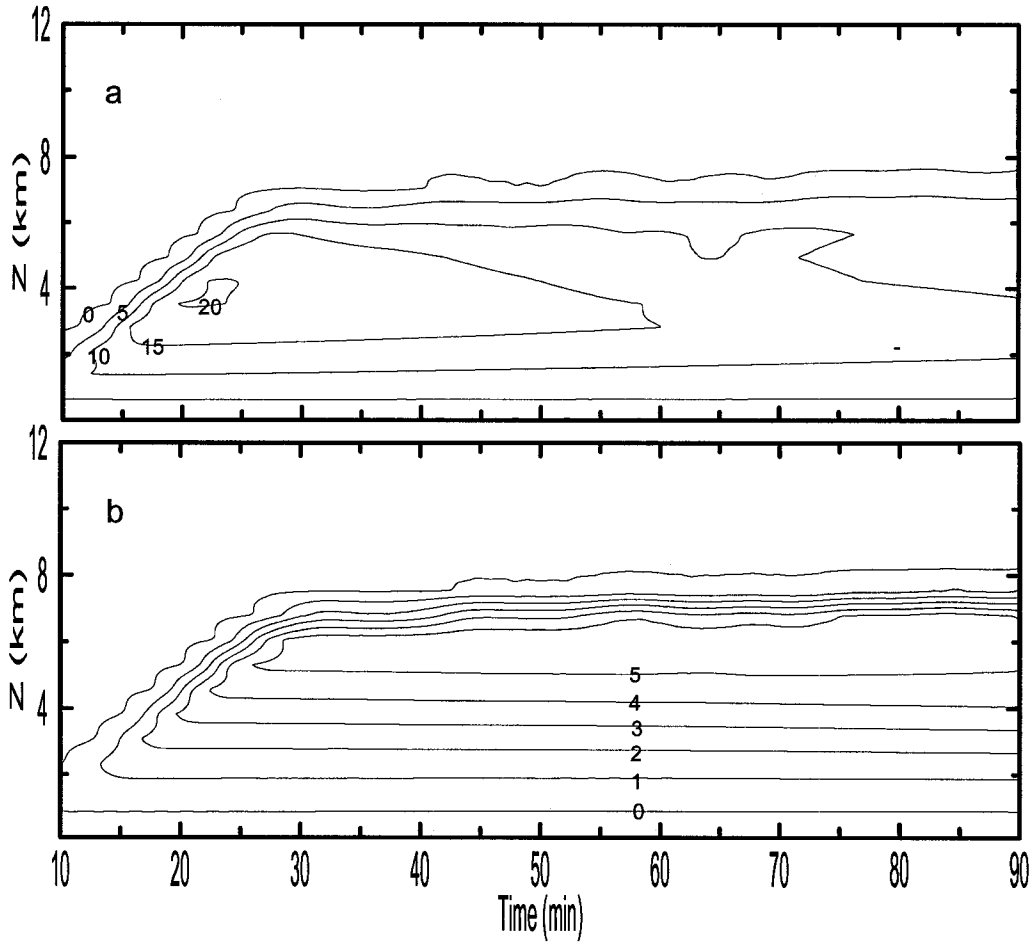

Figure 4.3: Model-derived cloud parameters plotted with height and time for the case of 24 August 1983, precipitation effects were switched off in the model running of F. (a) Vertical velocity in ms^{-1} with the interval of $5\,ms^{-1}$ beginning from zero, and (b) Cloud water mixing ratio in gkg^{-1}.

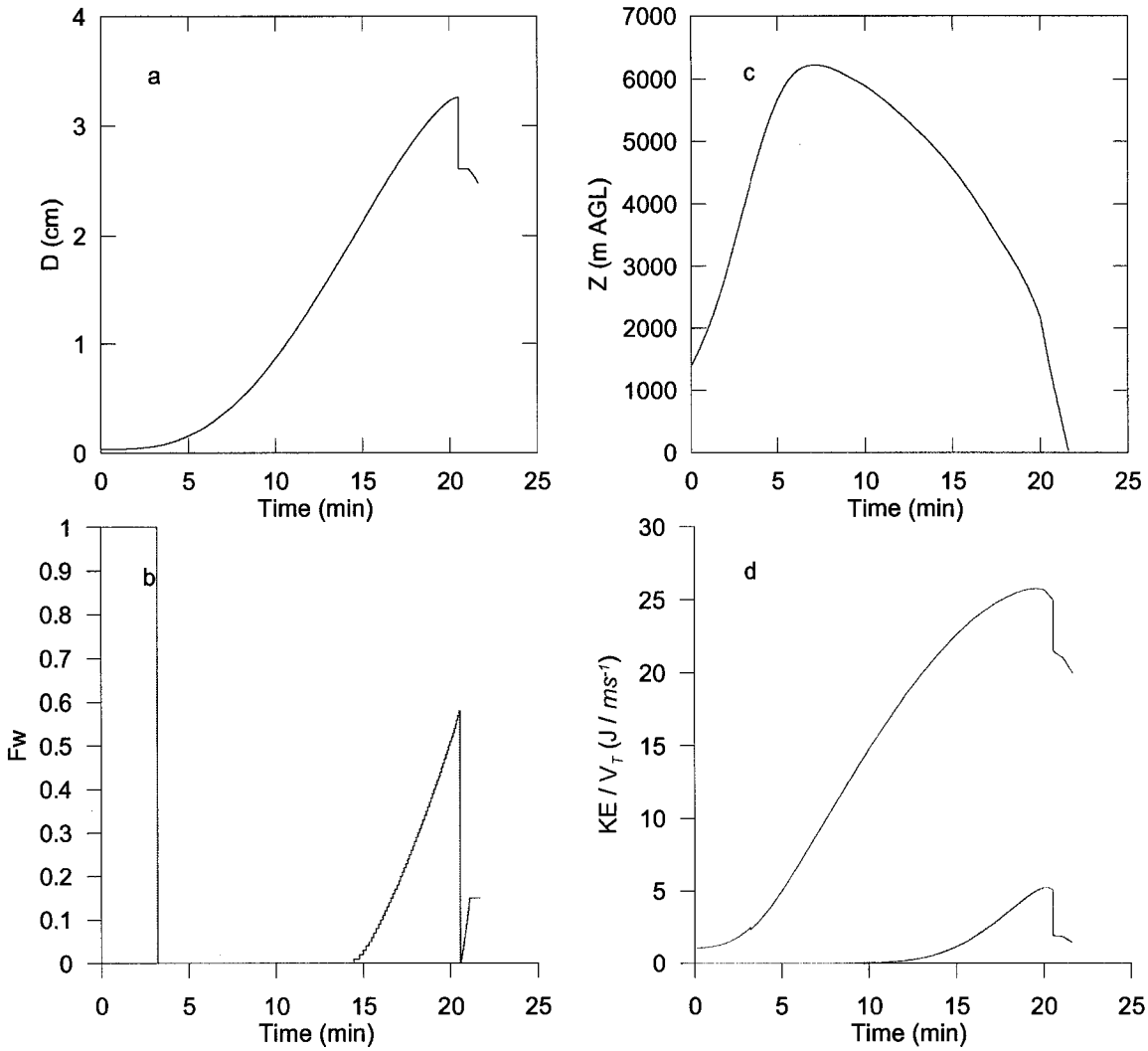

Figure 4.4: Hail growth history for the case of 24 August 1983 using F. (D_f=2.5 cm, τ_f=22 min).

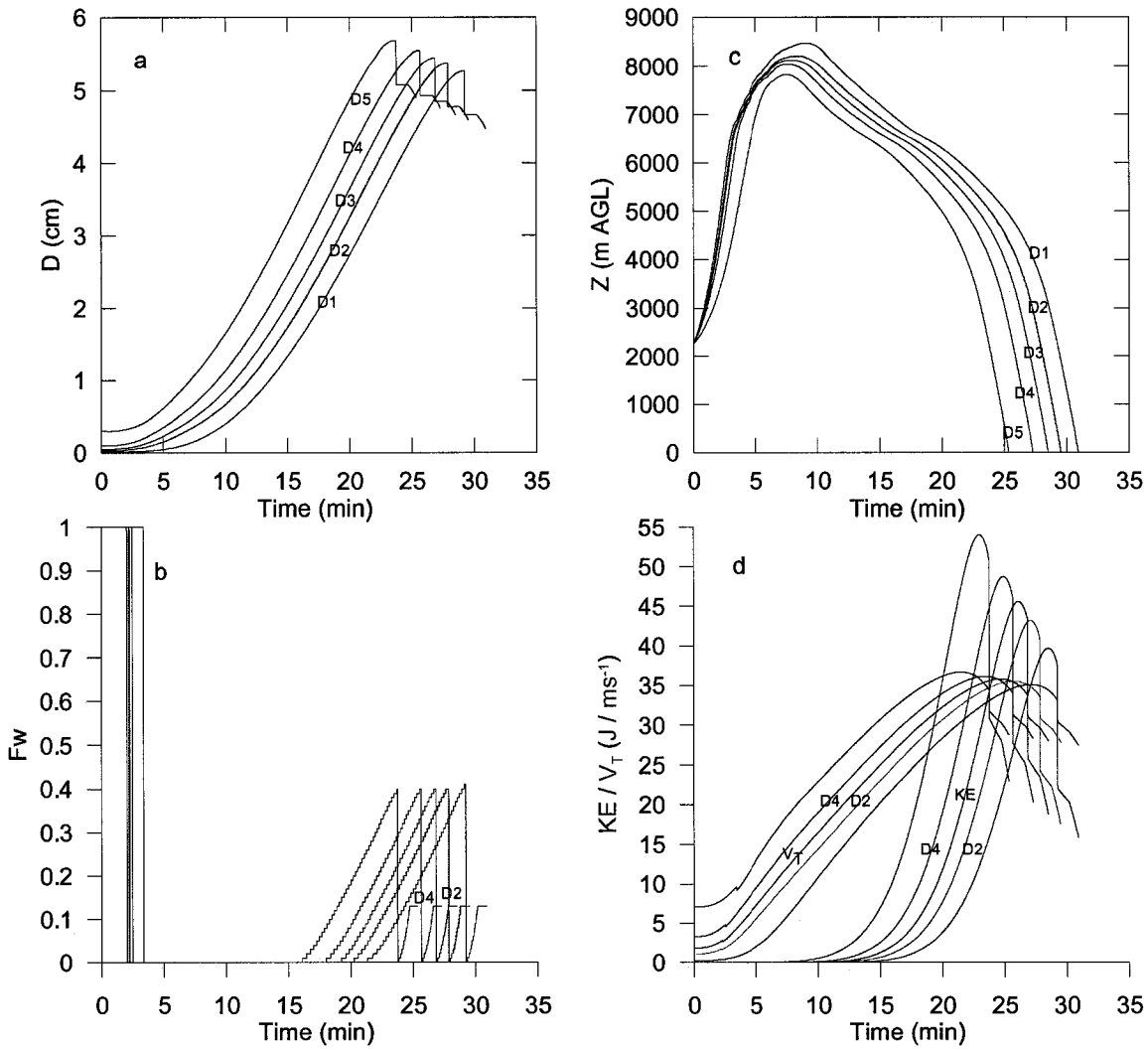

Figure 4.5: Hail growth time histories of sensitivity experiments on different hail embryo initial size for the case of 11 July 1985.

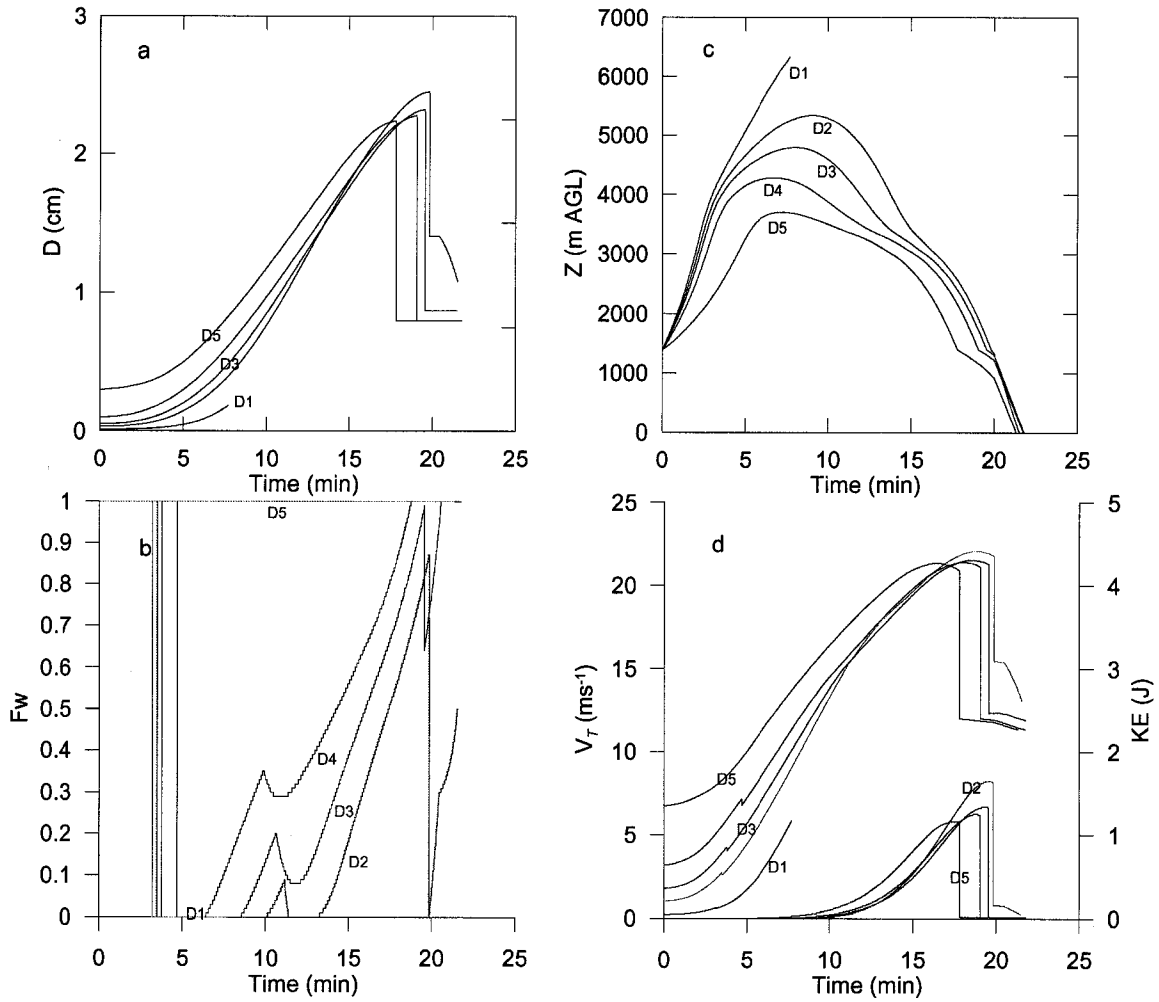

Figure 4.6: Hail growth time histories of sensitivity experiments on different hail embryo initial size for the case of 24 August 1983. (Different initial size of hail embryo)

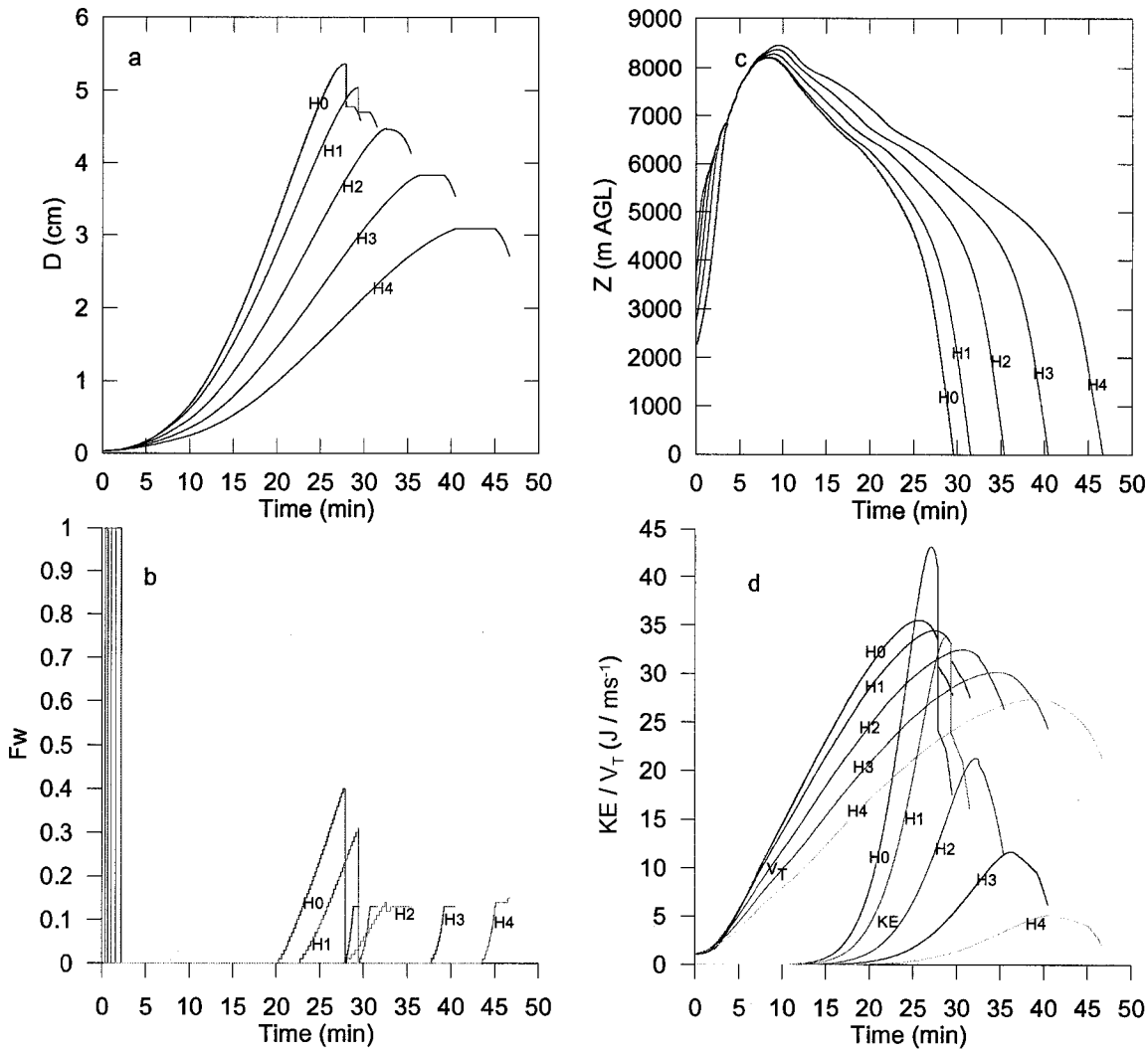

Figure 4.7: Time histories of hail growth for embryos initially lifted from different heights ACB. Same sorts of hail parameters are used as those in Figure 3.10 except different initial heights of embryos. H0 lifted form cloud base. H1, H2, H3, H4 are lifted from 500m, 1000m, 1500m and 2000m ACB, respectively. (Different initial heights of embryo for the case of 11 July 1985).

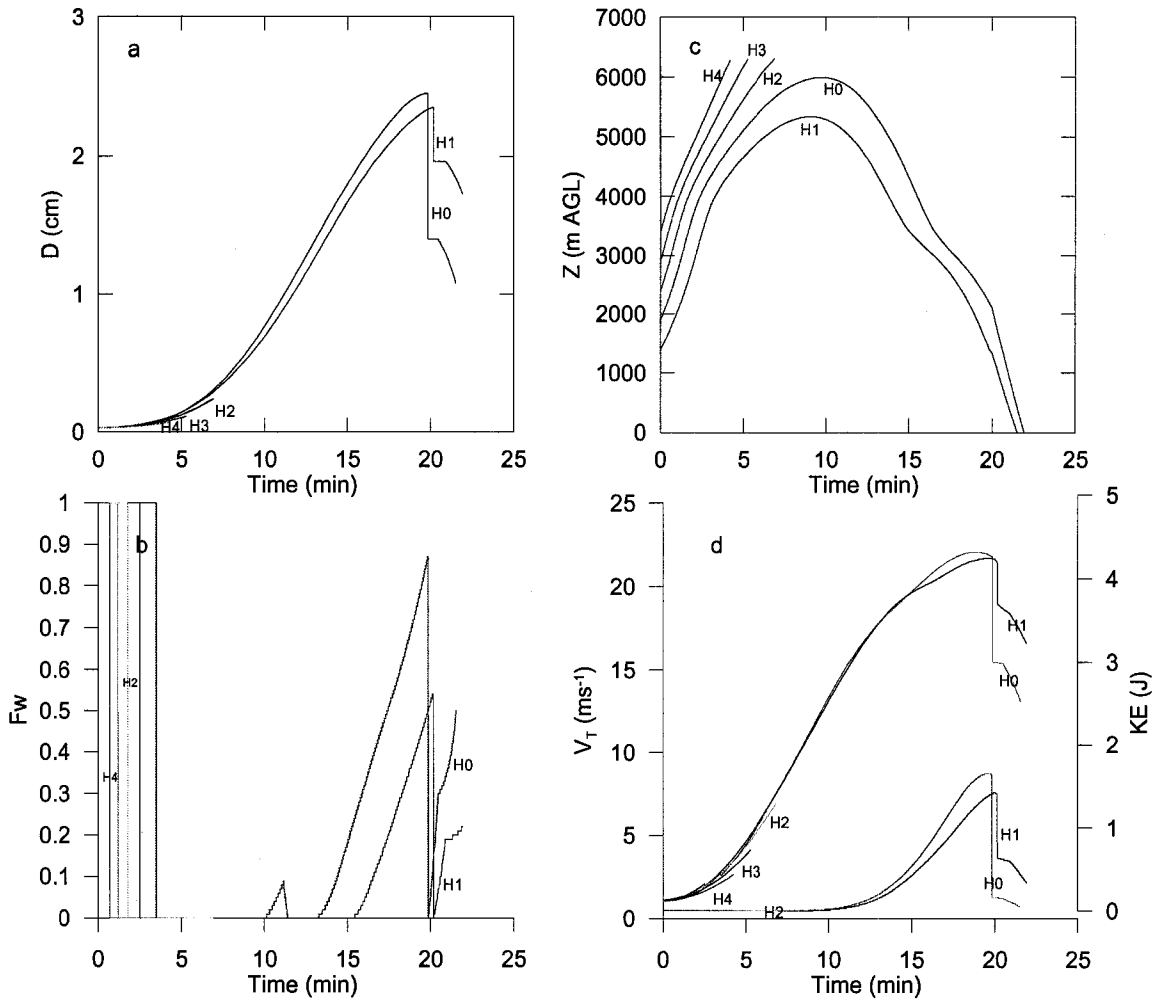

Figure 4.8: Sensitivity experiments for different initial height of embryo on the case of 24 August 1983.

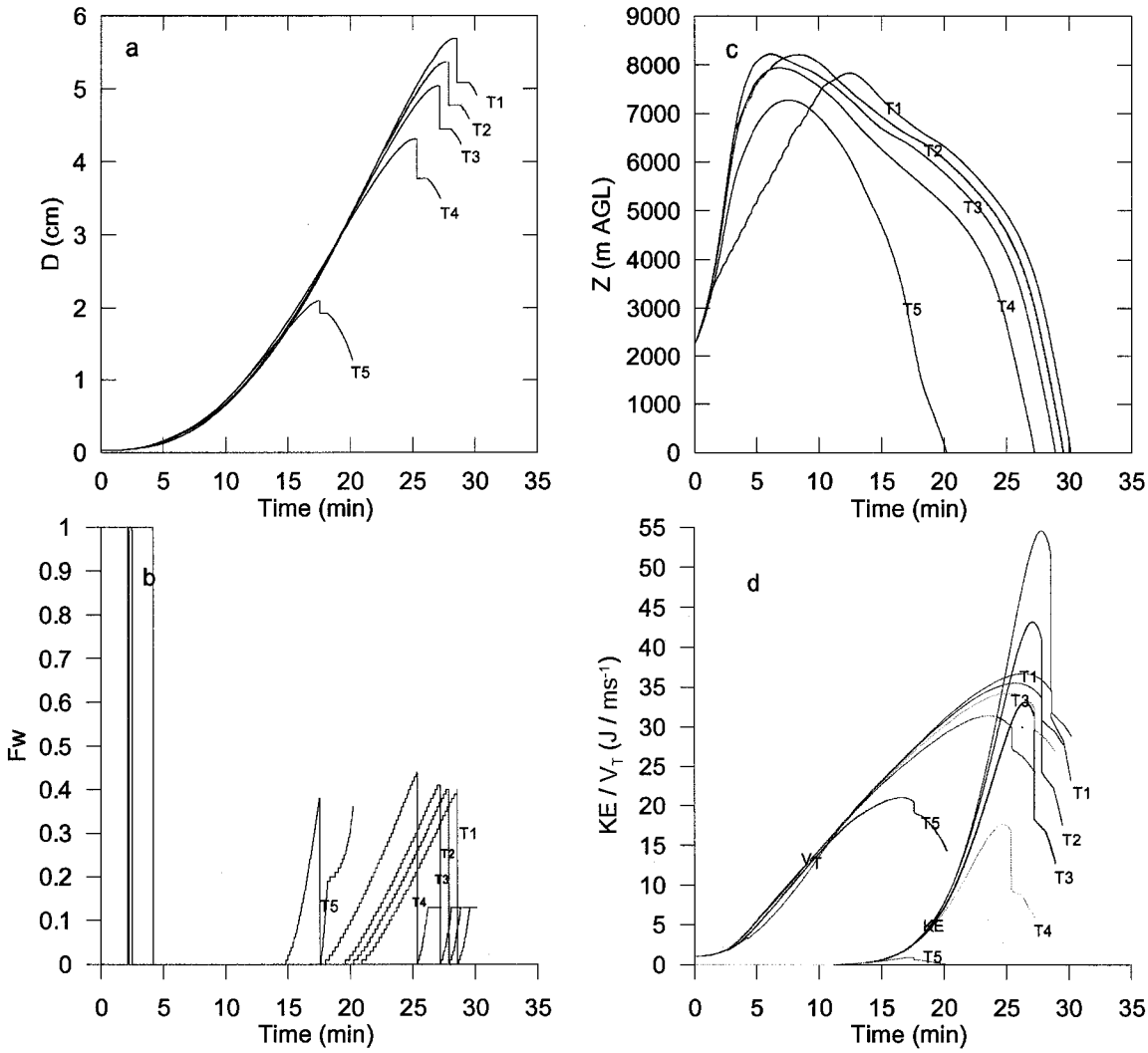

Figure 4.9: Sensitivity experiments for different initial time of embryo introduced into cloud for the case of 11 July 1985.

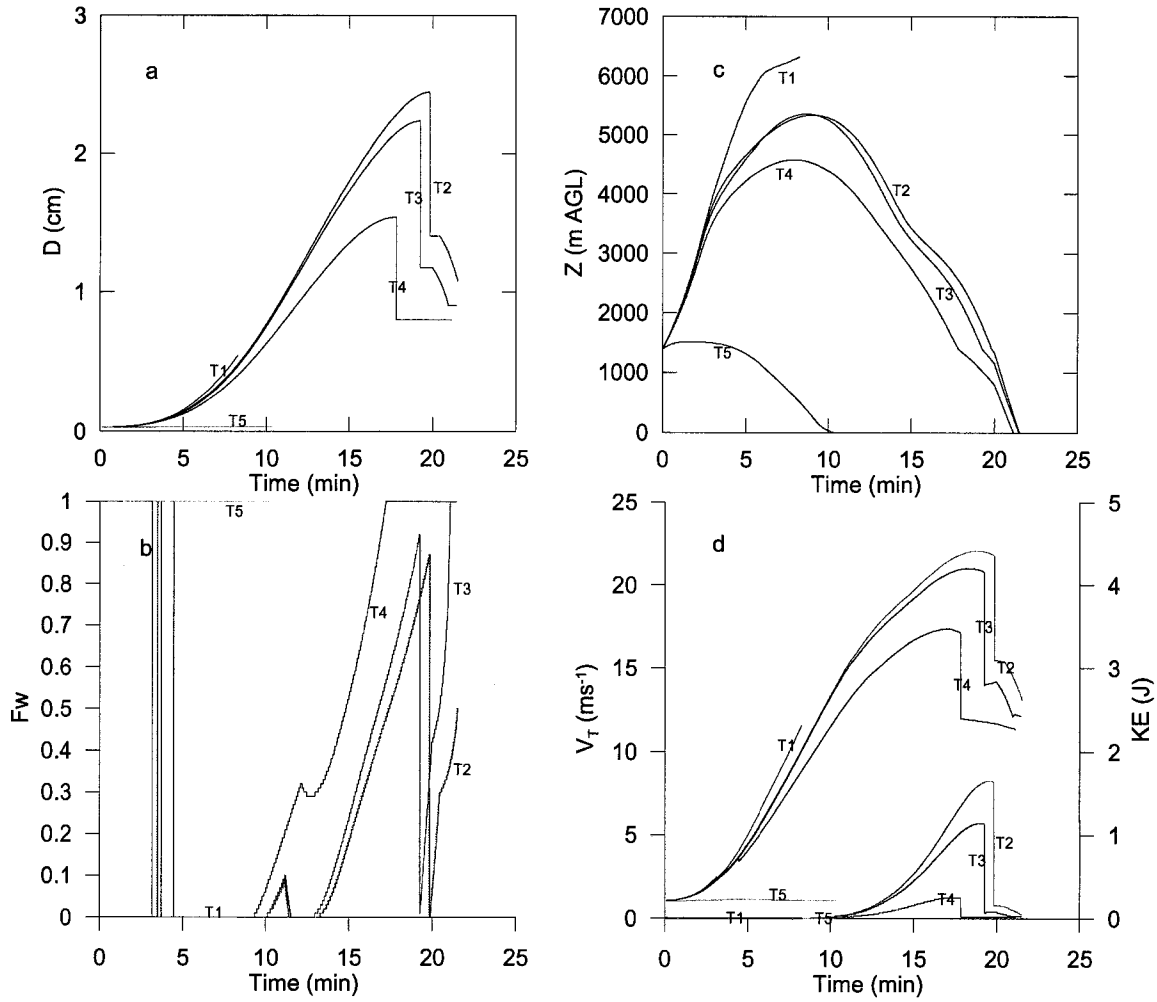

Figure 4.10: Sensitivity experiments for different initial time of embryo introduced into cloud for the case of 24 August 1983.

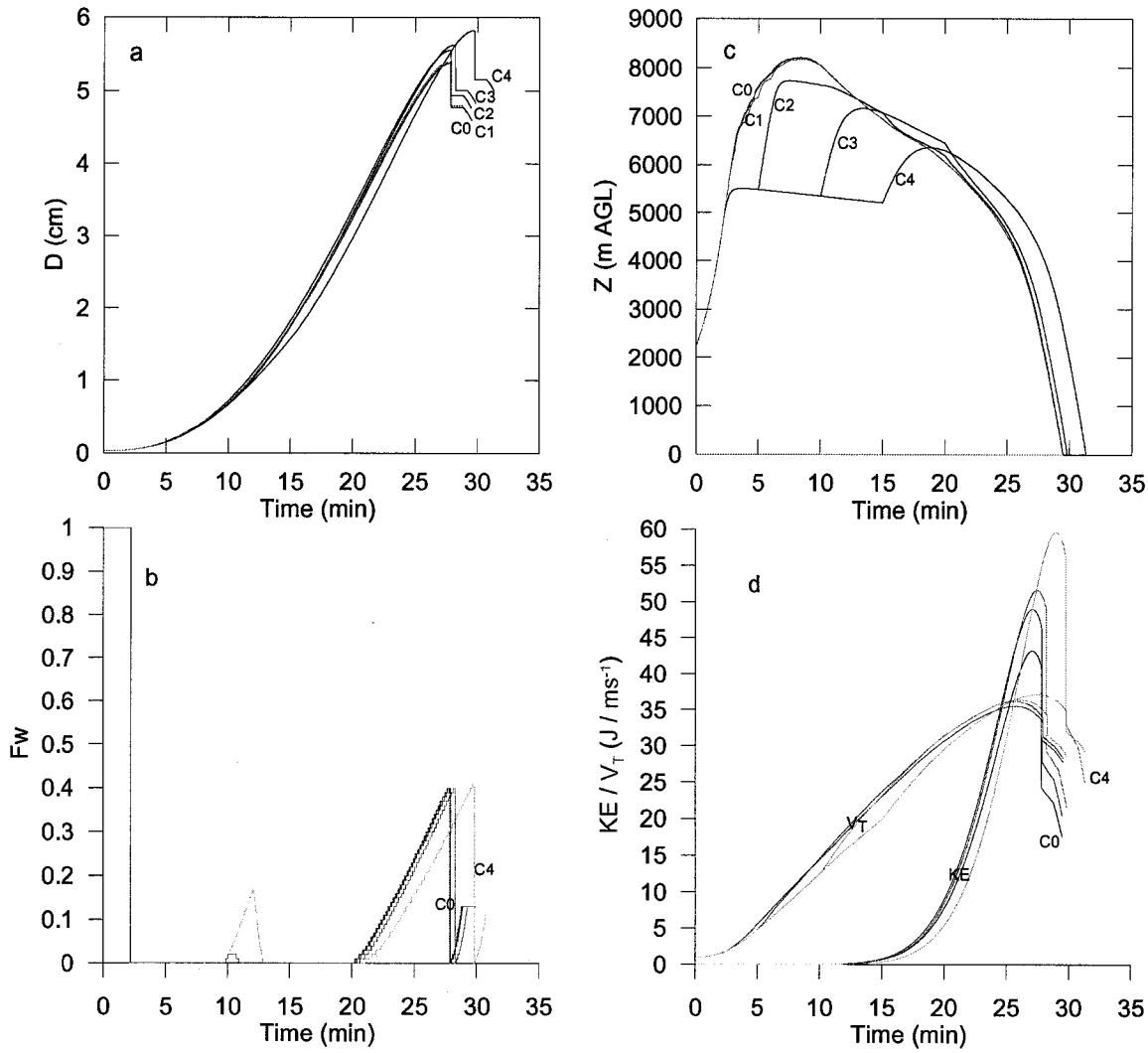

Figure 4.11: Time histories of hail growth in sensitivity experiments for different time span of cloud. Symbols C0 through C4 in the figure represent individual experiment. C1 is overlaid with C0. (Different time span of cloud parameter profiles for hail growth for the case of 11 July 1985).

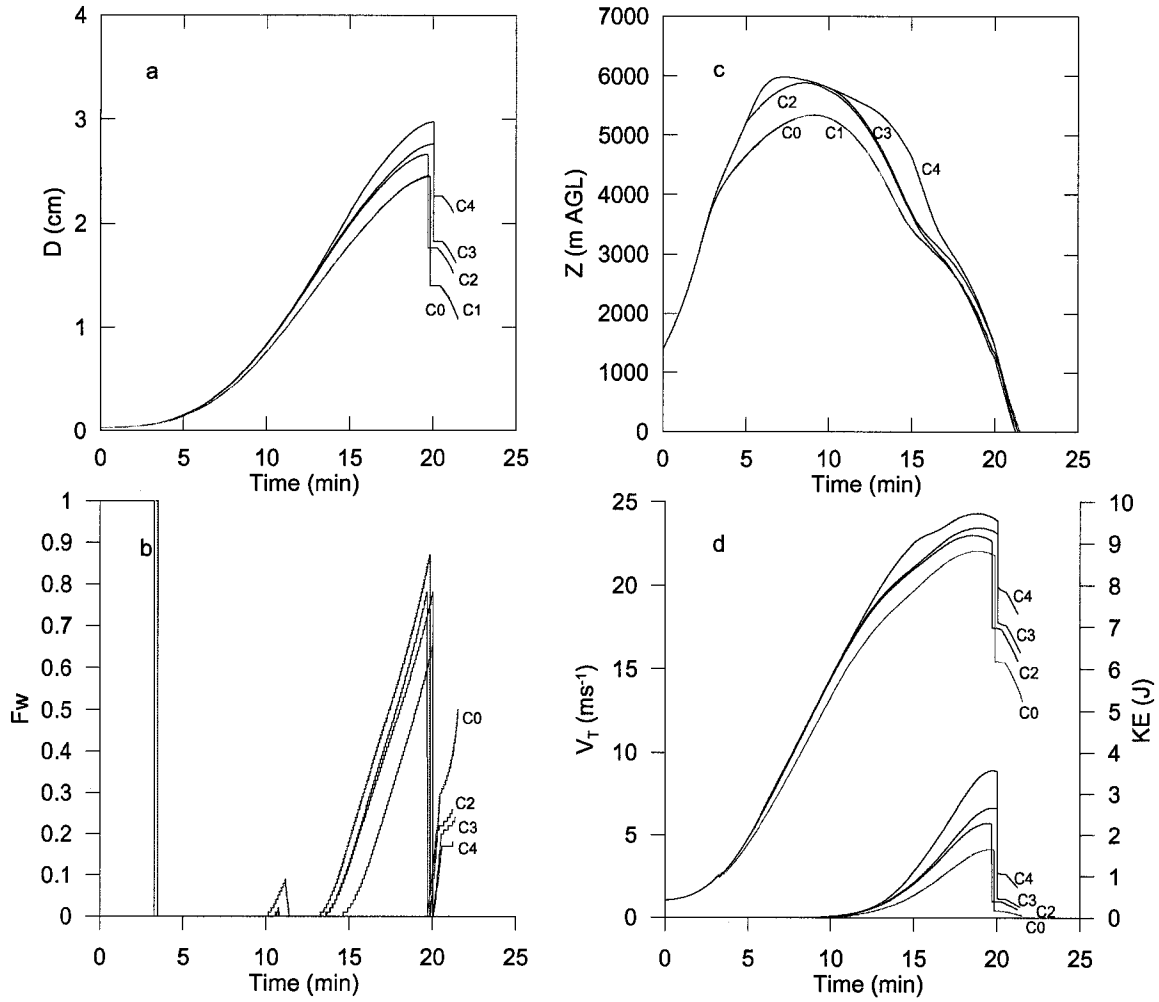

Figure 4.12: Different time span of storm cloud parameters for hail growth on the case of 24 August 1983.

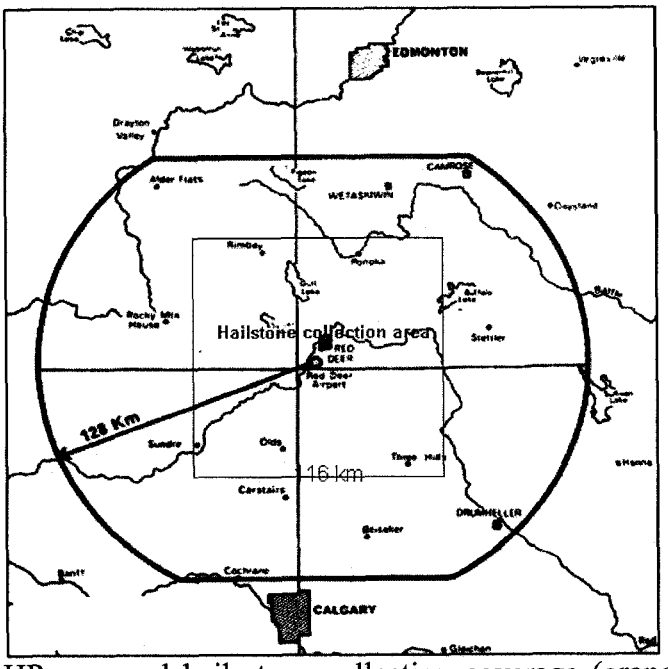

Figure 5.1: The AHP area and hail stone collection coverage (orange rectangular) for verification.

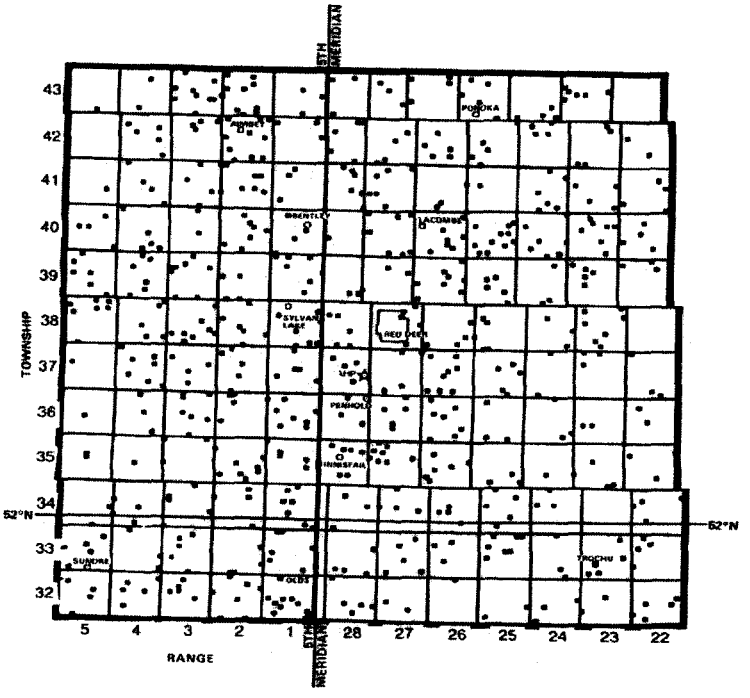

Figure 5.2: The hailstone collection network consisted of 653 volunteer operated volunteer stations within a 13,400 (116×116) km^2 area, which is correspondent to the rectangular area in orange color in Figure 5.1.

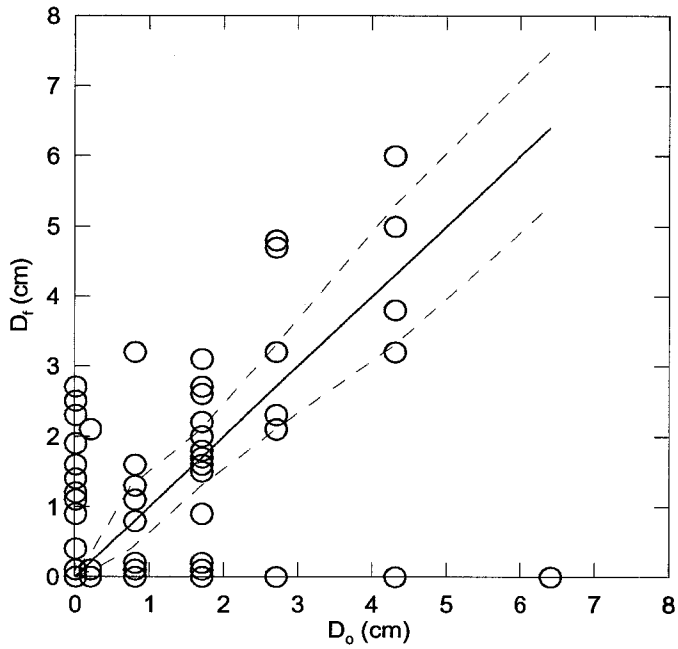

Figure 5.3: Distributions of forecasted maximum hail size using the coupled cumulus-hail model considering precipitation effects (P) plotted against observations. Some of them are overlapped together.

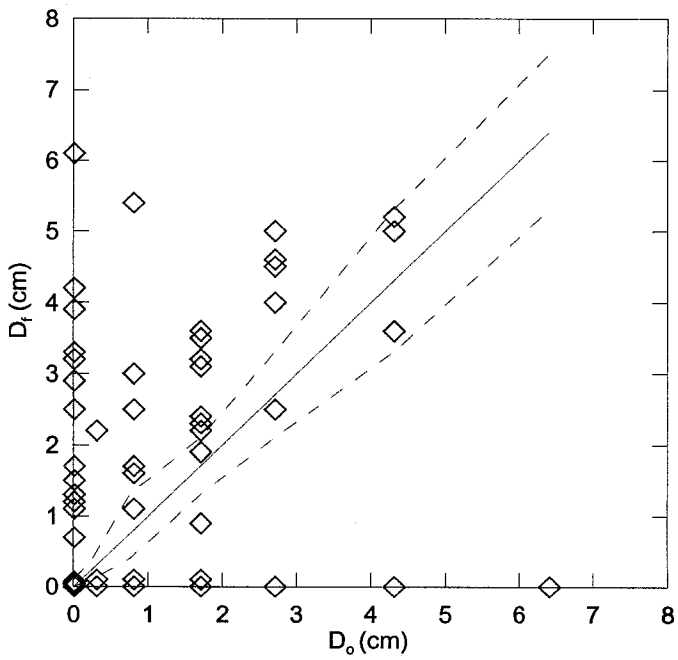

Figure 5.4: Distributions of forecasted hail size using the coupled cumulus-hail model without precipitation effects (F) plotted against observations.

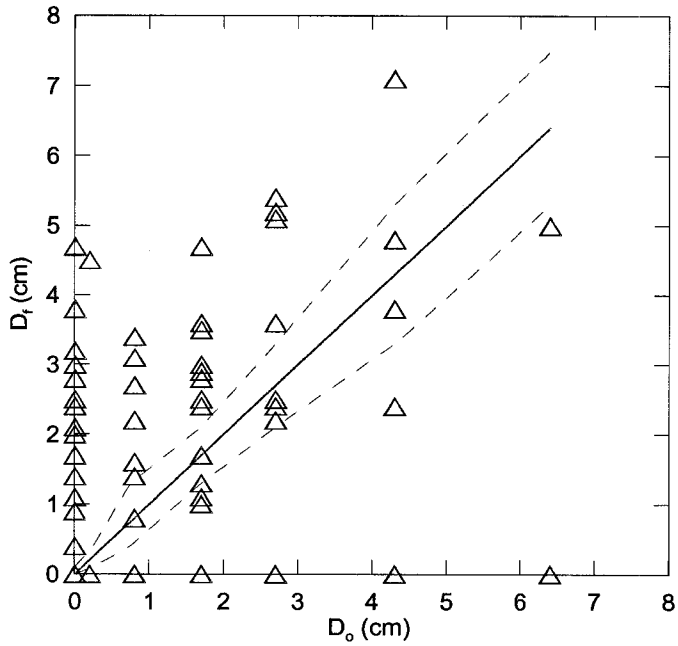

Figure 5.5: Distributions of forecasted hail sizes using HAILCAST (H) plotted against observations.

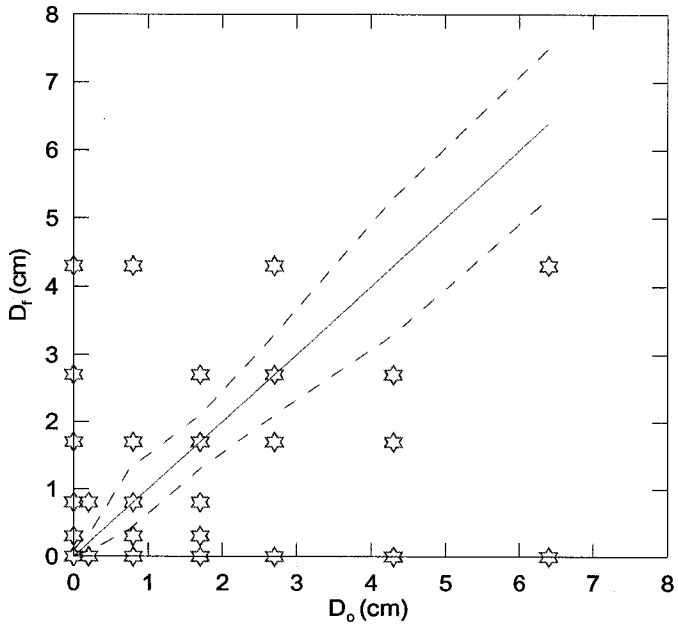

Figure 5.6: Distributions of forecasted hail sizes using NOMOGRAM (N) plotted against observations.

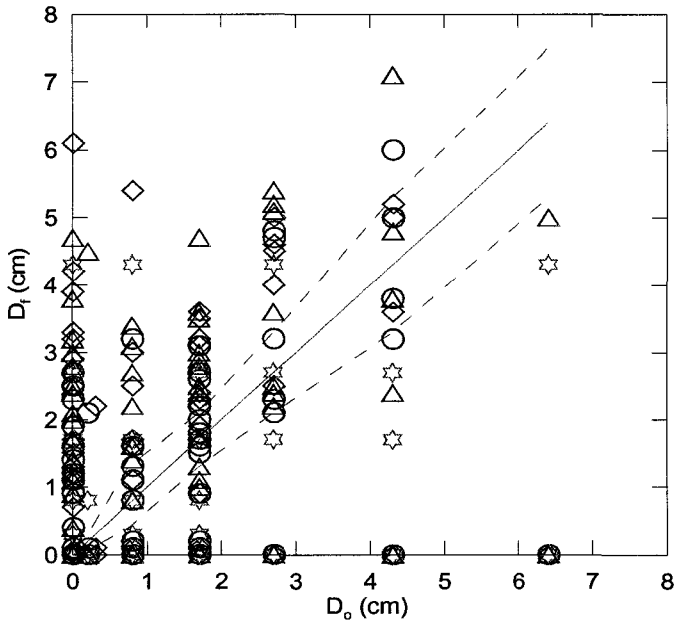

Figure 5.7: Comparisons of model forecasting techniques for AHP data. Forecasted hail size based on different model techniques plotted against observations. P (circle), F (diamond), H (triangle), and N (star).

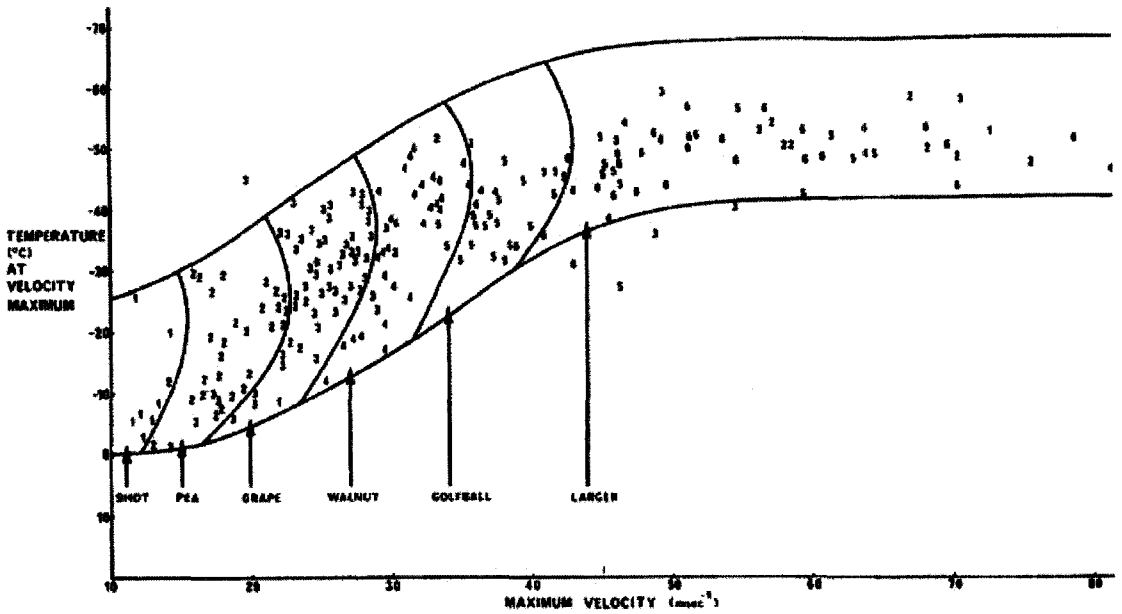

Figure 5.8: NOMOGRAM (N), which related the maximum hail size on the ground to the maximum updraft velocity and the temperature at the altitude of maximum updraft. Numbers 1 to 6 correspond to shot through larger than golf ball size hail. Courtesy of Rinick and Maxwell.

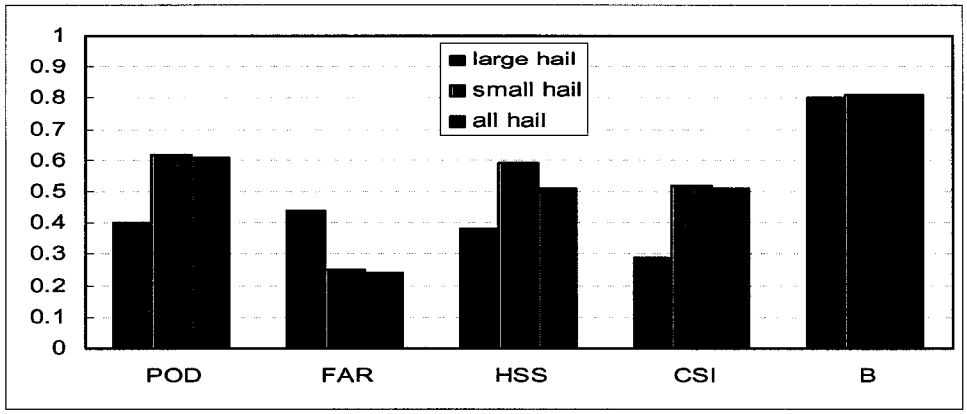

Figure 6.1: Skill scores for model P.

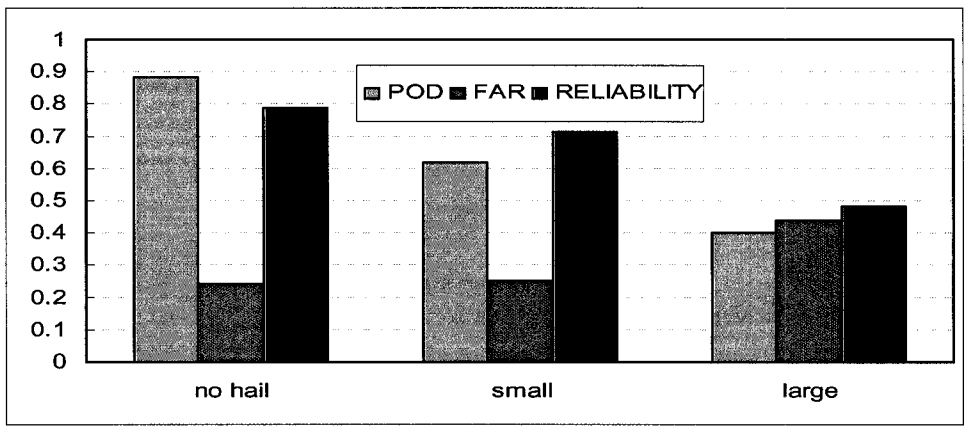

Figure 6.2: Model P reliability for hail size category forecast.

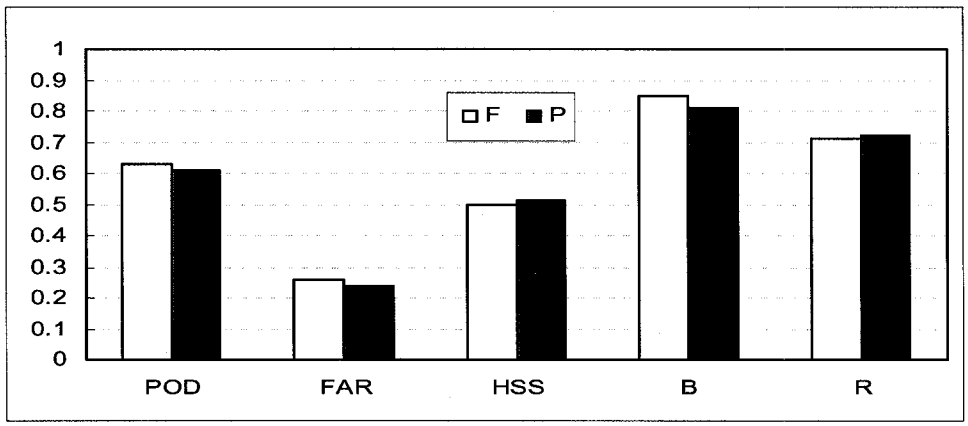

Figure 6.3: Comparison of forecasting skill scores for all hail days between P and F.

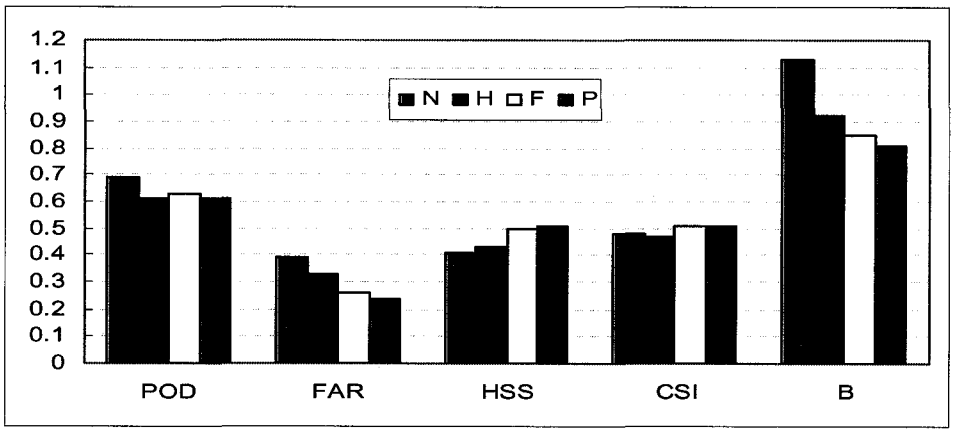

Figure 6.4: Different model technique forecasting skill scores for all hail days.

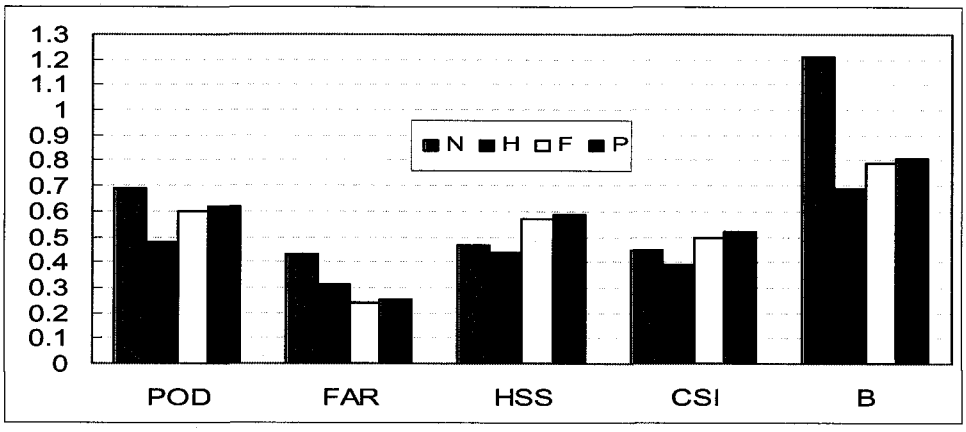

Figure 6.5: Different model technique forecasting skill scores for small hail days.

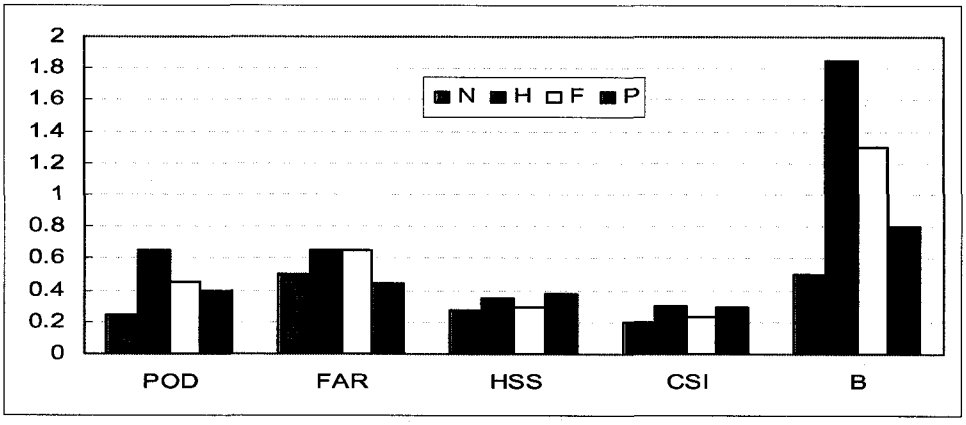

Figure 6.6: Different model technique forecasting skill scores for large hail days.

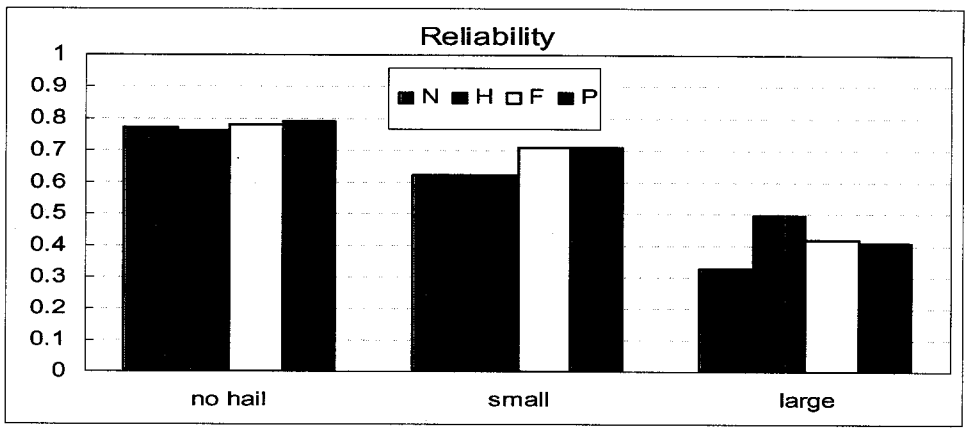

Figure 6.7: Reliabilities of category forecasts using different model techniques.

TABLES

Table 3.1: Comparisons between two cases as one is severe and the other is small hail.

	19850711 (yyyymmdd)	**19830824** (yyyymmdd)
Surface T (°C)	28	22
Surface Td (°C)	10	11
CAPE (J/kg)	756	1063
W_{max} / $H_{W_{max}}$ (ms^{-1} / m AGL)	32/7400	21/3200
T at W_{max} (°C)	-22	-3.7
Maximum Qc (g/kg)	3	2
Maximum Or (g/kg)	10.5	8.5
Cloud top (m AGL)	9800	9000
Cloud base (m AGL)	2300/696.6mb T/Td=6/-2	1384 / 771.7mb T/Td=7.7/2.8
Cloud life (min)	60	30 ~ 40
D_f (cm)	4.6	1.1
τ_f (min)	29	22
FW_f (%)	10	45
KE_f (J)	16	0.1

Table 3.2: Comparison between P and H for two cases.

Parameters	**Case of 19850711**		**Case of 19830824**	
Used model	**P**	**H**	**P**	**H**
$W_{max}/H_{W_{max}}$ (ms^{-1}/ m AGL)	32 / 7400	27 / 7000	21 / 3200	14 / 3000
T at W_{max}	-22	-19	-3.7	-2.2
Maximum Qc (g/kg) / h (m)	3 / 5000	3.5 / 7000	2 / 3500	4.0 / 4800
Maximum Qr (g/kg)	10	0	8	0
Cloud top (m AGL)	9800	9700	9500	6000
Cloud base (m AGL) T & Td at cloud base	2300 / 697mb T/Td=6/-2	2300	1384 / 772mb T/Td=7.7/2.8	1400
Cloud life (min)	60	infinitive	30 ~ 40	infinitive
D_f (cm)	4.6	4.8	1.1	1.4
τ_f (min)	29	62	22	24
FW_f (%)	10	12	50	30
KE_f (J)	16	20	0.1	0.2

Table 4.1: Comparison of cloud and hail parameters affected by precipitation effects for two cases.

Case	**19850711**		**19830824**	
Model	**P**	**F**	**P**	**F**
$W_{\max}(ms^{-1})$	32	30	21	20
$T_{W\max}$(°C)	-22	-20	-3.7	-2.9
Z_{top} (m)	9800	9000	9500	7000
$Q_{c\max}/Z_{Qc\max}(gkg^{-1}/\text{m})$	3/5000	6/7900	2/3500	6/6300
$Q_{r\max}(gkg^{-1})$	10	0	8	0
τ_C(min)	60	>60	30 ~ 40	>60
D_f(cm)	4.6	5.1	1.1	2.5
τ_f(min)	29	30	22	22

Table 4.2: Sensitivity experiments for hail embryo size and initial height of embryo.

Expt	D_i (cm)	Z_i (m ACB)	D_f(cm)		τ_f(min)	
			19850711	*19830824*	19850711	*19830824*
D1	0.01	0	4.5	*0.2 at cloud top*	31	*8 blown out*
D2	**0.03**	**0**	**4.6**	***1.1***	**29**	***22***
D3	0.05	0	4.7	*0.9*	29	*22*
D4	0.1	0	4.8	*0.8*	27	*22*
D5	0.3	0	4.9	*0.8*	25	*22*
H0	**0.03**	**0**	**4.6**	***1.1***	**29**	***22***
H1	0.03	500	4.5	1.7	32	22
H2	0.03	1000	4.1	0.24 *at cloud top*	35	7 *blown out*
H3	0.03	1500	3.5	0.1 *at cloud top*	40	5 *blown out*
H4	0.03	2000	2.7	0.1 *at cloud top*	47	4 *blown out*

Table 4.3: Sensitivity experiments on the introduction time of hail embryo into cloud and the changes of time span period of cloud parameters.

Expt	τ_i (min)	τ_d (min)	D_f (cm)		τ_f (min)	
			19850711	*19830824*	19850711	*19830824*
T1	20	0.5	4.9	*0.5* *at cloud top*	30	*8* *blown out*
T2	**25**	**0.5**	**4.6**	***1.1***	**29**	***22***
T3	30	0.5	4.2	*0.9*	29	*22*
T4	40	0.5	3.5	*0.8*	27	*21*
T5	60	0.5	1.3	*0.0* *at cloud base*	20	*10* *Can't uphold*
C0	**25**	**0.5**	**4.6**	***1.1***	**29**	***22***
C1	25	1	4.61	1.1	29.5	22
C2	25	5	4.76	1.5	29.5	21
C3	25	10	4.83	1.6	29.8	21
C4	25	15	4.99	2.1	31.3	21

Table 5.1: Categories used for classify hail size during the AHP.

Class	Range (cm)	Representative Diameter (cm)
None	[0.0 ; 0.1]	0.0
Shot	[0.1 ; 0.4]	0.2
Pea	[0.4 ; 1.3]	0.8
Grape	[1.3 ; 2.1]	1.7
Walnut	[2.1 ; 3.3]	2.7
Golf ball	[3.3 ; 5.3]	4.3
>Golf ball	$\geq$5.3	6.4

Table 5.2: Summary of different model techniques for hail forecast.

Name of model technique	Cloud model	Hail growth model	Coupling technique
P	Time-dependent two-cylinder cumulus model, involving basic microphysical processes, warm precipitation scheme.	Time-dependent hail growth model involving detailed hail growth microphysics.	Time changing profiles of cloud parameters involving vertical velocity, cloud and rain water mixing ratio, in-cloud temperature etc coupled with hail growth.
F	Switched off precipitation effects from the cumulus model in P.	Same with P.	Same as above except rain water mixing ratio.
H	Steady-state one-dimensional cloud model, excluding cloud physics and precipitation effects.	Same as above.	Steady-state profiles of cloud parameters involving updraft velocity, cloud water content and in-cloud temperature coupled with hail growth.
N	No cloud model, just maximum updraft velocity and temperature at W_{max}.	No hail growth microphysics.	No coupling technique.

Table 6.1: 2×2 contingency table for calculations of model skill scores.

		Observation		
		Yes	No	
Forecast	Yes	Hits (HT)	False Alarms (FA)	Yes Forecasts (HT+FA)
	No	Misses (MS)	Correct Nulls (CN)	No Forecasts (MS+CN)
		Yes Observations (HT+ MS)	No Observations (FA + CN)	Sample Size (N = HT + MS+ FA + CN)

Table 6.2: Summary of skill scores used to evaluate model performance of hail forecast.

Score	Measure	Calculation
Probability of Detection (POD)	Measures the ability to detect an event	POD=HT/(HT+MS)
False Alarm Ratio (FAR)	Measures the tendency to "cry wolf"	FAR=FA/(FA+HT)
Heidke Skill Score (HSS)	Measures the true skill of a rare event forecast	HSS=[2*(HT*CN-MS*FA)]/ [MS*MS+FA*FA+2*HT*CN+(MS+FA) *(HT+CN)]
Critical Success Index (CSI)	Measure of overall performance	CSI=HT/(HT+MS+FA)
Bias (B)	Indicates the degree of under /over-forecasting of an event	B=(HT+FA)/(HT+MS)
Reliability (R)	Shows the credit of believable forecast	R=POD/(POD+FAR)

Table 6.3: Examples of miss forecast cases for large hail days.

Date (yymdd)	Do (cm)	Surface T (°C)	Surface Td (°C)
83622	2.7	17	9
84706	4.3	16	8
85623	4.3	16	7
85712	2.7	16	11
85723	2.7	19	7
85830	2.7	16	9